

**UCLA**

**UCLA Electronic Theses and Dissertations**

**Title**

Multiscale Characterization and Variability of Maya Blue Pigment in Jaina-Style Figurines

**Permalink**

<https://escholarship.org/uc/item/7793m9z3>

**Author**

Shin, Aileen

**Publication Date**

2017

Peer reviewed|Thesis/dissertation

UNIVERSITY OF CALIFORNIA

Los Angeles

Multiscale Characterization and Variability of Maya Blue Pigment in Jaina-Style Figurines

A thesis submitted in partial satisfaction  
of the requirements for the degree Master of Science  
in Materials Science and Engineering

by

Aileen Shin

2017





## ABSTRACT OF THE THESIS

Multiscale Characterization and Variability of Maya Blue Pigment in Jaina-Style Figurines

by

Aileen Shin

Master of Science in Materials Science and Engineering

University of California, Los Angeles, 2017

Professor Ioanna Kakoulli, Chair

Maya Blue is considered a significant organic-inorganic hybrid pigment and the oldest known nanostructured material, produced in Mesoamerica during the Pre-Hispanic period. Experimental and theoretical research conducted on its manufacturing technique and composition indicated that its hue and unique stability comes from the intercalation between the organic indigo dye ( $C_{16}H_{10}N_2O_2$ ) and the inorganic fibrous clay palygorskite  $[(Mg,Al)_4(Si)_8(O,OH,H_2O)_{26} \cdot nH_2O]$ . Maya blue is known particularly for its resistance against chemical corrosion and biodegradation; however, there is still an ongoing debate on how the indigo's interaction with the clay helps achieve the stability of the pigment. In this research, we investigate the variability in composition, microstructure and properties of ancient Maya blue pigment, decorating a set of funerary Jaina-style figurines now at the collection of Fowler Museum at the University of California, Los Angeles (UCLA) and San Miguel Museum in Campeche, Mexico. For the

analysis, we employed a multiscale and multianalytical approach from the macro to the micron length scale using forensic imaging combined with optical microscopy, fiber optics reflectance spectroscopy, scanning electron microscopy-coupled with energy dispersive X-ray spectroscopy and Raman spectromicroscopy.

The thesis of Aileen Shin is approved.

Jaime Marian

Charlene Villaseñor Black

Ioanna Kakoulli, Committee Chair

University of California, Los Angeles

2017

## TABLE OF CONTENTS

<b>1</b>	<b>Introduction</b> .....	<b>1</b>
1.1	<i>Maya civilization</i> .....	1
1.2	<i>Jaina-style figurines</i> .....	4
1.3	<i>Statement of significance</i> .....	5
1.4	<i>Maya blue: literature review</i> .....	5
<b>2</b>	<b>Materials and Methods</b> .....	<b>9</b>
2.1	<i>Sampling and sample preparation</i> .....	9
2.2	<i>Analytical imaging and documentation</i> .....	17
2.3	<i>Preparation of polished cross sections</i> .....	17
2.4	<i>Digital microscopy</i> .....	17
2.5	<i>Scanning electron microscopy (SEM) and energy dispersive X-ray spectroscopy (EDS)</i> .....	18
2.6	<i>Fiber optics reflectance spectroscopy (FORS)</i> .....	18
2.7	<i>Raman spectromicroscopy (<math>\mu</math>RS) and surface enhanced Raman scattering (SERS)</i> .....	19
<b>3</b>	<b>Results</b> .....	<b>20</b>
3.1	<i>Color and molecular characterization of Maya blue</i> .....	20
3.2	<i>Chemistry of blue pigment</i> .....	23
3.3	<i>Microstructural and elemental characterization of Maya blue</i> .....	27
<b>4</b>	<b>Discussion</b> .....	<b>34</b>
4.1	<i>Variability of Maya blue</i> .....	34
4.2	<i>Influence of the raw materials and production methods in chemistry and microstructure of Maya blue</i> .....	34
<b>5</b>	<b>Conclusions</b> .....	<b>35</b>
<b>6</b>	<b>Appendices</b> .....	<b>37</b>
6.1	<i>Appendix A – FORS spectra</i> .....	37
6.2	<i>Appendix B – Raman spectra</i> .....	40
6.3	<i>Appendix C – Raman shifts (wavenumbers - <math>\text{cm}^{-1}</math>)</i> .....	54
6.4	<i>Appendix D – SEM-EDS micrographs and elemental mapping</i> .....	59
<b>7</b>	<b>References</b> .....	<b>72</b>

## LIST OF FIGURES

Figure 1. Map of the Maya region courtesy of Fine Art Museums of San Francisco. Redrawn by Richard Grides. (McVicker, 2012) .....	2
Figure 2. The chemical structure for (a) indigotin and (b) indirubin. Images courtesy of David and Sue Richardson (Richardson and Richardson, 2016).....	6
Figure 3. A compilation of FORS spectra of the blue paint layer on select Jaina-style figurines. The highlighted area notes the absorption band in the visible-region attributing to Maya blue.....	21
Figure 5. Raman spectra of Kremer Pigmente standards, (a) indigo (green) and (b) Maya blue (red), against spectrum of (c) ancient Maya blue Sample 04 (blue). The dotted lines denote notable shifts, disappearances, and intensity in the bands. ....	26
Figure 6. SEM micrographs of the cross-sections of select Maya blue samples (a) 01, (b) 05, (c) 06, (d) 08, (e) 09, and (f) 25 at 5000x magnification. (a) shows greater contrast round-shaped particles, whereas (c) and (f) display larger particles with less contrast, and (b) and (e) show elongated particles sparsely distributed. (d) appears to have an irregular distribution of impurities in a longitudinal fashion. The complete collection of SEM micrographs can be found in Appendix D – SEM-EDS micrographs and elemental mapping. ....	28
Figure 7. The plot of Al in respect to Si against Mg in respect to Si.....	29
Figure 8. EDS elemental mapping of the major elements in Sample 25, indicating a difference in concentration of Mg, Al, and Si within the paint layer and ceramic. A complete elemental map of all samples can be seen in (Appendix D – SEM-EDS micrographs and elemental mapping). ....	30
Figure 9. Backscattered electron micrographs of Sample 01 at (a) 3000x magnification showing the Maya blue and clay substrate interface and at (b) 5000x magnification showing a closer view at the Ca-rich region within the Maya blue.....	33
Figure 10. Backscattered electron micrographs of Sample 20 at (a) 500x and (b) 5000x magnification, showing the high distribution of Ca-rich inclusions throughout the blue paint layer.....	33

## LIST OF TABLES

Table 1. List of Jaina-style figurines from the Fowler Museum collection sampled for this research. ....	9
Table 2. Color values of the blue paint layer on select Jaina-style figurines.....	23
Table 3. Raman bands (wavenumbers $\text{cm}^{-1}$ ) of Maya blue (MB) and indigo.....	24
Table 4. Bulk major and minor elements (at. wt. %) in blue paint layer.....	32

## ACKNOWLEDGEMENTS

I would like to thank Dr. Sergey Prikhodko for training me in using the scanning electron microscopy coupled with energy dispersive X-ray spectroscopy. Many thanks also go to Dr. Christian Fischer for sharing the FORS spectra and for his support throughout my studies. I am grateful to Christian De Brer, Head of Conservation at the Fowler Museum at UCLA for access to the Jaina-style figurines. I would also like to express my gratitude for my committee members, Dr. Jaime Marian and Dr. Charlene Villaseñor Black, for taking the time to review and improve upon this thesis.

I am also thankful towards Roxanne Radpour, Yuan Lin, Xiao Ma, and Xuanyi Wu for their assistance in helping me learn how to utilize different analytical techniques. In addition, I appreciate the other members of the UCLA Archaeomaterials Group for their continuous support throughout this research.

This work would not have been possible without my principle investigator and committee chair, Dr. Ioanna Kakoulli, who dedicated time and effort into not only helping me through completing this publication but also through my academic endeavors.



# 1 Introduction

## 1.1 Maya civilization

There is some consensus amongst archaeologists that the Maya culture, where the ancient civilization possibly dated from over 3,000 years ago up until its collapse during 750-900 A.D. (Hodell et al., 1995), altogether has an Olmec origin (Sharer and Traxler, 2006) due to the similarities in culture regardless of the diverse customs existing within Mesoamerica. Before the discovery and conquest on Maya cities by the Europeans, the Maya civilization thrived for many years (Sharer and Traxler, 2006). There are three eras that describe the chronology of the ancient Maya: Preclassic (300 B.C. - A.D. 240), Classic (A.D. 250 - 900), and Postclassic (A.D. 900 - 1519) (Henderson, 1997, Broda, 2000). It is during the Preclassic period that the Mesoamericans were establishing their earliest societies along the Southern area of the Mexican Gulf Coast, central Mexico, and in the Maya located in the Mesoamerican southeast region (Šprajc, 2009). Moving down the timeline into the Classic period, strong geographic differences were formed, and with it, a rich diversity in language, ethnic groups, and culture (Broda, 2000). This includes a growth in their writing system, fine arts, and architecture (Šprajc, 2009). Following this flourishing era into the Postclassic period, it became more common for a number of Mesoamerican polities to trade goods and share ideas with neighboring cities (Smith and Berdan, 2003), whilst also increasing in migrations, political fragmentation, and militarization (Šprajc, 2009), eventually leading into the Late Classic Maya collapse.

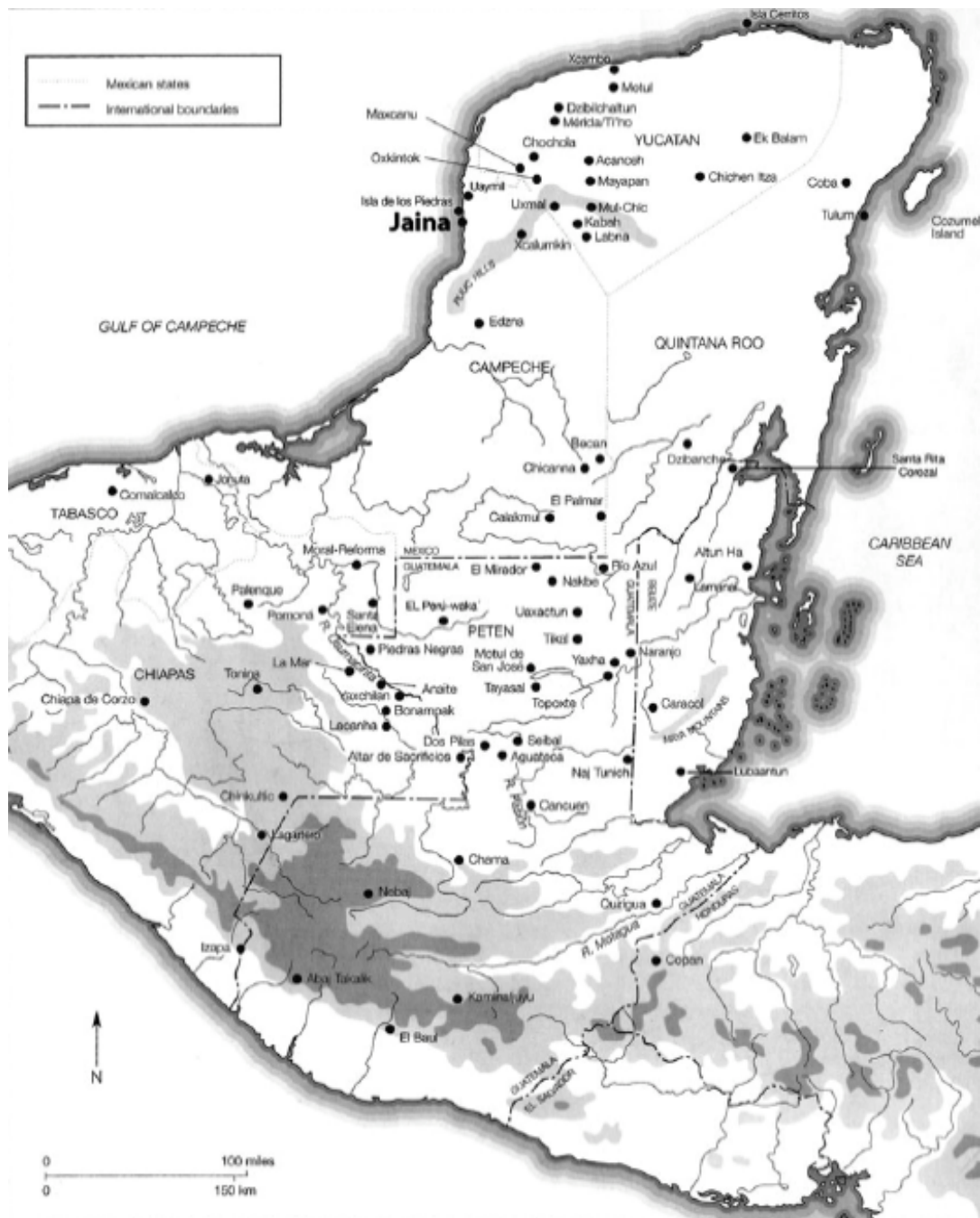


Figure 1. Map of the Maya region courtesy of Fine Art Museums of San Francisco. Redrawn by Richard Grides. (McVicker, 2012)

The ancient Maya preoccupied the region that was coined by anthropologist Paul Kirchoff as “Mesoamerica” (Creamer, 1987). The Maya had a notable geographic unity during the Spanish Conquest, unlike the more scattered regions of the other indigenous people of

Mexico and Central America. They occupied a single, cohesive area covering around 324,000 km<sup>2</sup> of land that includes the Yucatan Peninsula, Guatemala, Belize, a section of Tabasco and Chiapas, as well as the west side of Honduras and El Salvador. Owing to the inclusion of multiple lands, there is great diversity in geography from the Pacific coastal plain in the southern margin, to the highlands in the central region, to the lowlands in the northern area (Sharer and Traxler, 2006, Coe and Houston, 2015). The Pacific Coastal Plain extends from Chiapas in Mexico to southern Guatemala and El Salvador. Due to the volcanic activities in the highlands north of the coast, the volcanic sediments make up a part of the soil. The Maya highlands are defined to exist above an average of 800 m in elevation, the terrain including volcanoes and a richness in a variety of natural resources (Sharer and Traxler, 2006). The southern highlands are of importance to the historical documentation of Maya civilization since the earliest known village societies were discovered in this region during the tenth century, thus providing recordings of early Maya practices (Demarest, 2004, Coe and Houston, 2015). The lowlands in general have a mainly flatter terrain that was once covered by lush subtropical rain forests and also carried a variety of resources due to the range in environment.

Though the Maya civilization covered a great deal of land, it was common amongst the diverse Maya culture to perform rituals for religious and ceremonial practices, from sacrificing living beings to funerary traditions (Lucero et al., 2003). It is through these practices that archaeological sites, structures, and artifacts can be found and studied today, providing insight on not only the achievements of the ancient Maya but also the cultural context behind those accomplishments.

## 1.2 Jaina-style figurines

On the coast of Campeche, Mexico lies an artificial burial site of the Maya: the presumably titled Jaina Island. As part of the cultural ritual, the deceased, regardless of social status, were typically buried alongside a Jaina-style figurine and ceramic pottery or other ceremonial objects, where these figurines can range from rattles to whistles to statuettes. Although these type of figurines have been studied, mainly from an archaeological and art historical perspective (Fernández, 1946, Cook de Leonard, 1964, Miller, 1975, Corson, 1976, Goldstein, 1980, Piña Chán, 1996, McVicker, 2012, Halperin, 2014, Tzadik, 2014), there are still unanswered questions on the significance they hold in the past society due to the peculiarity of the event that they accompanied both on the higher and lower end of the hierarchy. How the figurines are defined in relation with whom it was placed beside has been an ongoing debate, but it has mostly been a matter of interpretation due to the difficulty of determining the initial layout of the ancient site. Because the graves have been tampered with as seen by the visual signs of looting and forgery, determining the original geographical scene, and therefore interpreting the historical context, becomes even more challenging (McVicker, 2012).

Little is also known about the production of these Jaina-style figurines in a cultural and social context; however, it has been revealed that these figurines were produced through hand-modeled or molded clay, where the latter was a technique for a more progressive adaptation to the hand-modeling technique and used for mass production (McVicker, 2012). It has been suggested that the figurines were not manufactured in quantity on Jaina or even the coast of Campeche due to the lack of workshops evident on the locations, although workshops have been found in the surrounding regions, Tabasco and Peten, which could explain the many sources of clay that were used in the figurines production.

### 1.3 Statement of significance

Maya blue is not only the oldest nanostructured material known to human history, but also a chemically and optically stable organic-inorganic hybrid pigment. The application of materials science principles and methods to study this ancient pigment can therefore provide insight on the selection of the raw materials and the processes involved for its production. Understanding the relationships between structure and synthesis can further inform cultural context and the social process involved in its manufacture.

In this research, we apply non-destructive scientific techniques, which do not consume the sample to yield results, to investigate the structure of Maya blue. More specifically, the research has a twofold goal: first to examine the extent of the variability in the production of Maya Blue in the Jaina-style figurines from the Fowler Museum collection, and second to identify potential fingerprint markers that may provide clues to artifact authentication studies.

### 1.4 Maya blue: literature review

Maya blue is an organic-inorganic hybrid pigment created by the ancient Maya during the pre-Hispanic times through low firing, at around 105° to 150°C (Van Olphen, 1966), of a mixture of indigo dye ( $C_{16}H_{10}N_2O_2$ ) with the fibrous clay palygorskite  $[(Mg,Al)_4(Si)_8(O,OH,H_2O)_{26} \cdot nH_2O]$ . This blue color has been used by the Maya people to decorate textiles, pottery, figurines, and wall paintings, showcasing a varying hue of blue to bluish-green, the probable cause being the dependence on the heating conditions or the ratio of indigo to the clay when it was produced (Doménech et al., 2006). Indigo has a poor light fastness, and therefore can degrade in its original shade of blue over time when exposed to light; however, when chemically bound to the clay to produce Maya blue, its color durability to light and resistance against harsh conditions, including chemical corrosion and biodegradation, increases (José-Yacamán et al., 1996, Giustetto et al., 2005, Dejoie et al., 2011). Despite this common knowledge of the stable

characteristic of Maya blue, the question at large is how the indigo molecules bond with the clay in order to achieve the pigment's high chemical and photochemical stability.

Before attempting to understand the origin of the strength of Maya blue, it is important to take note of the two elements that make up its chemical structure. Indigo is an organic blue dye with two main coloring components, indigotin and indirubin. The Maya extracted indigo through processing the leaves of the species *Indigofera suffruticosa* of the genus *Indigofera*, also known as añil, a plant native to Central America (Giustetto et al., 2005, Sanz et al., 2012, Splitstoser et al., 2016). Indigotin provides the main blue colorant of the indigo dye which comes from the presence of N-H donor groups and the substitution of C=O acceptor groups for the C=C double bond located towards the center of the molecule (Dejoie et al., 2011). Indirubin is a structural isomer of indigotin that is just as present (Sanz et al., 2012, Splitstoser et al., 2016).

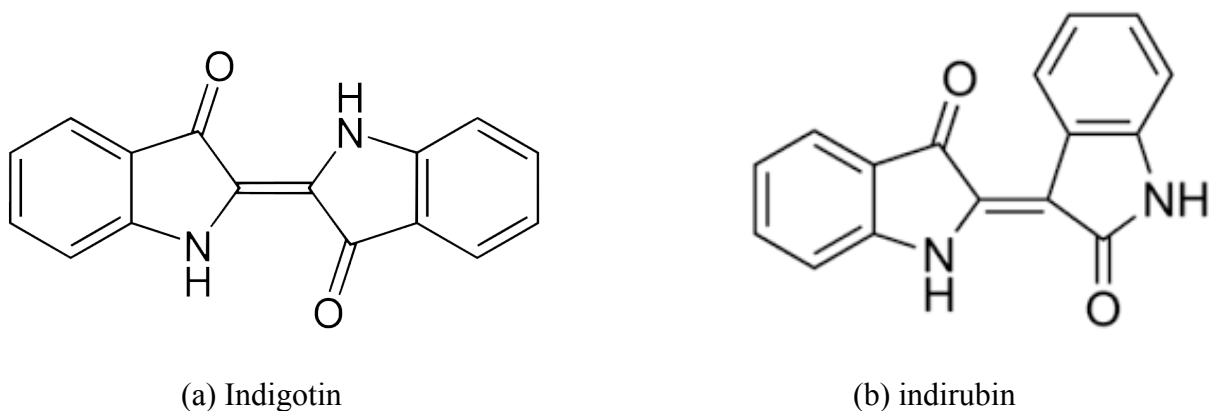


Figure 2. The chemical structure for (a) indigotin and (b) indirubin. Images courtesy of David and Sue Richardson (Richardson and Richardson, 2016).

The clay known as palygorskite is a type of dioctahedral phyllosilicate, a zeolite whose molecular structure is formed by alternating layers of continuous Si-based tetrahedral sheets and discontinuous (Mg,Al) octahedral sheets that extends in the c-direction (Giustetto et al., 2005). There are varying compositional forms of this clay depending on the source location, particularly

when impurities are introduced into the matrix, one such instance of Ca, Na, K, Fe, and Ti found in an area from within the Yucatán peninsula of Mexico (de Pablo Galán, 1996).

Palygorskite has been discovered to have three types of adsorbed water molecules: a weakly-bound physisorbed water surface that covers the fibers, weakly-bound zeolitic water molecules within the channels, and tightly-bound structural water molecules that completes the geometrical arrangement of the (Mg,Al) cations bordering the octahedral layers (Giustetto et al., 2005, Dejoie et al., 2011). It is during thermal treatment when synthesizing Maya Blue that the indigo molecules are able to bind to the palygorskite structure, but there is still the issue of determining where exactly the indigo dye adsorbs onto the clay.

Before the chemistry of Maya blue was fully understood, it was suggested that the ferrous iron ( $\text{Fe}^{2+}$ ) was the only chromogenic element in this synthetic pigment. This was based on the findings of Gregory P. Baxter, a chemist of Harvard University, who identified Ca, Mg, Si, Al, and Fe in a spectrogram of the ancient pigment (Gettens, 1962). Through X-ray diffraction studies, Gettens was later able to identify the clay mineral attapulgite, now commonly known as palygorskite, as an inorganic, colorless material within Maya Blue, but was still unable to determine what causes the bluish tint (Gettens, 1962). Following the acceptance of the presence of palygorskite as one of the major constituents of Maya Blue, the archaeologist Anna Shepard posed a hypothesis that the blue pigment is created by the combination of an inorganic and an organic material, later supported by the experimental research of van Olphen, who studied the formation of the attapulgite-indigo complex, since indigo was a dye that would have been available to the Maya (Shepard and Gottlieb, 1962, Van Olphen, 1966). Van Olphen suggested that the indigo molecules could only occupy the surface grooves of the clay as the indigo molecules were too large to fit through the palygorskite tunnels, and it is because of the palygorskite covering the indigo molecules that the latter is able to receive protection from

external oxidant or acid attacks (Van Olphen, 1966). José-Yacamán *et al.* would later form a theory by studying the Maya blue structure at the nanoscale level, where it was thought that Fe, Cr, Ti and Mn particle impurities may influence the appearance of the colorization due to the encapsulation of not only indigo molecules but also the oxidation and encapsulation of the metallic nanoparticles, where the latter would also contribute to the acid resistance of the hybrid pigment (José-Yacamán *et al.*, 1996).

Another theory proposes that the tunnels, a term used interchangeably with channels, are partially inaccessible after heat treatment; therefore concluding that the indigo molecules reside at the entrance of the channels, where hydrogen bonds form between the carbonyl and amino groups of the indigo and the silanol groups at the border of the clay micropores, effectively trapping the water within (Hubbard *et al.*, 2003). Giustetto *et al.* suggested that indigo molecules enter the microporous channels by substitution of the zeolitic water molecules that are lost at higher temperatures, thus encapsulating the indigo molecules within (Giustetto *et al.*, 2003). An opposing model supporting van Olphen's previous claims further suggests that by elevating the temperature of the water adsorbed in the grooves of the clay, thereby effectively removing the water, the indigo molecules are able to occupy the now vacant areas on the surface (Chiari *et al.*, 2008).

The most recent finding explaining the unique properties and color of Maya blue is based on the transformation of indigo to dehydroindigo through oxidation. Through analyzing electrochemical data, it was observed that dehydroindigo and indigo are favored thermodynamically as noted through their attachment to the clay matrix at elevated temperatures. In addition to this latest concept, it is still proposed that the indigo dye is dispersed within different sites of the palygorskite matrix (Doménech *et al.*, 2009).










## 2 Materials and Methods





### 2.1 Sampling and sample preparation





Using the sharp edge of a scalpel, thirty microsamples containing Maya blue were taken from Jaina-style figurines that are now at the collection of the Fowler Museum of University of California, Los Angeles (Table 1 & Appendix D – SEM-EDS micrographs and elemental mapping).

**Table 1. List of Jaina-style figurines from the Fowler Museum collection sampled for this research.**




Sample #	Description	Figurine Museum Accession #	Figure
01	Light blue taken from drape over the left arm	X91.2264	
02	Blue taken from cloth hanging over right shoulder	X91.2261	
03	Light blue taken from neck clothing	X91.2252	





04	Dark blue taken from right earring	X91.2253	
05	Blue taken from bottom left of pedestal	X91.2262	
06	Light blue taken from middle of headdress	X91.2263	
07	Blue taken from bottom-right of robe near foot	X91.2269	





08	Blue taken from bottom-right near foot	X91.2274	
09	Blue taken from backside towards the right	X2010.16.4	
10	Light blue taken from above the head, at the bottom of head piece	X91.2268	
11	Light blue taken from figurines right side	X2010.16.21	





12	Light blue taken from backside of head	X2010.16.16A	
13	Blue taken from backside of head piece	X2010.16.10	
14	Blue taken from backside of head	X2010.16.17	
15	Blue taken from under the arm on the article of clothing towards the left	X2010.16.2	



16	Blue taken from lower garment	X2010.16.19	
17	Light blue taken from right side	X2010.16.1	
18	Light blue taken from left side of the head piece	X2010.16.7	

19	Light blue taken from right side, towards the front	X76.760	
20	Light blue taken from garment above the left foot	X91.625	
21	Blue taken from underneath belt area	X2010.16.23(A,C,D,E,F)	
22	Light blue taken from under chin towards the left	X76.788	

23	Light blue taken from back on right shoulder	X76.791	
24	Light blue taken from back	X96.8.37	
25	Light blue taken from right of head piece	X75.1740	
26	Blue taken from midsection towards the right	X2010.16.15	

27	Light blue taken from the midsection in the back towards right	X2010.16.12	
28	Blue taken from midsection towards the left	X2010.16.13	
29	Blue taken from midsection towards the left	X2010.16.11	
30	Greyish blue taken from top of head piece	X76.722	



## **2.2 Analytical imaging and documentation**

Following the examination of the figurines using reflectance and fluorescence imaging to detect possible surface and structural alterations (Tzadik, 2014), the figurines were photographed using diffuse light. The photographs were used as base images with annotations indicating the location of the microsamples (Appendix D – SEM-EDS micrographs and elemental mapping).

## **2.3 Preparation of polished cross sections**

Each microsample was prepared as a polished cross section to expose the stratigraphy of the paint layer and interface with the ceramic body. Samples were prepared using an EpoxiCure™ 2 Resin cured with EpoxiCure™ 2 Epoxy Hardener using a mixture of 4:1 resin to hardener ratio by volume. The mixture was then poured to fill in half of square- and rectangular-shaped rubber molds and allowed to cure for roughly three hours until the epoxy reached a thicker, amorphous viscosity. The stratigraphic samples were then placed on top of the epoxy near the edge of the mold with the paint surface flat on the epoxy, and more resin was poured to fill in the remainder of the mold. Once the resin was completely set, the samples went through a process of grinding (perpendicular to their surface to expose the entire stratigraphy) followed by polishing using a Spectrum System 1000 rotating table. The samples were first ground using ethanol and an 800 grit silicon carbide sheet to expose the cross-section to show the Maya Blue and occasionally the clay it was applied onto, then polished using ethanol with a 3 micron followed by a 1 micron microid diamond compound paste on the respective Buehler polishing pads to achieve a smooth finish.

## **2.4 Digital microscopy**

Digital Photomicrographs at 200x magnification were taken of the cross section polished samples using a KEYENCE VHX-1000 digital microscope for visual comparison in terms of the location of the Maya blue with respect to the SEM micrographs.

## **2.5 Scanning electron microscopy (SEM) and energy dispersive X-ray spectroscopy (EDS)**

The polished cross section samples after examination using digital microscopy, were placed on aluminum scanning electron microscopy (SEM) stubs using carbon tape and transferred to a Balzers Union CED 020 carbon evaporator to apply a thin layer of carbon coating. This was done by placing three to six samples inside the evaporator chamber and allowing the vacuum to pump for about half an hour, or until the pressure reached 0.05 mbar, then switching on the high current to allow the carbon to coat the samples. In addition, any remaining Maya blue flakes also originating from the Jaina-style figurines were placed directly on a glass slide to be analyzed using the Raman spectroscopy utilizing non-destructive techniques.

In order to study the contrast between the transitioning phases from within the Maya blue to the clay substrate, samples were analyzed in high vacuum using a FEI NOVA NanoSEM™ 230 scanning electron microscope (SEM) equipped with a Backscattered Electron Detector (BSED). The spot size was maintained from 3.0 to 3.5 with an accelerating voltage of 10 to 15 kV, increasing no higher than those values so to reduce charging effects on the non-conductive samples. The SEM was coupled with a Thermo Scientific NORAN System 7 Energy Dispersive X-Ray Spectrometer (EDS) for the qualitative and quantitative analysis of the elemental compositions, where the current was increased to above 1 nA for better detection of the elements by increasing spot size to 4.5 whilst ranging the voltage between 10, 12, 15 and 18 kV depending on detection functionality.

## **2.6 Fiber optics reflectance spectroscopy (FORS)**

Reflectance spectra of the blue paint were taken using a LabSpec 4 Benchtop Analyzer equipped with a high intensity contact probe. The instrument enables the acquisition of spectral data between 350-2500 nanometers (nm). The size of the analyzed surface is ~10 mm in diameter.

Supplemental spectra were also taken with the FieldSpec® 3 (ASD), which is a portable and rugged version of Labspec 4 (Tzadik, 2014).

## **2.7 Raman spectromicroscopy ( $\mu$ RS) and surface enhanced Raman scattering (SERS)**

By utilizing a Renishaw inVia Raman spectrometer, characteristic molecular vibrational frequencies of the Maya blue samples can be detected for chemical analysis. This confocal system was equipped with a Leica microscope with a 50x objective lens and a Charge Coupled Device (CCD) Detector. An excitation of 633 nm laser probe was used with 1200 mm diffraction grating. The laser power was maintained at no more than 0.01 mW to avoid degradation or potential thermal damage to the samples. Additional parameters included an integration time of 10 seconds and 3 accumulations, as well as 5 seconds of photobleaching time in order to reduce the effect of fluorescence. The spectrum was recorded in extended mode from 150  $\text{cm}^{-1}$  to 1750  $\text{cm}^{-1}$  for comparable results with previous data (Tatsch and Schrader, 1995, Witke et al., 2003, Leona et al., 2004, Giustetto et al., 2005).

### 3 Results

#### 3.1 Color and molecular characterization of Maya blue

The blue pigment of the figurines was previously studied non-invasively using fiber optics reflectance spectroscopy (FORS) (Tzadik, 2014). When analyzing the near infrared (NIR) reflectance spectra (Figure 3) (Appendix A – FORS spectra), the Maya blue archaeological samples appear to collectively show absorbance bands at ~1420, ~1920, and ~2200 nm. These bands are attributed to the palygorskite clay (Leona et al., 2004).

The visible-region provides information on the blue coloration. The maximum absorption and curve profile of the reflectance spectrum allow differentiation of Maya blue from the pure indigo dye. In the visible, the spectral differences between Maya blue and indigo postulate modifications affecting charge distribution of the indigo molecule following its fixation in palygorskite with the formation of hydrogen bonds between the carbonyl groups (C=O) of the indigo/dehydroindigo dye and the hydroxyl-groups from structural water in the channels of palygorskite. This change in the chemical environment moves the absorption to lower energies causing a bathochromic shift.

In Maya blue, the absorption maximum (~660-670 nm) is red shifted in comparison to that of indigo (~650-660 nm), caused by changes in the chemical environment due to the formation of hydrogen bonds, from the fixation of the indigo molecules on the palygorskite clay (Reinen et al., 2004, Leona et al., 2004). The variability within the ancient Maya blue samples such as subtle band shifts may be due to variance in dehydroindigo and indigo ratio in the palygorskite (Sánchez del Río et al., 2011).

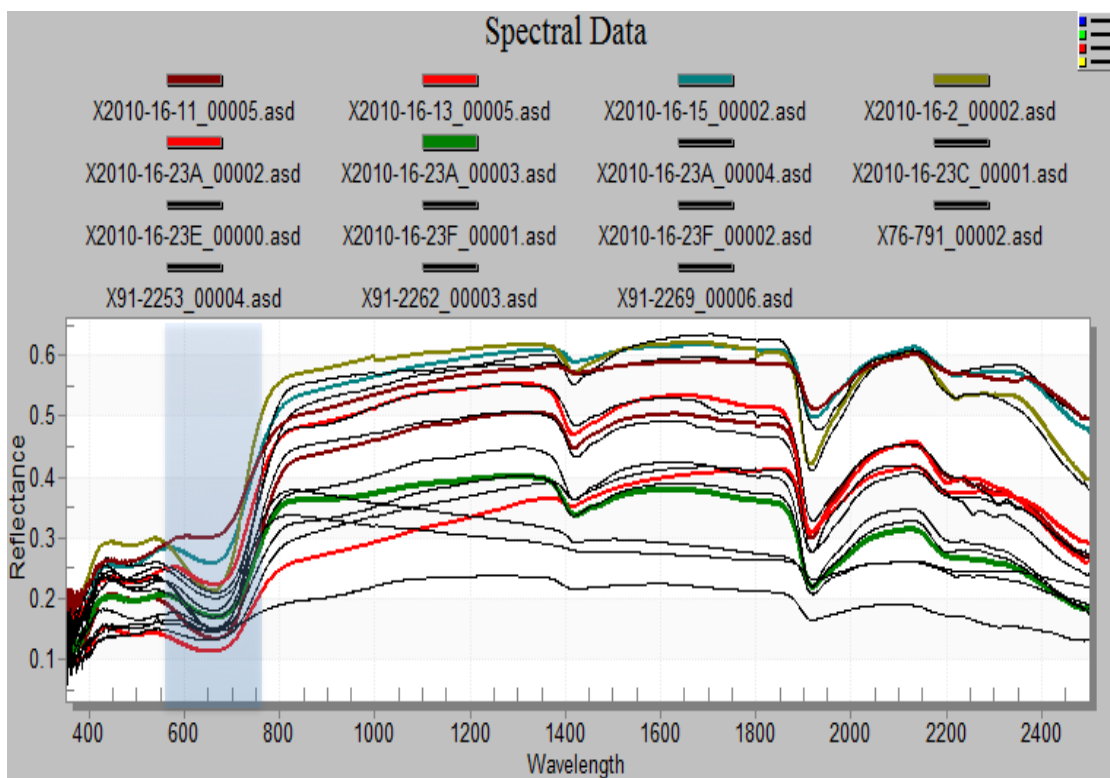


Figure 3. A compilation of FORS spectra of the blue paint layer on select Jaina-style figurines. The highlighted area notes the absorption band in the visible-region attributing to Maya blue.

From the FORS analysis, the color values can also be calculated based on the Commission Internationale de l’Eclairage (CIE) 1976 model of a three-dimensional color space of coordinates  $L^*$ ,  $a^*$ , and  $b^*$  (Hunter and Harold, 1987). These three values are represented by what the human eye perceives as opposites:  $L^*$  provides information on the lightness of the color from a scale of 0 to 100, where a value of  $L^*=0$  is the darkest color achievable and  $L^*=100$  is the brightest;  $a^*$  represents red and green, where a positive value is associated with red and negative associated with green;  $b^*$  represents the colors yellow and blue, where yellow is denoted by a positive number and blue by a negative (Whetzel, 2016). In order to quantify color and evaluate the color difference of the ancient Maya blue, delta  $L^*$  ( $\Delta L^*$ ), delta  $a^*$  ( $\Delta a^*$ ), and delta  $b^*$  ( $\Delta b^*$ ) were computed by subtracting the respective values of the ancient blue paint layer from that of the blue paint layer on Jaina-style figurine museum accession number X2010.16.2 (JF15) (Table

1 & Figure 4). In this assessment, it has to be taken into consideration that the color values of the archaeological Maya blue were calculated from the spectrum of the surviving traces of Maya blue from the paint layer applied over the ceramic body with or without a white layer underneath (as ‘slip’) or mixed into the blue. Owing to this inherent heterogeneity of measurements, results presented here are only intended to provide a rough quantitative assessment of the color difference in the blue paint on the archaeological figurines as perceived by the eye.

The delta E ( $\Delta E^*$ ) value, a measure of perceived visible difference of two given colors on a scale ranging from  $\Delta E=0$  to 100, was calculated using the CIELAB 1976 formula (Brainard, 2003):

$$\Delta E_{ab}^* = \sqrt{(L_2^* - L_1^*)^2 + (a_2^* - a_1^*)^2 + (b_2^* - b_1^*)^2}$$

where any value lower than  $\Delta E^*=1$  is said to be indiscernible to the human eye; however, for the difference in color space that can be visibly observed, a lower number means a greater similarity in color and a greater number means the colors are contrast more in terms of how the human eyes perceive opposites.

While the majority of the blue paint layers from select Jaina-style figurines showed a negative  $b^*$  value, indicating an influence of a bluish hue, an almost equal number of ancient

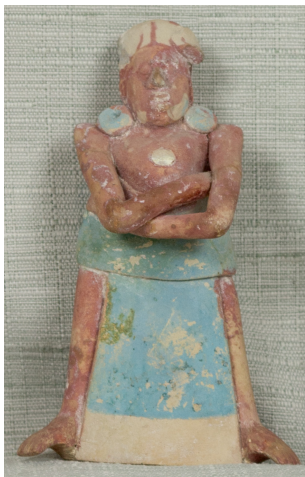


Figure 4. Jaina-style figurine X2010.16.2.

Maya blue interestingly showed a positive value for yellow (Table 2). However, the consistent negative  $a^*$  values suggest that all the pigments have some amount of green coloration. The values relating to the lightness of the colors generally ranged between ~43 to ~60. The ancient Maya blue pigments in respect to figurine X2010.16.2 (Table 1 & Figure 4) have  $\Delta E^*$  values ranging between ~4 to ~17, indicating discernable difference in the blue hue among the figurines.

Table 2. Color values of the blue paint layer on select Jaina-style figurines.

Sample # Associated	Figurine Museum Accession #	L*	a*	b*	\Delta L*	\Delta a*	\Delta b*	\Delta E*
JF23	X76.791	44.820	-2.876	1.803	14.970	3.035	3.228	15.612
JF04	X91.2253	54.034	-5.158	-3.867	5.756	0.753	2.442	6.298
JF05	X91.2262	55.977	-4.757	1.962	3.813	1.154	3.387	5.229
JF07	X91.2269	53.755	-5.358	-3.543	6.035	0.553	2.118	6.420
JF15	X2010.16.2	59.790	-5.911	-1.425	-	-	-	-
JF29	X2010.16.11	50.055	-5.747	-3.377	9.735	0.164	1.952	9.930
JF28	X2010.16.13	43.409	-2.939	-2.777	16.381	2.972	1.352	16.703
JF26	X2010.16.15	59.198	-1.371	3.536	0.592	4.540	4.961	6.751
JF21	X2010.16.23A	56.132	-0.527	1.869	3.658	5.384	3.294	7.295
JF21	X2010.16.23A	51.720	-3.401	-0.120	8.070	2.510	1.305	8.551
JF21	X2010.16.23A	46.884	-0.456	1.445	12.906	5.455	2.870	14.302
JF21	X2010.16.23C	46.633	-2.032	1.608	13.157	3.879	3.033	14.048
JF21	X2010.16.23E	57.020	-3.008	-1.670	2.770	2.903	0.245	4.020
JF21	X2010.16.23F	52.230	-3.364	-4.721	7.560	2.547	3.296	8.632
JF21	X2010.16.23F	48.476	-0.003	-0.919	11.314	5.908	0.506	12.774

\*  $\Delta E^*$  values were calculated in respect to the color values of JF15. The  $a^*$  and  $b^*$  values are color coded to indicate what hue it represents.

### 3.2 Chemistry of blue pigment

As reflectance and vibrational spectroscopic techniques enable the differentiation between indigo (precursor in Maya blue production) and Maya blue, the two techniques provided important information on the composition of the blue pigment used for decoration of the Jaina-style figurines of the Fowler Museum collection. Comparing the Raman spectra of the ancient Maya blue samples from the Jaina-style figurines to those of the modern Maya blue, though the significant differences could be observed, the modern Maya blue sample from Kremer Pigmente showed Raman shifts, suggesting also the presence of indigo (free molecule) (Table 3).

**Table 3. Raman bands (wavenumbers  $\text{cm}^{-1}$ ) of Maya blue (MB) and indigo.**

Kremer Pigmente MB ( $\text{cm}^{-1}$ )	Kremer Pigmente Indigo ( $\text{cm}^{-1}$ )	Aldrich Indigo ( $\text{cm}^{-1}$ )	Indigo <sup>a</sup> ( $\text{cm}^{-1}$ )	Indigo <sup>b</sup> ( $\text{cm}^{-1}$ )	Reference Assignment of Vibration <sup>c</sup>
254	261	252		252	$\gamma(\text{C}=\text{C}), \gamma(\text{C}=\text{C})$
		266		266	$\delta(\text{S}-\text{C}=\text{C}), \delta(\text{C}-\text{C}=\text{C})$
		275		275	$\delta((\text{OC}-\text{C}=\text{C}))$
				310	$\delta(\text{N}-\text{C}=\text{C}), \delta(\text{C}-\text{C}=\text{C})$
				321	
554	548			401	$\gamma(\text{CH})$
				467	$\gamma(\text{CC})$
		546	545	544	$\delta(\text{C}=\text{C}-\text{CO}-\text{C})$
		600	599	598	$\delta(\text{C}=\text{O}), \delta(\text{CH}), \delta(\text{C}-\text{NH}-\text{C})$
				635	$\gamma(\text{NH}), \gamma(\text{CC})$
634				674	$\delta(\text{CC})$
672	675		674	674	
758	773		762	758	$\delta(\text{CH}), \delta(\text{N}-\text{C}-\text{C})$
				797	$\gamma(\text{CH}), \gamma(\text{C}=\text{C})$
864				868	$\nu(\text{CN})$
				921	$\delta\nu(\text{CC})$ Ring, $\delta(\text{C}=\text{C})$
950			940	940	$\gamma(\text{CH})$
				964	$\gamma(\text{CH})$
1018			1013	1015	$\delta(\text{CH})$
1111			1096	1097	$\delta(\text{CC}), \gamma(\text{CH})$
1151			1148	1147	$\delta(\text{CC})$
				1190	$\nu(\text{C}-\text{C})$ Ring
1226			1224	1224	$\delta(\text{CH}), \nu(\text{CN})$
1257		1249	1250	1248	$\delta(\text{CH}), \delta(\text{C}=\text{O})$
1317			1310	1310	$\nu(\text{CC})$
1367			1364	1365	$\delta(\text{NH}), \delta(\text{CH})$
				1400	
1464			1462	1460	$\nu(\text{CC}), \delta(\text{CH})$
				1482	$\nu(\text{CC}), \delta(\text{CH})$
1573	1581	1573	1573	1571	$\nu(\text{CC}), \nu(\text{C}=\text{C}), \nu(\text{C}=\text{O})$
				1582	$\nu(\text{C}=\text{C}), \nu(\text{C}=\text{O})$
1631	1634		1628	1625	$\nu(\text{CC}), \delta(\text{CH})$
		1703	1703	1701	$\nu(\text{C}=\text{O})$
				3052	$\nu(\text{CH})$
				3056	$\nu(\text{CH})$
				3060	$\nu(\text{CH})$
			3270	$\nu(\text{NH})$	

<sup>a</sup> (Karapanayiotis et al., 2004); <sup>b</sup> (Tatsch and Schrader, 1995); <sup>c</sup> (Tatsch and Schrader, 1995, Vandenabeele et al., 2005, Sánchez del Río et al., 2006); Bracketed “[ ]” bands in Kremer Pigmente Maya blue suggest the presence of indigo.



When comparing indigo colorant with its complexed form – intercalated with palygorskite clay – as in Maya blue, significant differences can be seen owing to changes in the chemical environment of the molecule that allow the differentiation between indigo and Maya blue (Leona et al., 2004). Starting at the lower end of the spectrum, the Raman shifts (attributed to the five-member ring in-plane and out-of-plane bending) between  $240\text{ cm}^{-1}$  and  $\sim 276\text{ cm}^{-1}$  in indigo (Tatsch and Schrader, 1995) (Table 3) merge into one band at  $\sim 256\text{-}261\text{ cm}^{-1}$  in Maya blue. The band at  $\sim 634\text{ cm}^{-1}$  (N-H out-of-plane motion) in indigo disappears in Maya blue as the hydrogen bonding conditions of the N-H group changes in the indigo-palygorskite complex (Leona et al., 2004, Giustetto et al., 2005, Sánchez del Río et al., 2006), whereas, the band corresponding to N-H in-plane bending at  $\sim 1365\text{ cm}^{-1}$  decreases in intensity in the complexed form. In the region between  $\sim 1570\text{ cm}^{-1}$  and  $1585\text{ cm}^{-1}$ , while two strong vibrations are characteristic of indigo, the first at  $\sim 1573\text{ cm}^{-1}$  (stretching of the C-C, six-member ring), and the second at  $\sim 1583\text{ cm}^{-1}$  (stretching vibration of the C=O, C=C system), only one band appears in Maya blue at  $\sim 1576\text{ cm}^{-1}$ . The change in vibrational frequencies may be attributed to charge distribution, symmetry and hydrogen bonding conditions caused by the intercalation of indigo molecule with the palygorskite clay (Figure 5) (Witke et al., 2003, Leona et al., 2004, Giustetto et al., 2005).

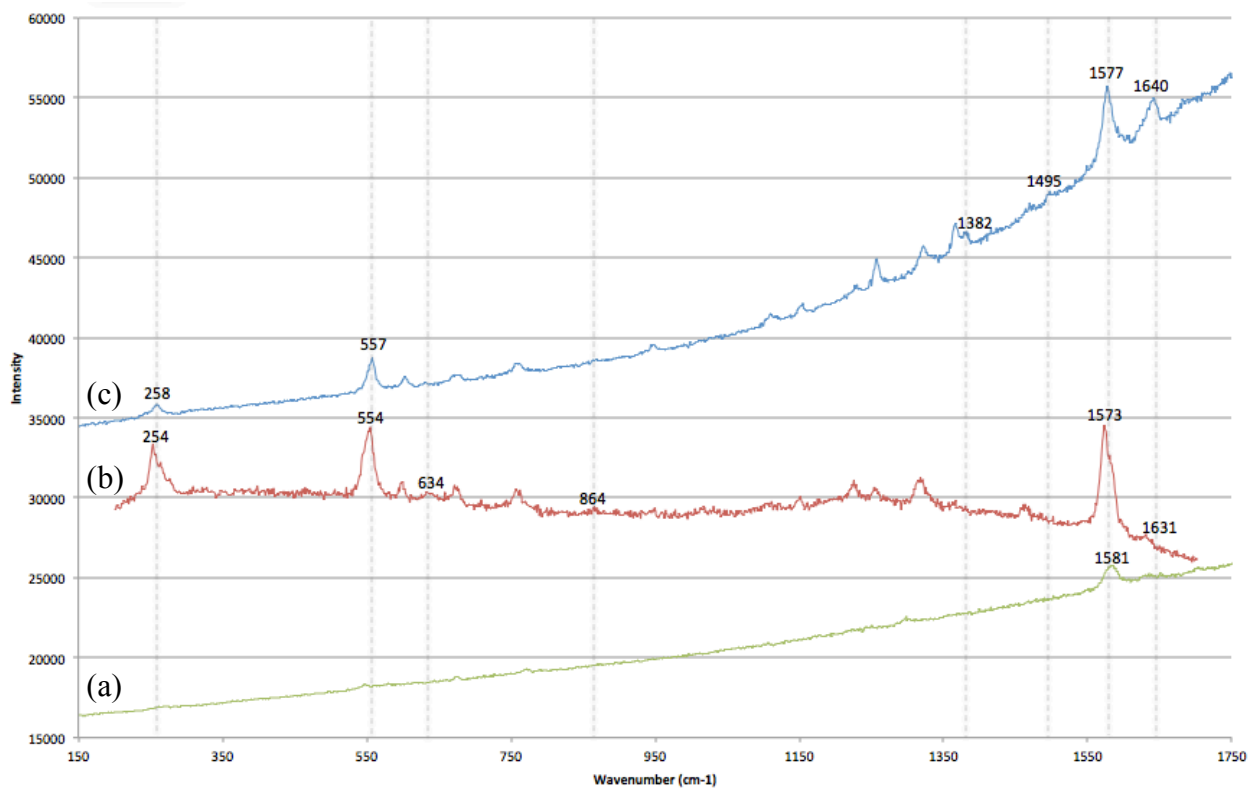


Figure 5. Raman spectra of Kremer Pigmente standards, (a) indigo (green) and (b) Maya blue (red), against spectrum of (c) ancient Maya blue Sample 04 (blue). The dotted lines denote notable shifts, disappearances, and intensity in the bands.

Overall, while changes in vibrational frequencies between indigo and Maya blue can differentiate the two, it remains challenging to distinguish archaeological Maya blue from its modern counterpart on the basis of Raman analysis alone. Both the archaeological and modern Maya blue might contain indigo in excess that has not been fully complexed with palygorskite. Sánchez del Río *et al.* (2006) stated that there is little difference in spectra between indigo mixed with palygorskite heated and unheated (Sánchez del Río *et al.*, 2006), as it is possible that there are still indigo molecules that may not have thoroughly incorporated into the palygorskite matrix and thus the clay does not interfere with the original structure of the indigo.

A band, however, found in the modern Kremer Maya blue at  $\sim 864\text{ cm}^{-1}$  attributing to the vibrations of the C-N bond in indigo, is overall lacking in the ancient Maya blue, though it weakly appears in Samples 18, 21 and 28. A band at  $1497\text{ cm}^{-1}$ , corresponding to C-H, N-H, and

C-C ring, appears in the majority of the ancient Maya blue samples, similar to the result from Witke *et al.* (2003), albeit exhibiting significantly weaker signals. This peak does not appear in the indigo standards analyzed, which is in opposition to the findings of Leona *et al.* (2004) and Giustetto *et al.* (2005). The  $1497\text{ cm}^{-1}$  peak is also absent in the Maya blue standard analyzed.

A band at  $1380\text{ cm}^{-1}$  assigned to N-H and C-H can also be seen in the majority of the ancient Maya blue pigments but not in the modern Maya blue. This peak has previously been identified in the Maya blue sample by Witke *et al.* (2003). It could possibly be due to the vibrational band activation from the interaction between indigo and palygorskite clay, suggesting a change in the centrosymmetry from the indigo adsorbing into the palygorskite.

### 3.3 Microstructural and elemental characterization of Maya blue

The polished Maya blue samples were analyzed using the scanning electron microscopy (SEM) coupled with energy dispersive X-ray spectroscopy (EDS). Using a backscattered electron (BSE) detector at high vacuum, it was possible to characterize the blue paint structure, interface and ceramic substrate. SEM-EDS enabled area and particle-specific elemental characterization and elemental mapping across the surface of the area analyzed. In using compositional contrast in BSE imaging, the blue paint layer could easily be distinguished from the substrate. The paint layer was characterized by a finer texture in contrast to the more coarse nature of the clay (Figure 6), most likely due to the manufacturing process and the treatment of palygorskite clay when integrating with the indigo molecules. Overall, the blue paint layer of thickness ranging from 10 to  $20\text{ }\mu\text{m}$  is characterized by a fine and fibrous structure characteristic of palygorskite, a type of phyllosilicate, with weak compositional contrast owing to the presence of predominantly low Z elements (clay) and the presence of indigo (organic molecule); though small inclusions, probably related to the manufacture of the pigment with higher Z elements, which appears brighter in the micrograph, can be seen (Appendix D – SEM-EDS micrographs and elemental mapping). The

EDS spot analysis on the blue paint layer confirmed the presence of the oxygen (O), magnesium (Mg), aluminum (Al) and silicon (Si) in all samples as expected in the palygorskite matrix  $[(\text{Mg},\text{Al})_4(\text{Si})_8(\text{O},\text{OH},\text{H}_2\text{O})_{26}\cdot n\text{H}_2\text{O}]$ . Carbon (C) was intentionally unaccounted for as carbon coating was placed on the polished samples to increase conductivity with the electron beam.

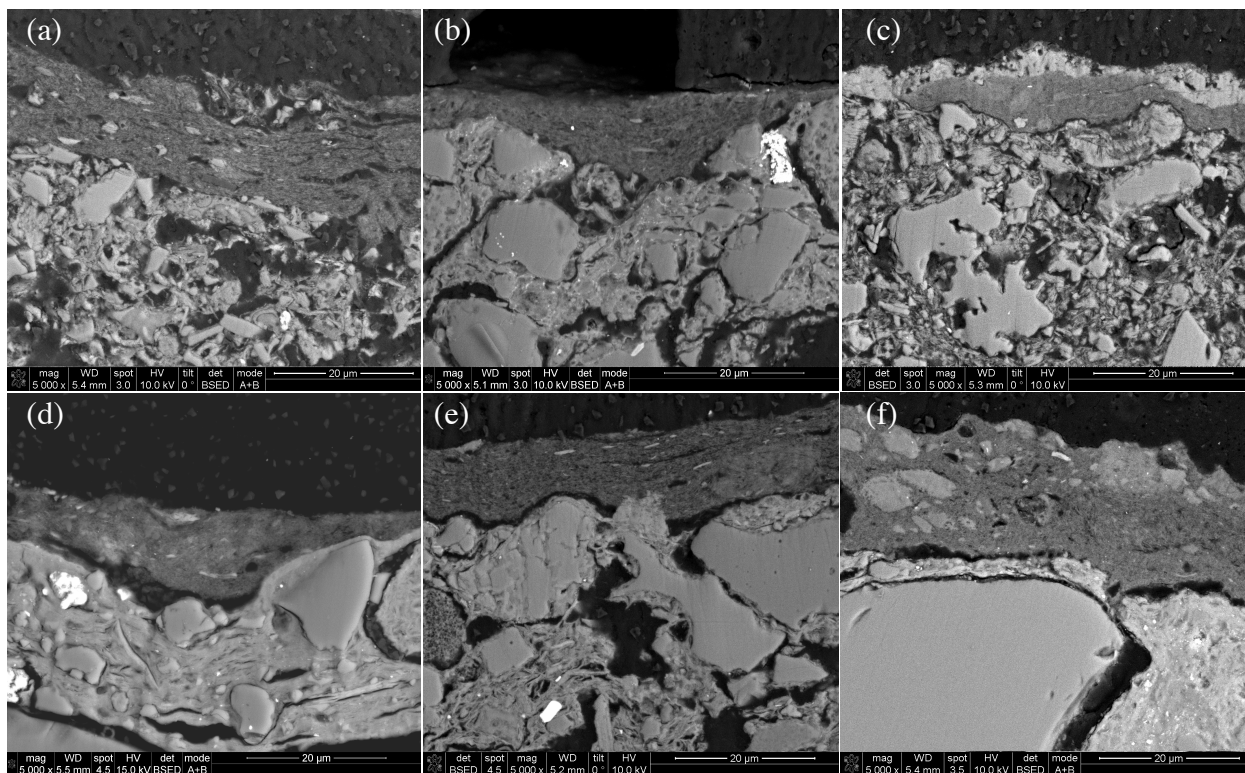


**Figure 6.** SEM micrographs of the cross-sections of select Maya blue samples (a) 01, (b) 05, (c) 06, (d) 08, (e) 09, and (f) 25 at 5000x magnification. (a) shows greater contrast round-shaped particles, whereas (c) and (f) display larger particles with less contrast, and (b) and (e) show elongated particles sparsely distributed. (d) appears to have an irregular distribution of impurities in a longitudinal fashion. The complete collection of SEM micrographs can be found in Appendix D – SEM-EDS micrographs and elemental mapping.

Atomic weight percent values of Al and Mg, two of the major elements in palygorskite, were normalized to Si and plotted in a bivariate plot (Al/Si at. wt. % versus Mg/Si at. wt. %). The two elements clustered into a cloud, indicating an overall 1:1 ratio of Al to Mg; however, there is a small variability in the atomic weight percentage ratio of the two elements (Figure 7) that may suggest insight on differing areas for the clay source material.

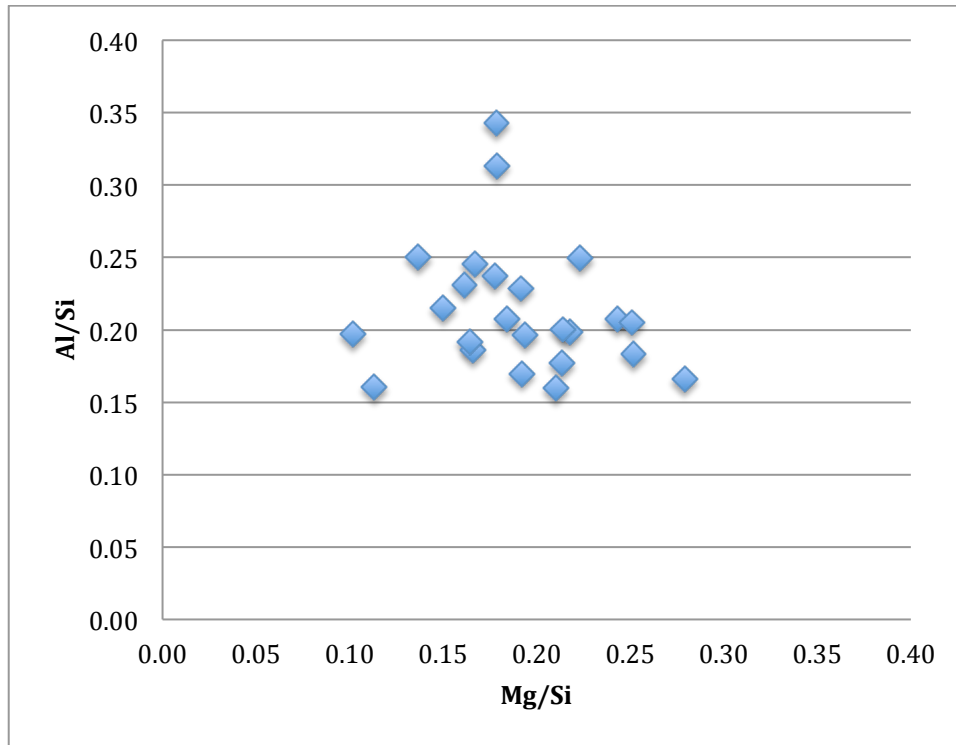


Figure 7. The plot of Al in respect to Si against Mg in respect to Si.

The ceramic bodies present higher heterogeneity and stronger compositional contrast containing various and larger inclusions, mainly quartz (Figure 6). Overall, the Maya blue paint layer appears to hold a greater presence of Mg in comparison to its presence in the clay substrate, whereas the clay has a higher concentration of Al and Si in comparison to their respective concentrations in the Maya blue (Figure 8).

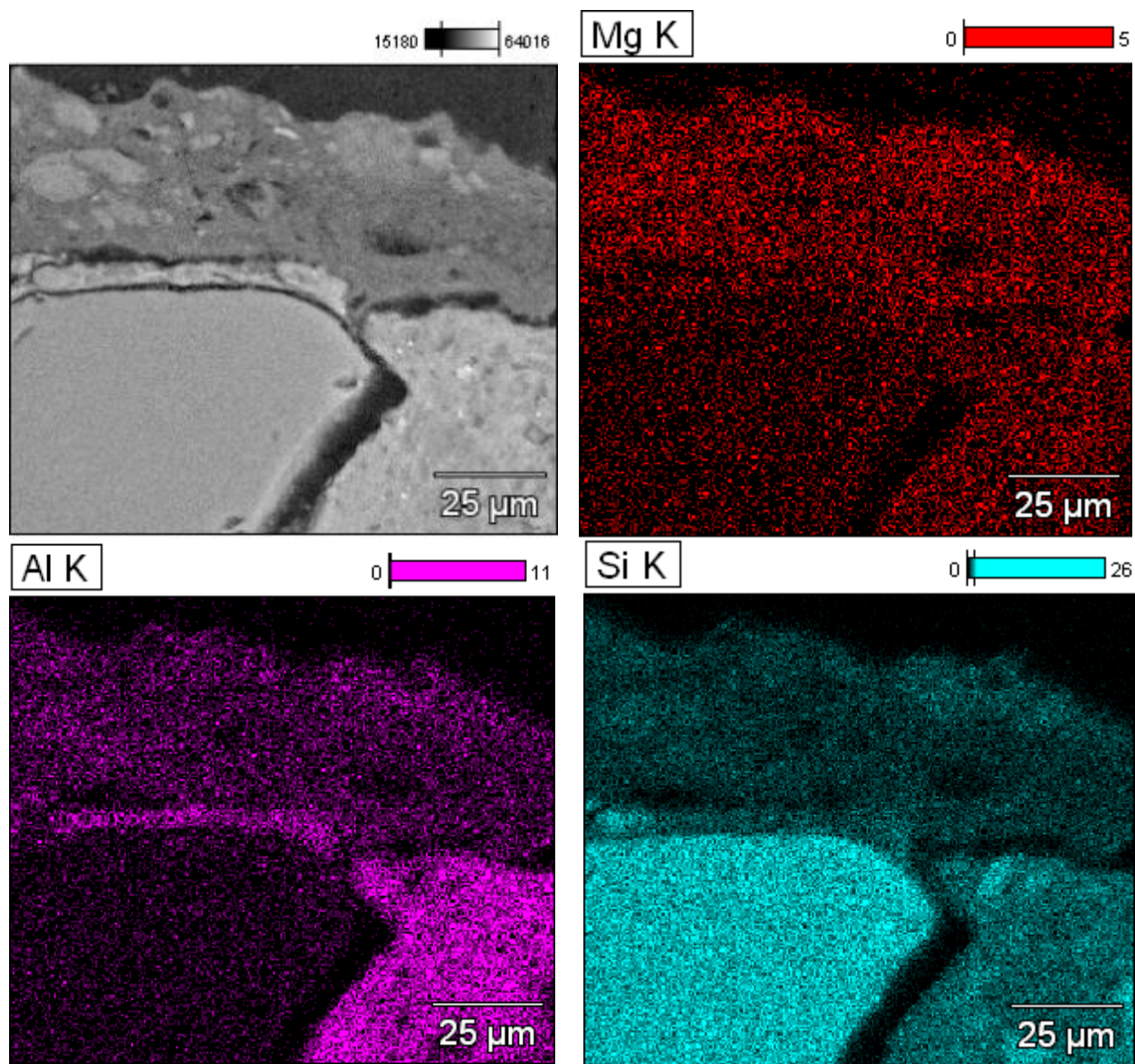


Figure 8. EDS elemental mapping of the major elements in Sample 25, indicating a difference in concentration of Mg, Al, and Si within the paint layer and ceramic. A complete elemental map of all samples can be seen in Appendix D – SEM-EDS micrographs and elemental mapping.

At the interface between the ceramic body and the blue paint layer, a distinctive layer rich in calcium (Ca) and sulfur (S) was identified in samples 06, 07, 10, 12, 13, 14, 18, 19, 22, and 23. This is most likely a gypsum ( $\text{CaSO}_4 \cdot 2\text{H}_2\text{O}$ ) layer (Tzadik, 2014), a type of slip (a slurry in water applied directly onto the ceramic body) providing a smooth and white surface for painting. In Sample 22, sodium (Na) and chlorine (Cl) were also detected with higher concentrations at the



surface of the paint; these are most likely contaminants suggesting the presence of the deliquescent salt, sodium chloride (NaCl).

BSE imaging revealed small inclusions, mainly round-shaped particles of varying size ranging from around 1 to 15 microns in the blue paint (Figure 6). There also appears to be elongated particles in Samples 01, 02, 05, 06, 09, 11, 12, 13, 18, 20, 21, 26, and 27, although the EDS spot analysis shows no clear distinctive chemical composition correspondence between the samples other than an increase in the Al atomic weight % in comparison to the Maya blue area as a whole.

In addition to the major elements, O, Mg, Al, and Si, in the clay matrix of the blue paint, EDS also indicated photon emissions of the characteristic X-rays of sodium (Na), chlorine (Cl), sulfur (S), potassium (K), calcium (Ca), and iron (Fe), titanium (Ti) and phosphorous (P) in varying concentrations (Table 4). Na, Cl and S are most likely weathering products. K, Ca, Fe and Ti could be associated with impurities in the clay, and possibly the processing of the indigo leaves used during the production of the blue paint. Titanium in particular could be an element that could help identify the location of the raw materials used and should be investigated further. Phosphorous is an element that suggests a funerary environment as its presence in this context could be linked to the decomposition of the body.

**Table 4. Bulk major and minor elements (at. wt. %) in blue paint layer.**

	<b>Mg</b>	<b>Al</b>	<b>Si</b>	<b>Na</b>	<b>Cl</b>	<b>S</b>	<b>K</b>	<b>Ca</b>	<b>Fe</b>	<b>Ti</b>	<b>P</b>
<b>JF01</b>	1.77	1.43	8.12	0.25	0.46	-	-	1.93	4.29	-	-
<b>JF02</b>	1.74	2.04	9.79	0.34	0.22	0.31	0.34	0.69	1.58	0.21	-
<b>JF03</b>	1.82	2.97	13.02	0.97	0.22	0.22	0.74	0.19	0.68	0.11	0.10
<b>JF04</b>	-	-	-	-	-	-	-	-	-	-	-
<b>JF05</b>	1.30	1.09	7.11	0.49	0.39	0.32	0.21	0.36	0.75	0.04	-
<b>JF06</b>	1.43	1.22	5.88	0.13	0.13	0.05	0.11	0.28	0.27	-	0.07
<b>JF07</b>	5.30	6.64	33.08	0.78	0.64	-	1.20	-	3.34	-	-
<b>JF08</b>	4.67	7.42	33.42	0.43	0.62	0.58	0.89	0.76	1.97	-	-
<b>JF09</b>	1.47	1.93	10.99	0.35	0.32	0.12	0.38	0.93	0.91	-	-
<b>JF10</b>	5.41	7.17	32.63	-	1.39	0.36	1.09	1.40	1.85	-	-
<b>JF11</b>	5.96	5.48	32.30	1.06	1.46	0.73	0.99	-	3.52	0.19	0.23
<b>JF12</b>	5.26	4.98	24.42	0.67	0.55	-	0.33	0.31	0.44	-	-
<b>JF13</b>	3.45	5.43	35.21	1.36	0.53	0.57	1.24	0.85	2.15	-	-
<b>JF14</b>	3.74	8.67	32.11	2.31	0.59	0.87	0.73	1.40	0.92	-	-
<b>JF15</b>	7.81	5.16	31.76	0.77	1.21	-	0.70	2.02	2.04	-	-
<b>JF16</b>	-	-	-	-	-	-	-	-	-	-	-
<b>JF17</b>	-	-	-	-	-	-	-	-	-	-	-
<b>JF18</b>	-	-	-	-	-	-	-	-	-	-	-
<b>JF19</b>	0.35	2.31	9.38	0.73	0.12	-	1.14	0.52	0.65	0.20	0.09
<b>JF20</b>	1.05	0.96	4.84	0.25	0.30	0.28	0.21	1.80	0.64	-	-
<b>JF21</b>	4.60	9.80	29.76	-	0.52	0.32	0.36	2.61	3.68	-	-
<b>JF22</b>	2.56	3.16	13.20	0.82	0.61	-	0.72	0.43	1.16	0.10	0.30
<b>JF23</b>	-	-	-	-	-	-	-	-	-	-	-
<b>JF24</b>	5.67	5.89	30.65	1.29	1.13	2.20	1.28	2.50	2.65	-	-
<b>JF25</b>	4.11	5.49	23.17	1.72	0.70	-	0.92	0.33	0.93	-	0.25
<b>JF26</b>	5.11	5.72	32.10	2.63	0.92	1.30	1.34	0.57	2.27	-	-
<b>JF27</b>	3.62	6.35	21.38	2.05	0.33	2.43	0.63	1.68	0.81	-	0.16
<b>JF28</b>	1.27	1.65	8.91	0.60	0.21	0.20	0.23	0.24	0.70	0.14	-
<b>JF29</b>	2.78	6.59	31.05	3.47	0.31	1.50	1.77	3.36	1.17	-	0.67
<b>JF30</b>	-	-	-	-	-	-	-	-	-	-	-

The Ti-rich particles that are found within a handful of samples are more or less irregularly distributed, seen as bright specks under backscattered electron analysis of the cross sections (Appendix D – SEM-EDS micrographs and elemental mapping).

A few of the ancient samples (Sample 01 and Sample 20) showed distinctive microstructure. Sample 01 shows at least two distinct phases within the blue paint layer, where



Ca was detected throughout the paint layer with a portion of the upper layer containing an increased amount of Ca (Figure 9).

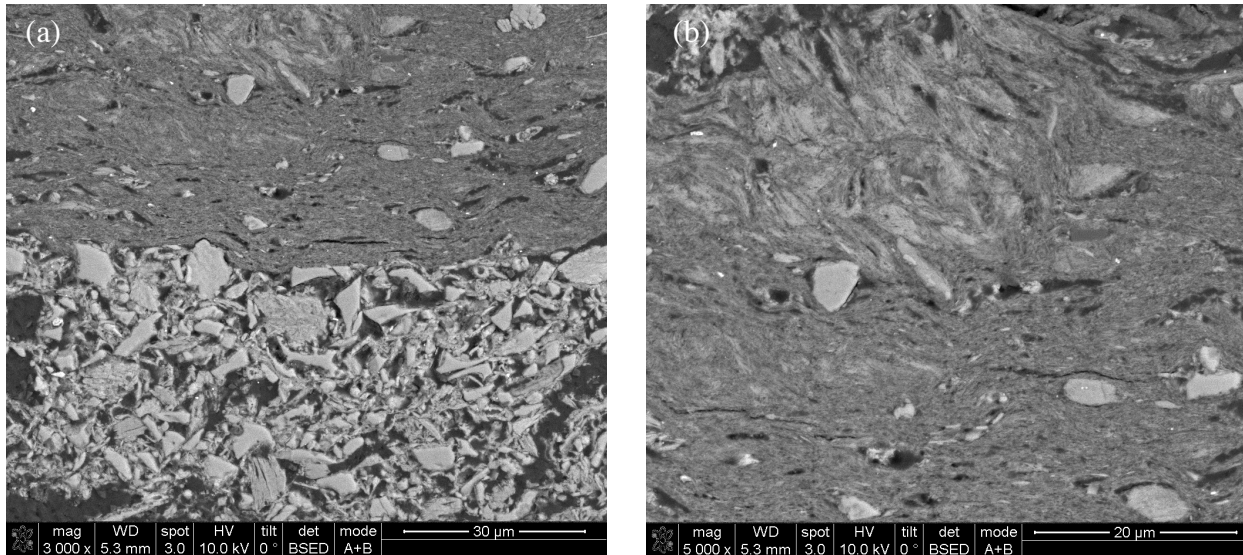


Figure 9. Backscattered electron micrographs of Sample 01 at (a) 3000x magnification showing the Maya blue and clay substrate interface and at (b) 5000x magnification showing a closer view at the Ca-rich region within the Maya blue.

In Sample 20, the blue paint layer contains Ca-rich particles uniformly dispersed within the paint layer (Figure 10). It is uncertain if these particles, most likely calcite, are contaminants from the manufacturing process, a distinction in the source material, or an intentional mixture between two colorants to influence a different shade of color.

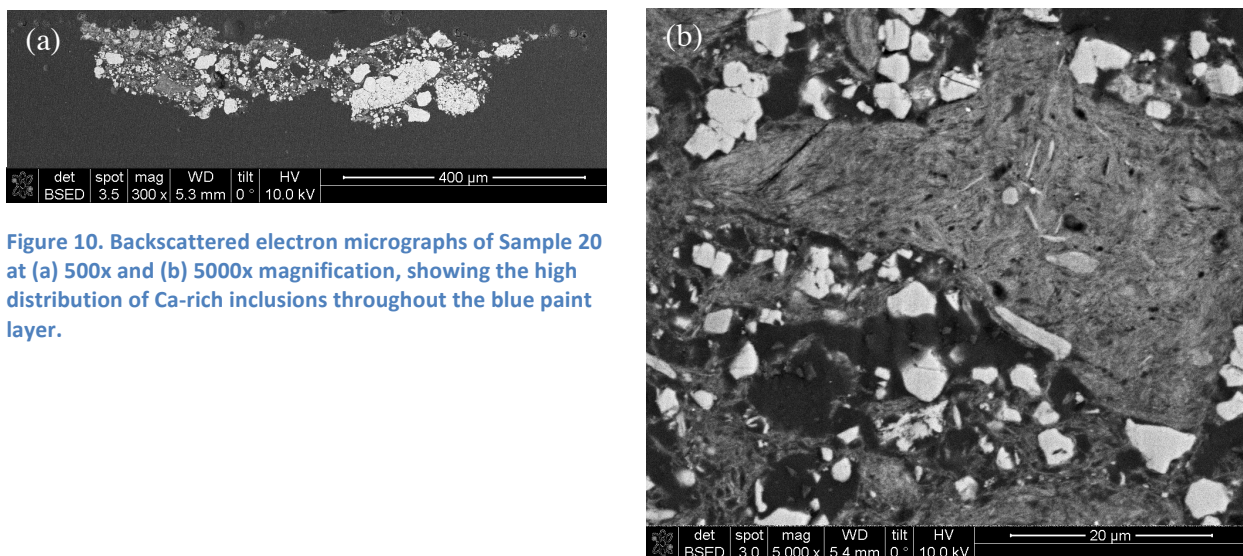


Figure 10. Backscattered electron micrographs of Sample 20 at (a) 500x and (b) 5000x magnification, showing the high distribution of Ca-rich inclusions throughout the blue paint layer.

## 4 Discussion

### 4.1 Variability of Maya blue

Based on minimally invasive non-destructive analyses performed on the blue pigment taken from the Jaina-style figurines, there seems to be some variability in the production and application of Maya blue on the figurines. The elements Al, Mg, Si and O are characteristic of all clays and therefore palygorskite, while assumed as the mineral of choice, has not been unambiguously confirmed. In addition to the clay matrix, there are also a number of varying inclusions that may be a feature of the geological source, where the clay has originated; though the possibility that these impurities derive from the processing of the indigo leaves (maceration, washing, etc.), and possibly other ritual or funerary practices or weathering cannot be entirely ruled out.

Samples 01 and 20 showed enrichment in Ca. Whereas the Ca-rich areas in Sample 01 appear to be due to processing during production, the Ca-rich particles present in Sample 20 seem to relate to deposition of calcite. This needs further investigation to better understand whether the presence of calcite was intentional (added to change the color of the paint layer) or a product of weathering.

### 4.2 Influence of the raw materials and production methods in chemistry and microstructure of Maya blue

Judging from the commonality of inclusions, such as the Ca-rich particles and other impurities, within the blue paint layer and ceramic body, it can be assumed that they originated from within the source material before or during production or due to weathering via post-depositional processes, most likely from burial soil that contain higher amounts of these impurities in the form of minerals. There has been evidence of a gypsum layer on top of some Maya blue samples, where gypsum can also be found in the soils of Mesoamerica.

## 5 Conclusions

There is still the question of the manufacturing process the ancient Mesoamericans used to create Maya blue, as well as how the inorganic and organic portion of the pigment chemically reconcile with one another, but through minimally invasive techniques, we are able to achieve an understanding of the variability in the Maya blue, and thus a possible insight on the variability in geosourcing and how the Maya blue was engineered. By analyzing the data obtained from microstructural and chemical analysis on thirty Jaina-style figurines, a collective documentation can give an insight on the characteristic behavior of Maya blue and any variation that could potentially lead to a better understanding on the ancient manufacturing process. The overall results have shown to be homogenous in that the Maya blue samples share the expected presence of the palygorskite through the SEM-EDS analysis and indigo through the Raman spectromicroscopy, but there have been small discrepancies within the samples.

In analyzing the FORS spectra and color values provided from previous work (Tzadik, 2014), the first evidence of the variability in the ancient Maya blue can be seen from the subtle shifts and change in broadness in absorption bands as well as a range in the measurement concerning how easily discernable to the human eye the ancient Maya blue is from one another. This may be the result from the variance in the dehydroindigo to indigo ratio, leading to the differing hues seen in Maya blue.

Data acquired from the SEM-EDS analysis provided quantitative information on the presence of Mg and Al in Maya blue, showing a nearly equal presence of the two elements in terms of atomic weight percent, but there was evidence that the palygorskite can have a slightly higher presence of Al than Mg. There were also impurities, elements that are usually found in common minerals, scattered throughout the ancient Maya blue samples, whether they were well incorporated into the Maya blue mixture or seen as particles that would range in size, shape,

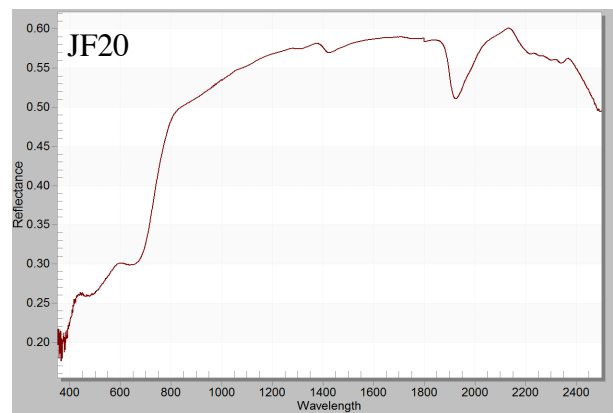
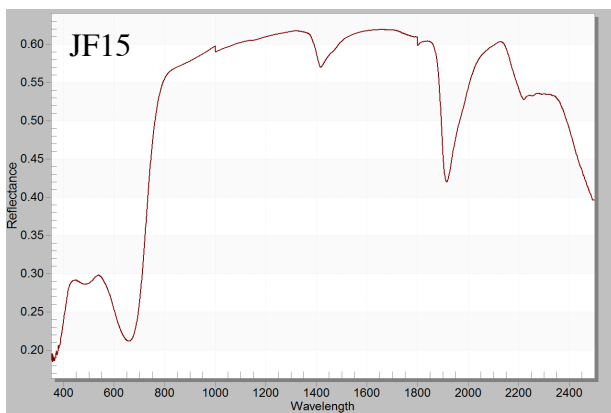
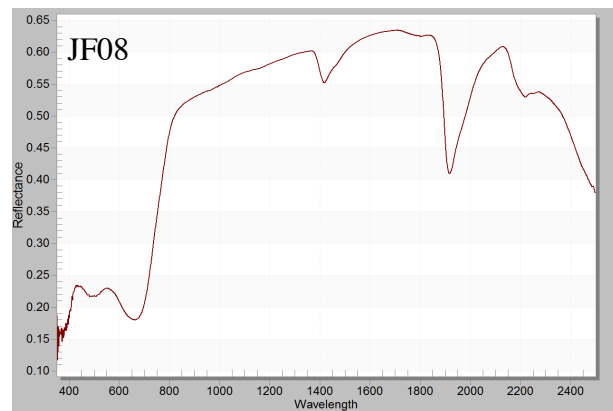
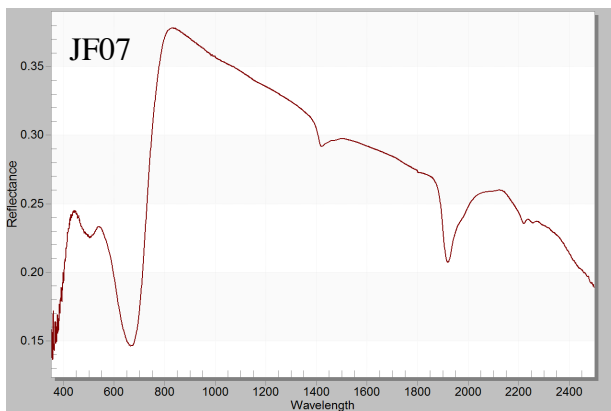
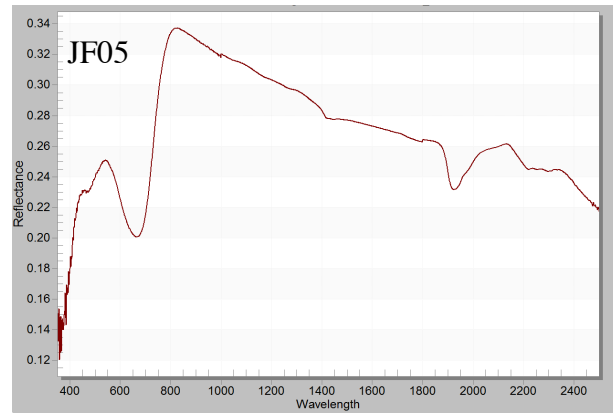
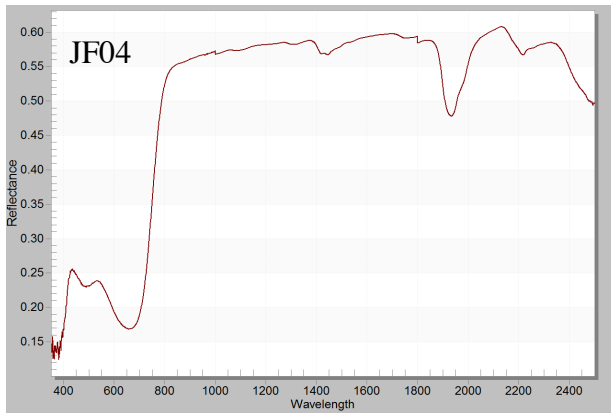
distribution, and composition. Salts and minerals in the form of sodium chloride and gypsum were also detected on the layer above some of the Maya blue samples. These varying conditions of the specimens suggest a dependence on the source of the raw materials or the site of burial.

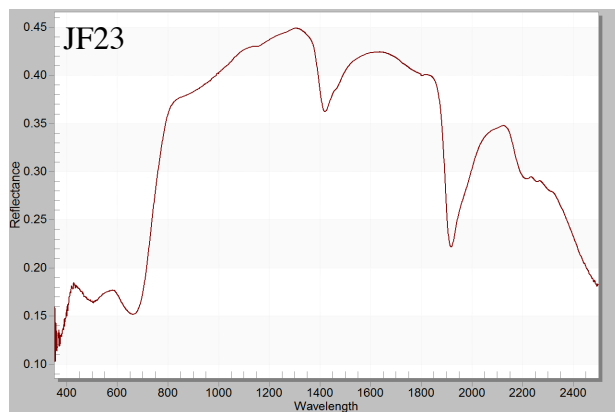
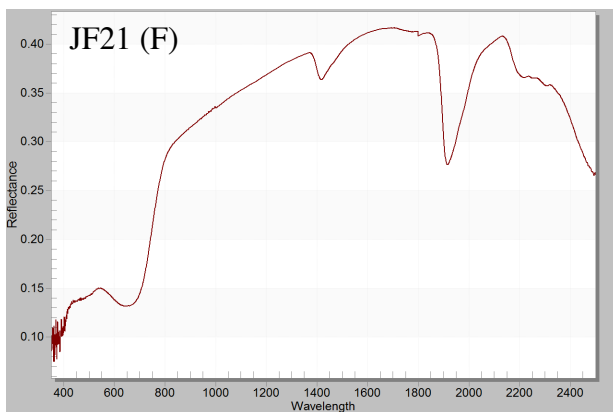
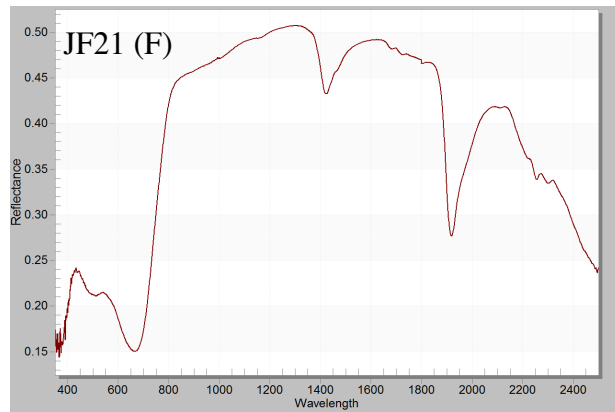
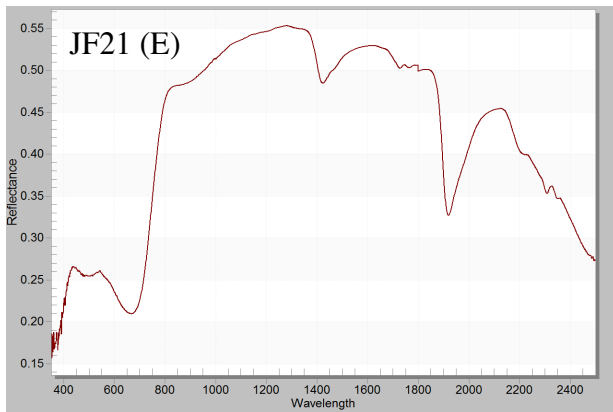
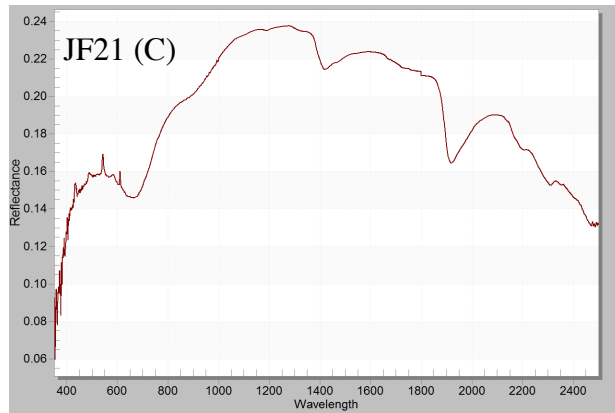
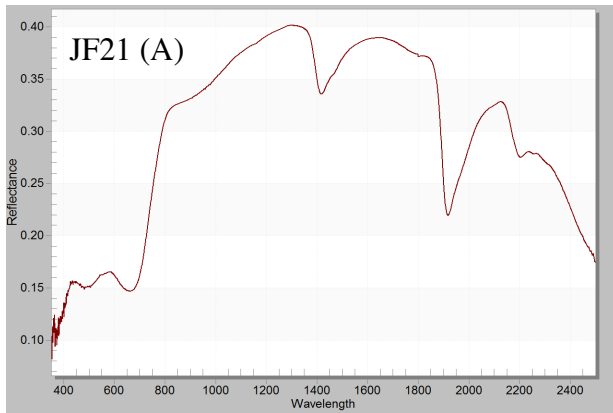
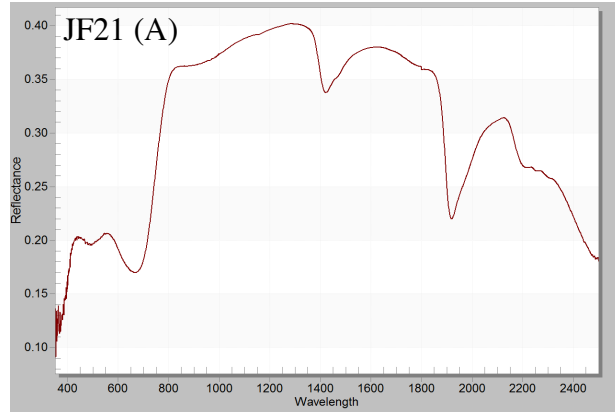
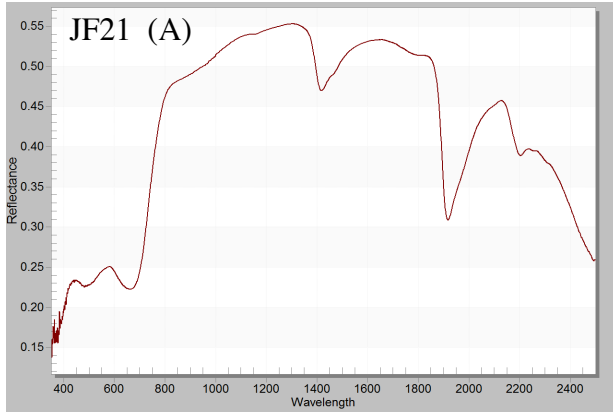
Raman spectroscopy of samples and reference materials indicating the intensity of characteristic Raman shifts (Appendix B – Raman spectra) and the assignment of the respective vibrational bands (Table 3) (Appendix C – Raman shifts (wavenumbers -  $\text{cm}^{-1}$ )) allow a more accessible documentation for comparison. There appears to be no large deviation between the ancient Maya blue specimens; however, it is evident that Raman shifts range between indigo and the Maya blue, which can be due to activated vibrational bands and a change in the centrosymmetry of the indigo when adsorbed onto the palygorskite. There is also the possibility that peak intensities differ between ancient and modern Maya blue, most likely dependent on the production process of the blue pigment.

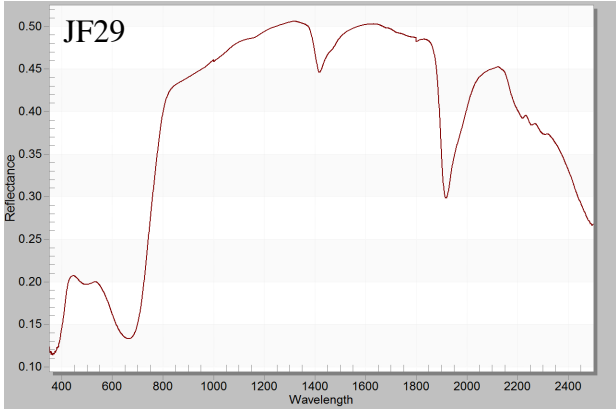
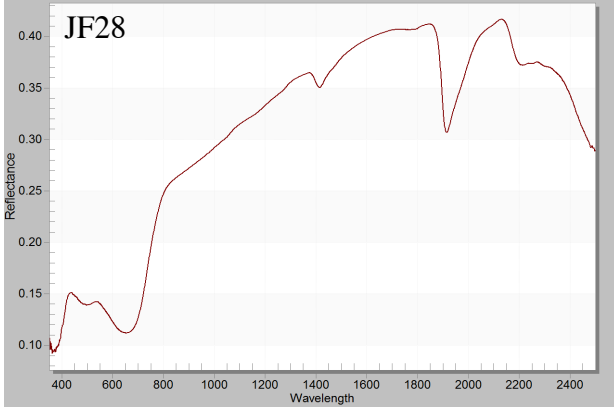
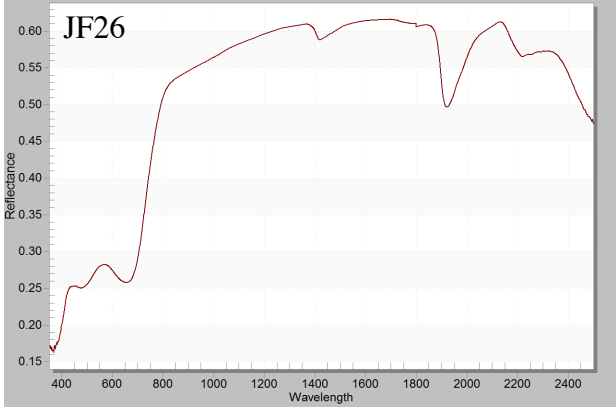
Although the microanalytical techniques utilized in this study provided a great deal of information on Maya blue originating from Jaina-style figurines, further research would need to be done to explore other characteristic properties, especially for distinguishing the ancient and modern productions of the pigment. Investigations would also need to be done to identify the chemical composition of the impurities within the Maya blue, which could potentially lead to further insight on the Jaina-style figurine burial practice and Maya blue manufacturing process as well as the cultural and historical understanding of the ancient Maya civilization.

## 6 Appendices

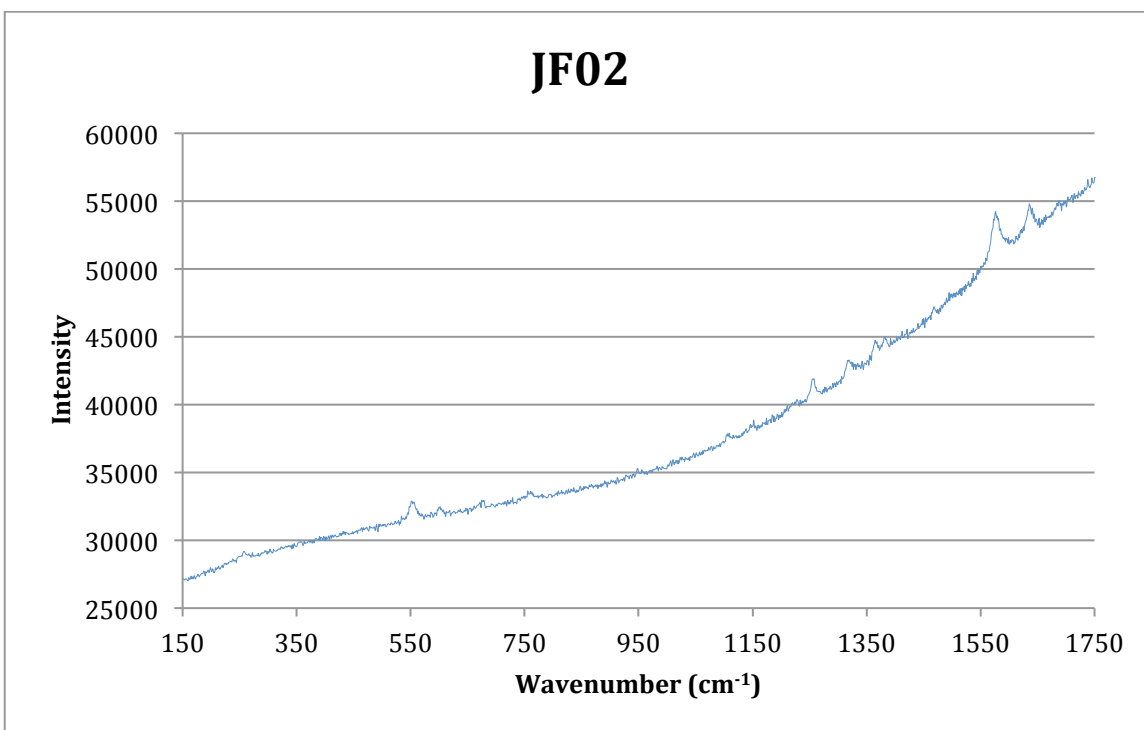
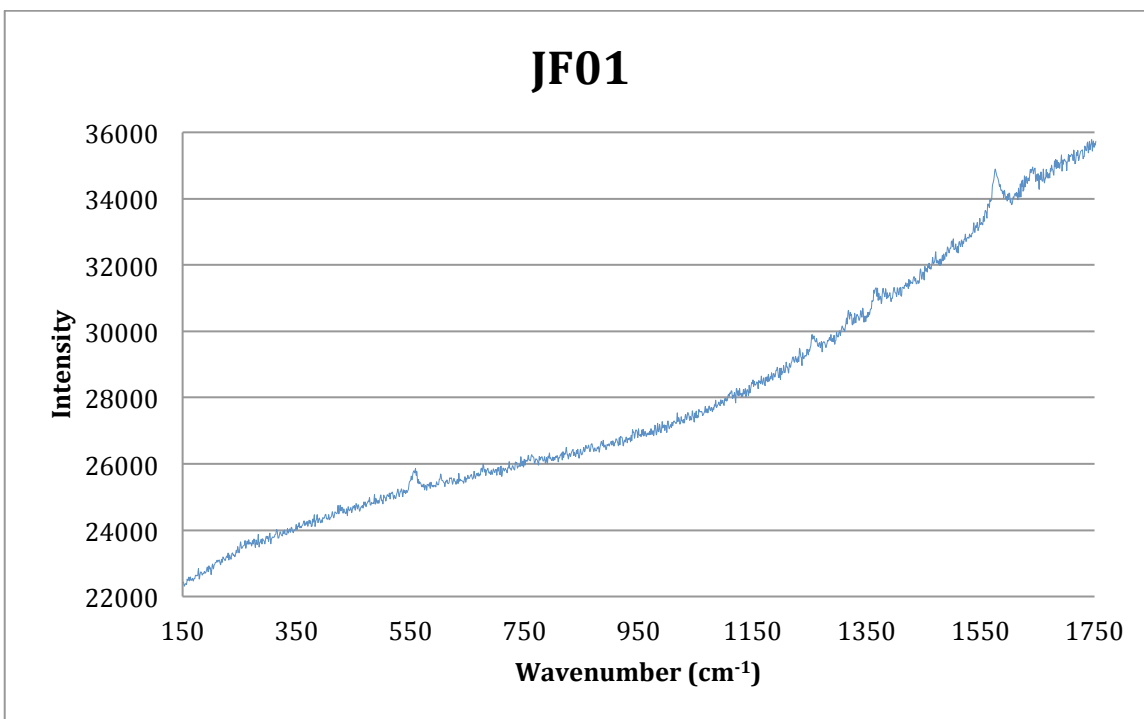
### 6.1 Appendix A – FORS spectra





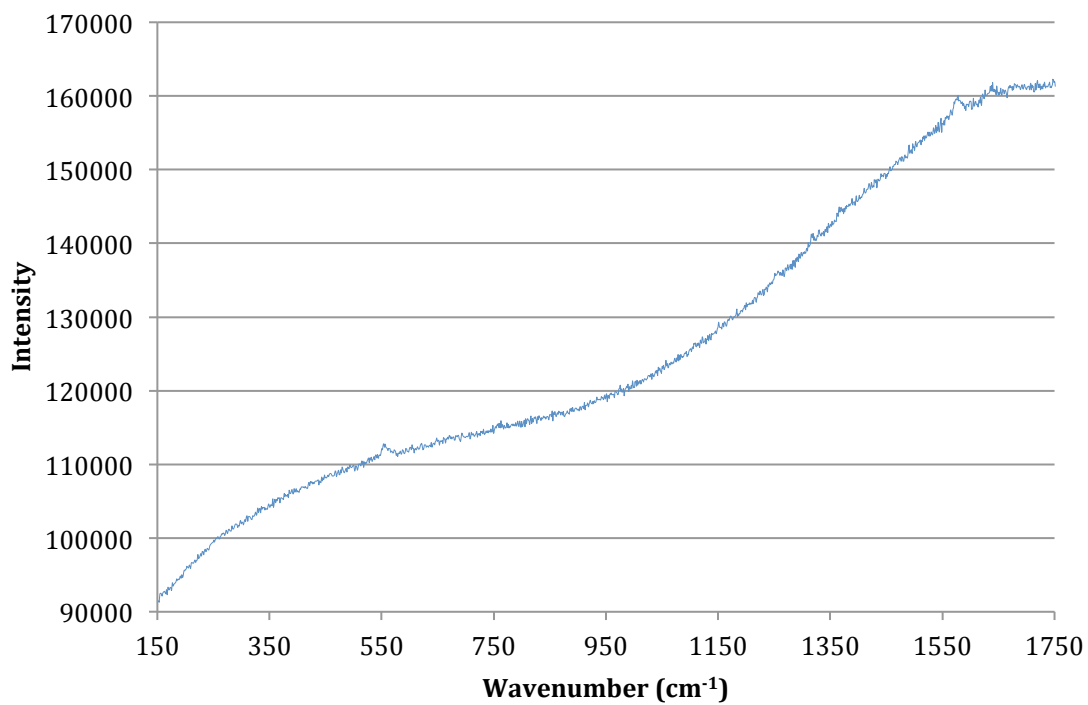


## 6.2 Appendix B – Raman spectra

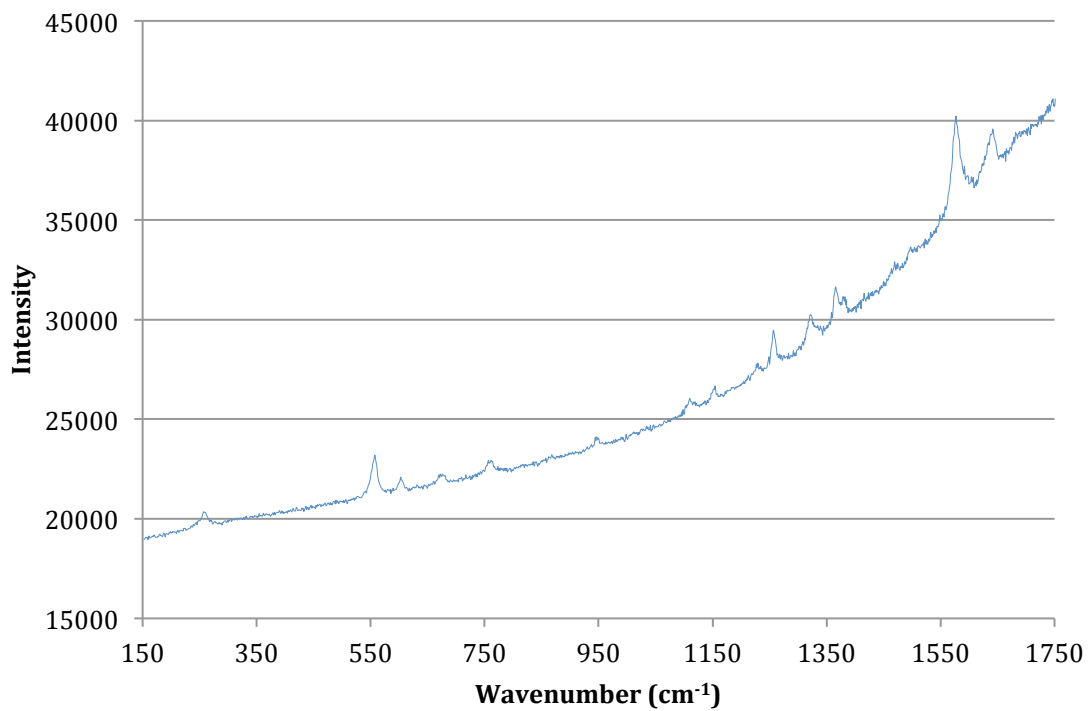


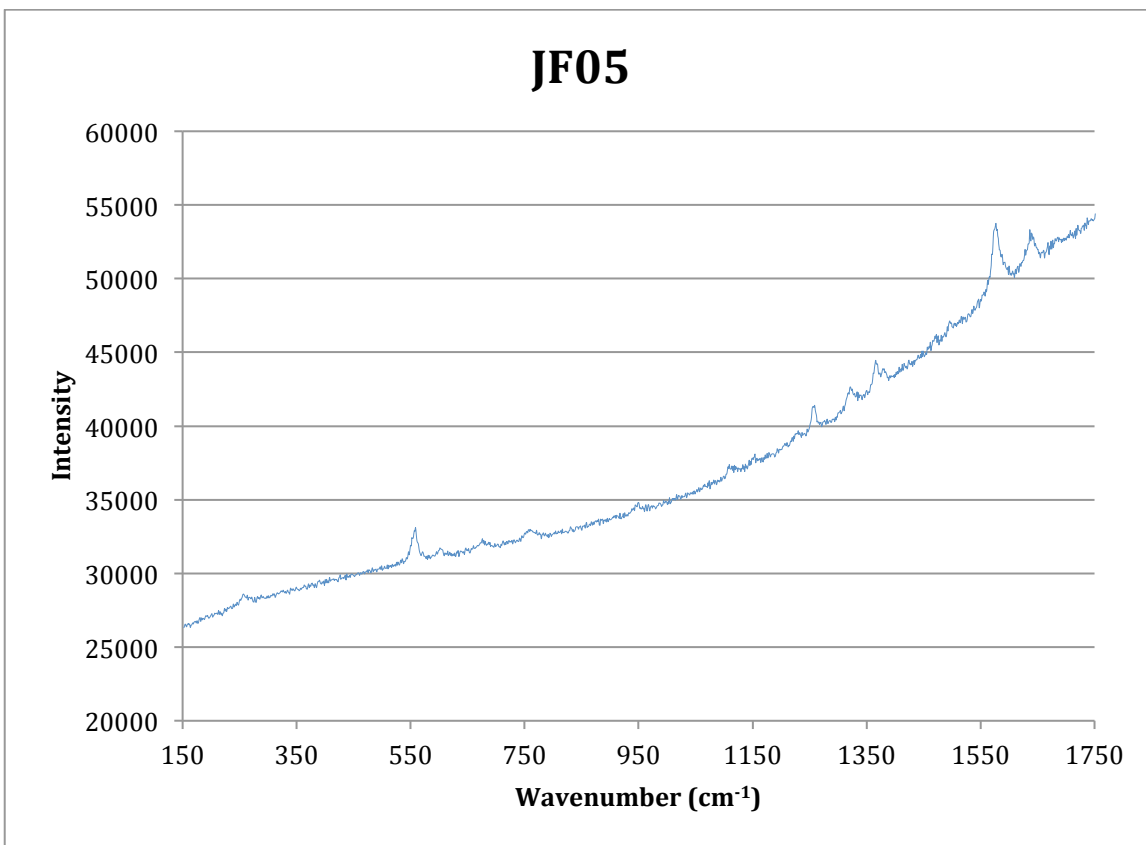


### JF03

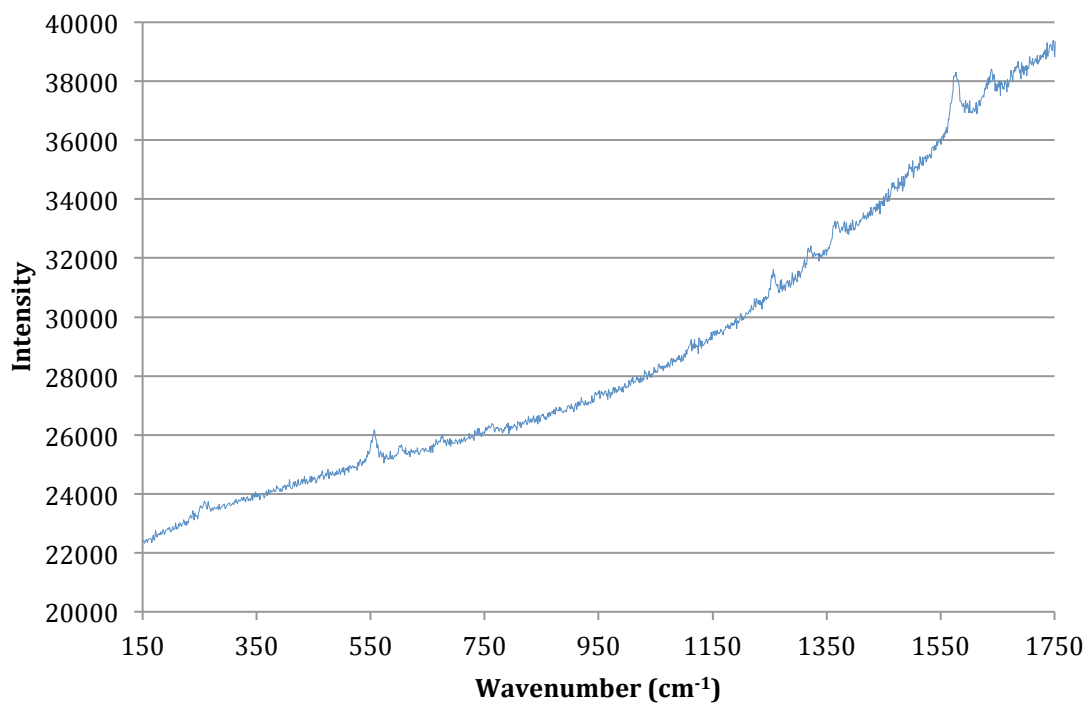


### JF04

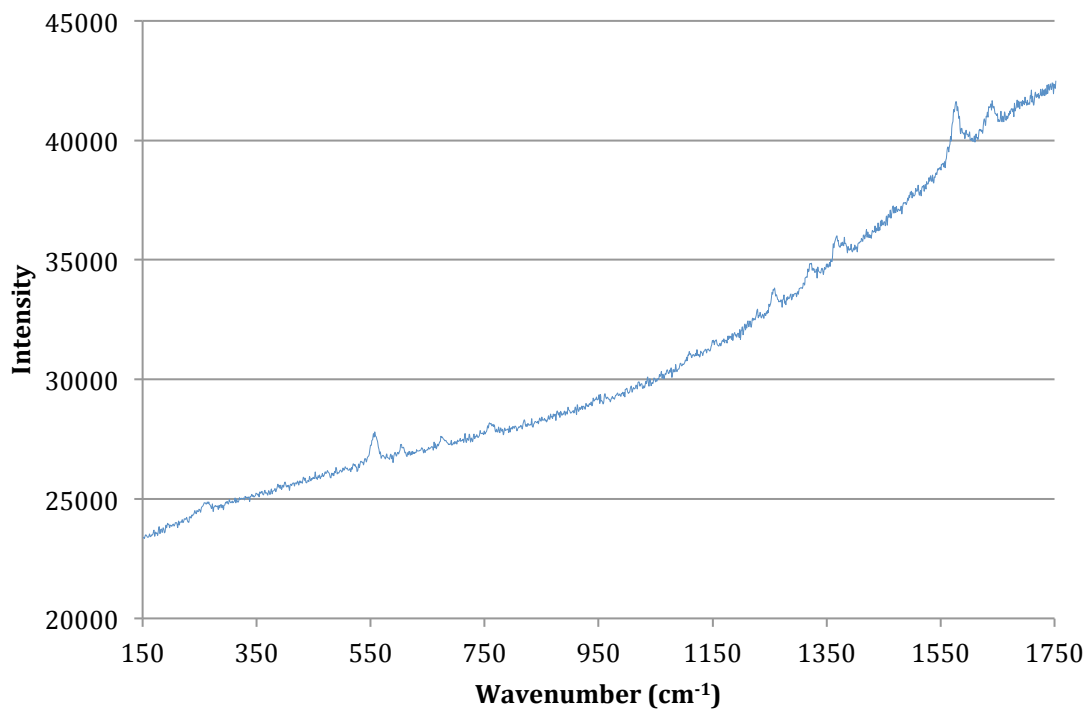


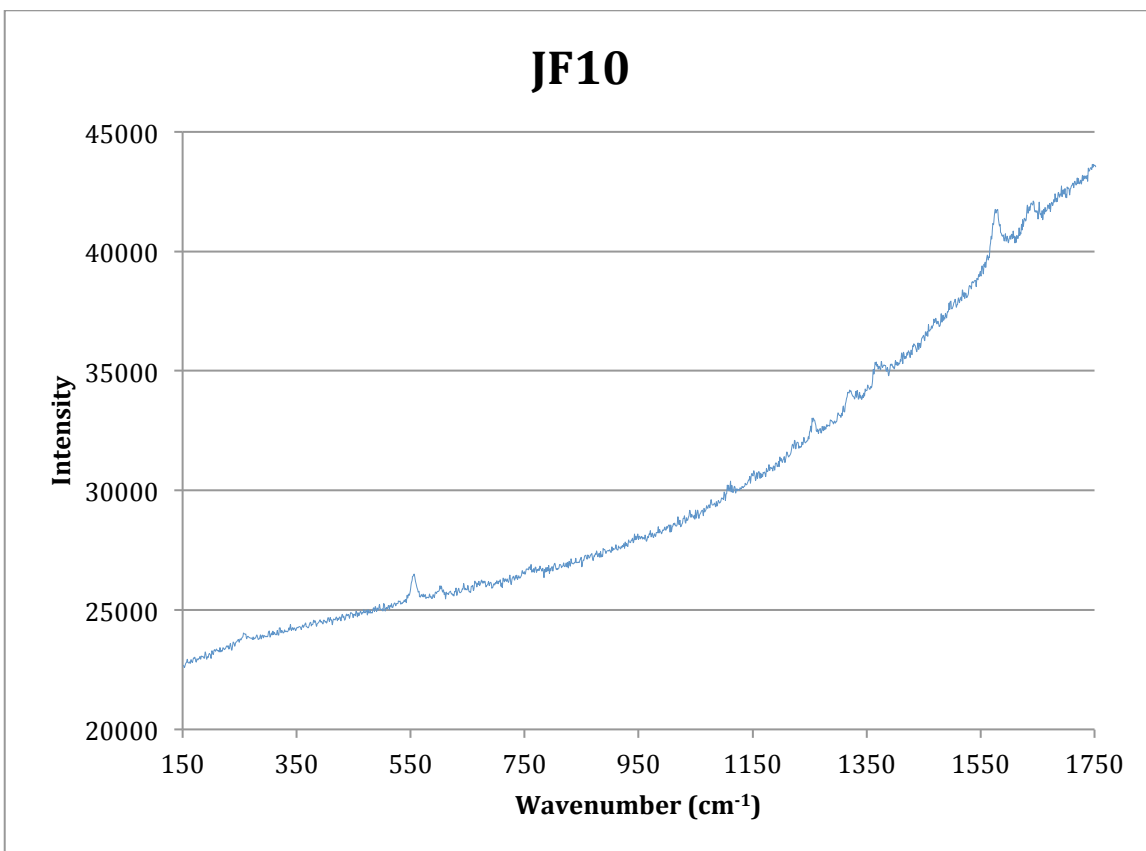
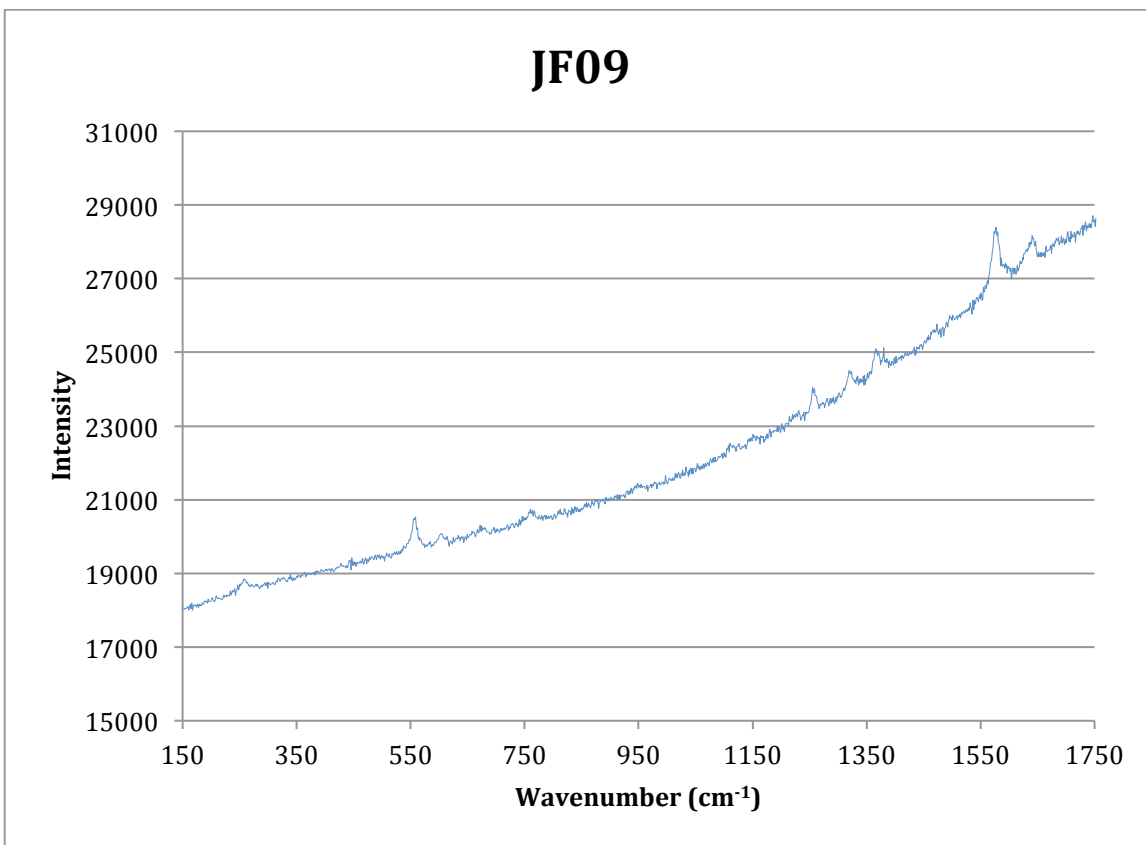


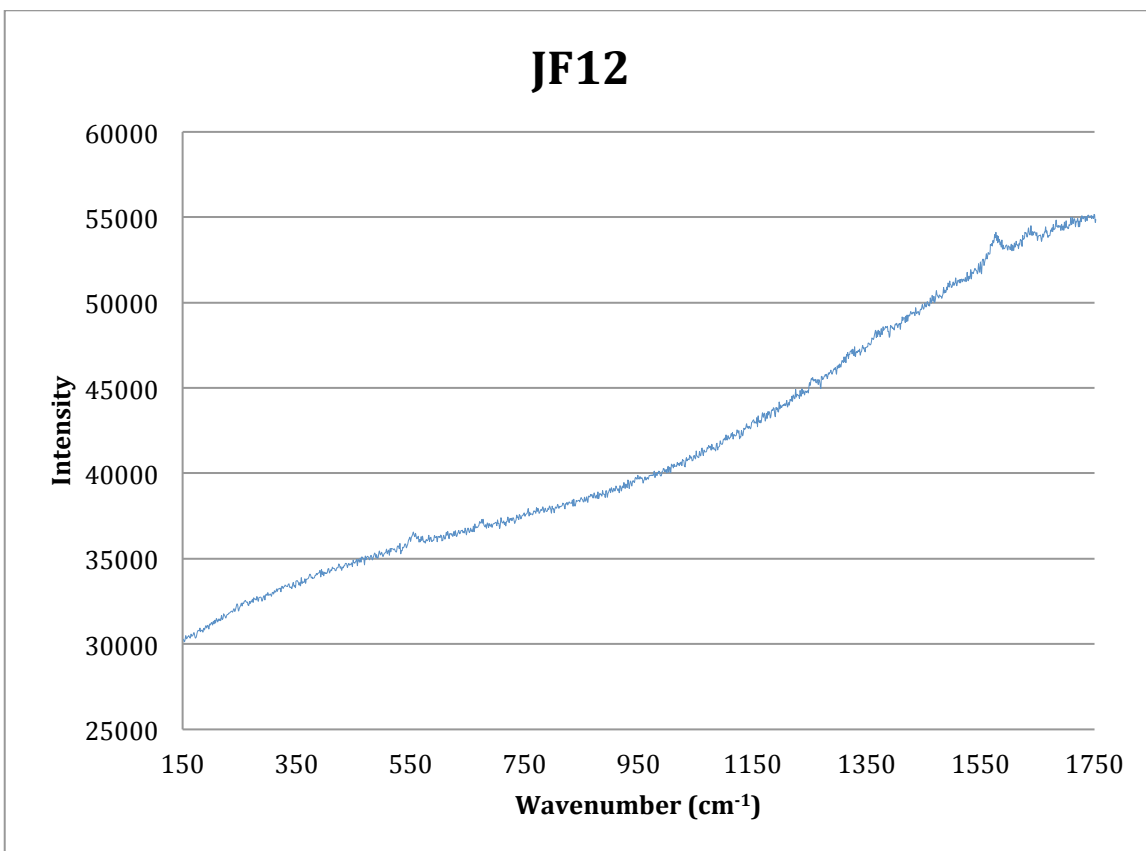
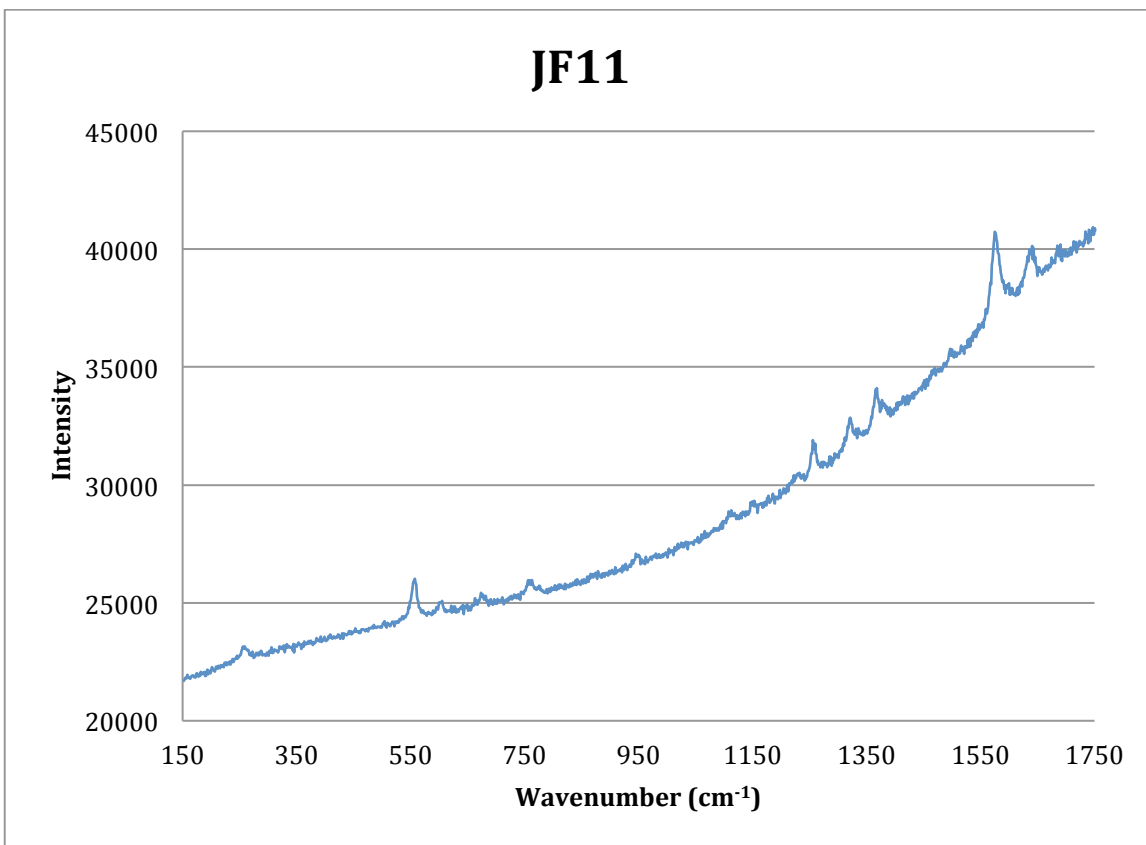
# JF07



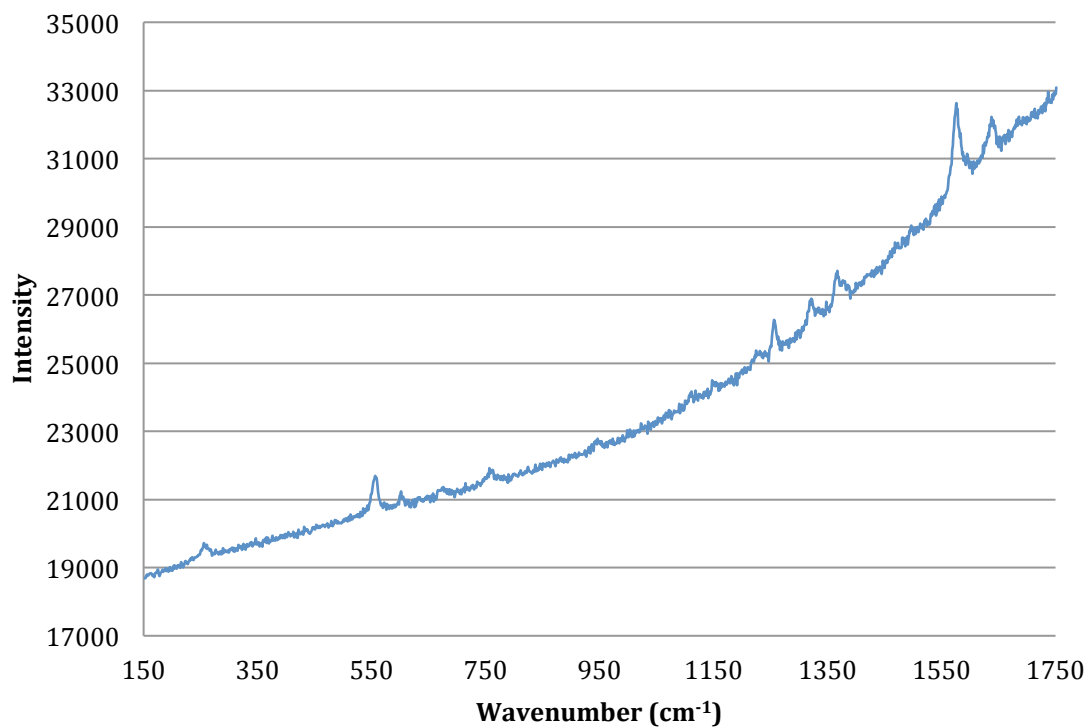
# JF08



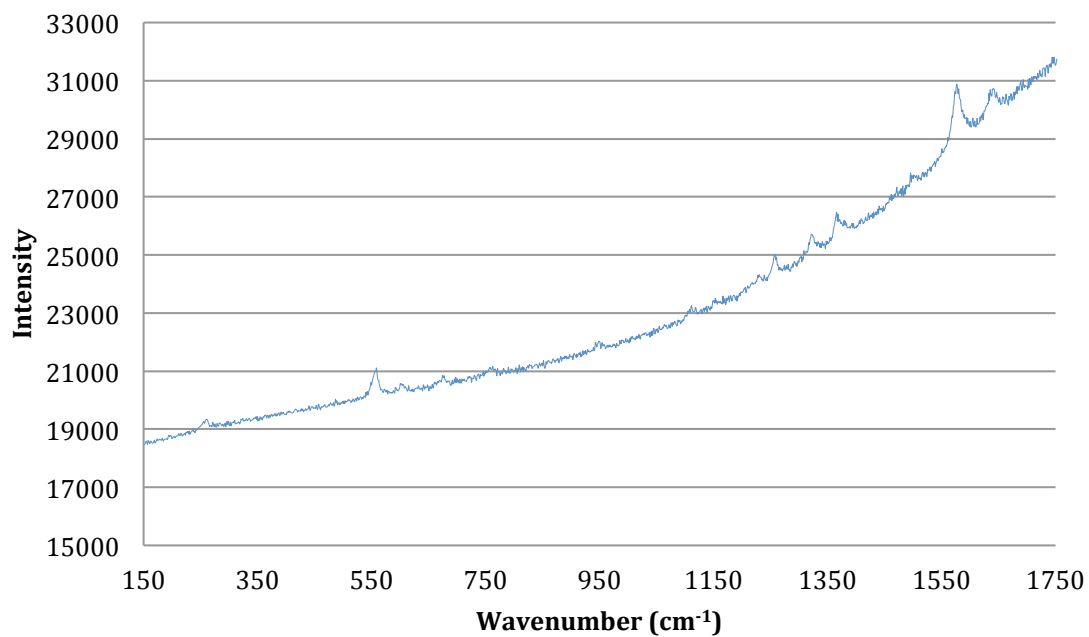




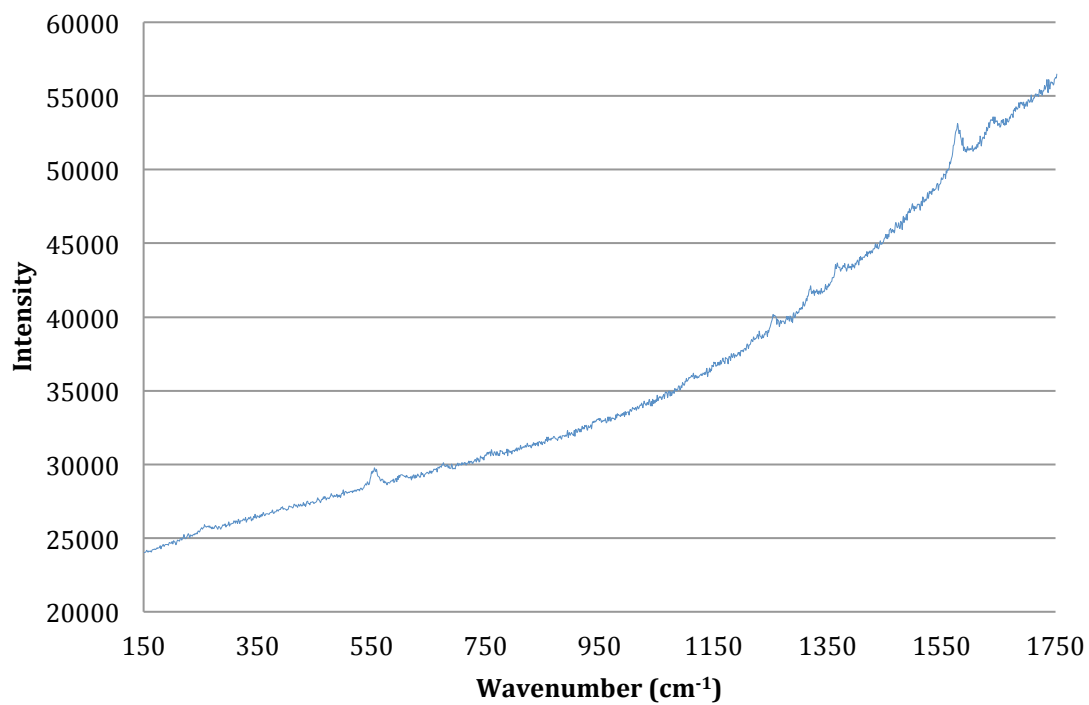
### JF13



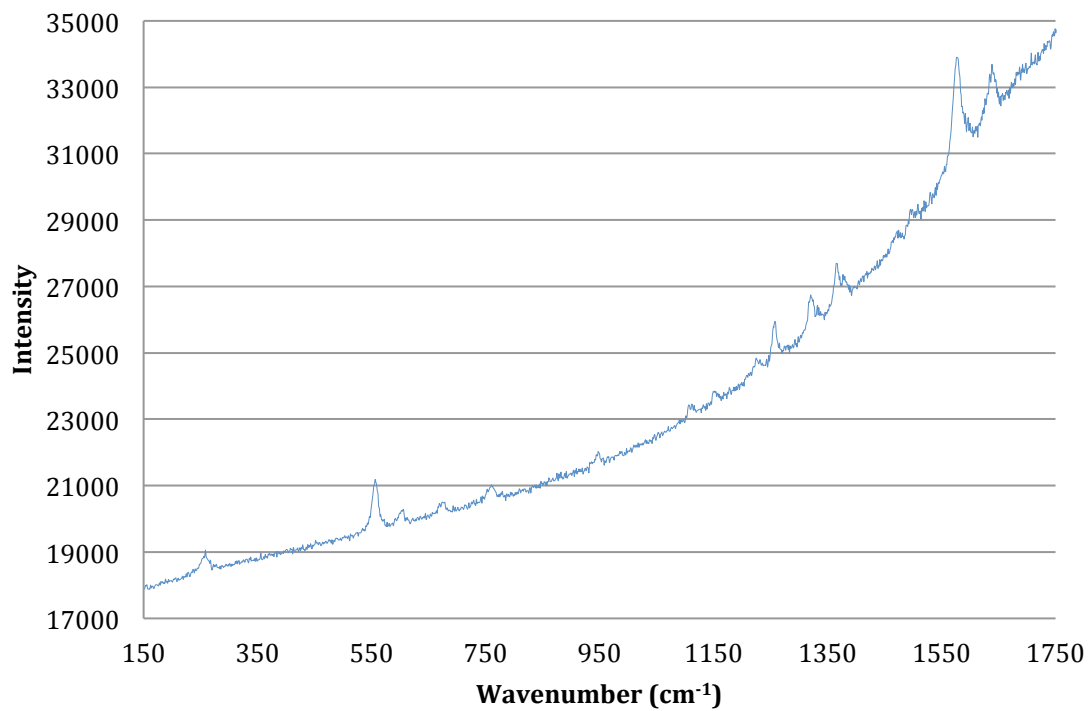
### JF14



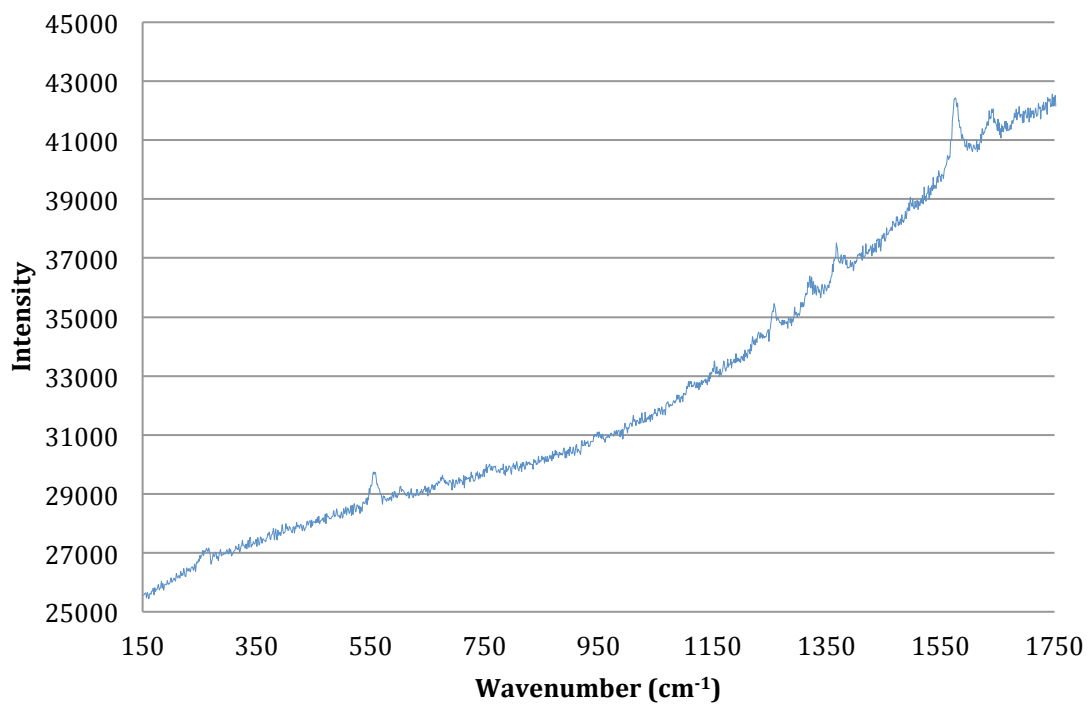
## JF15



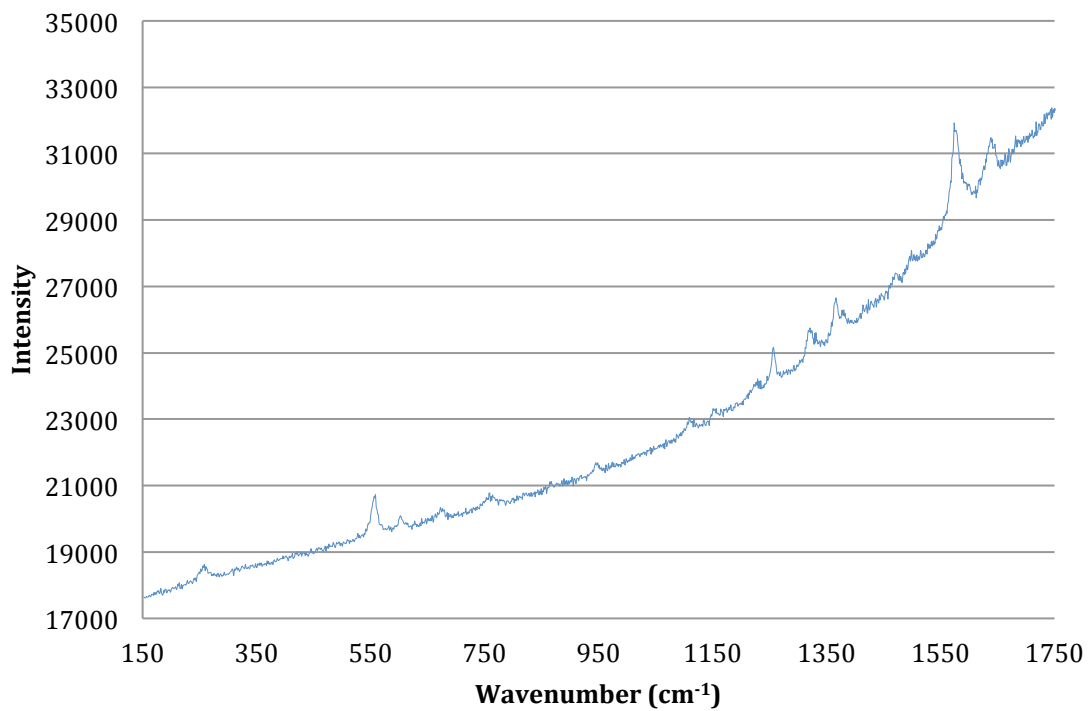
## JF16



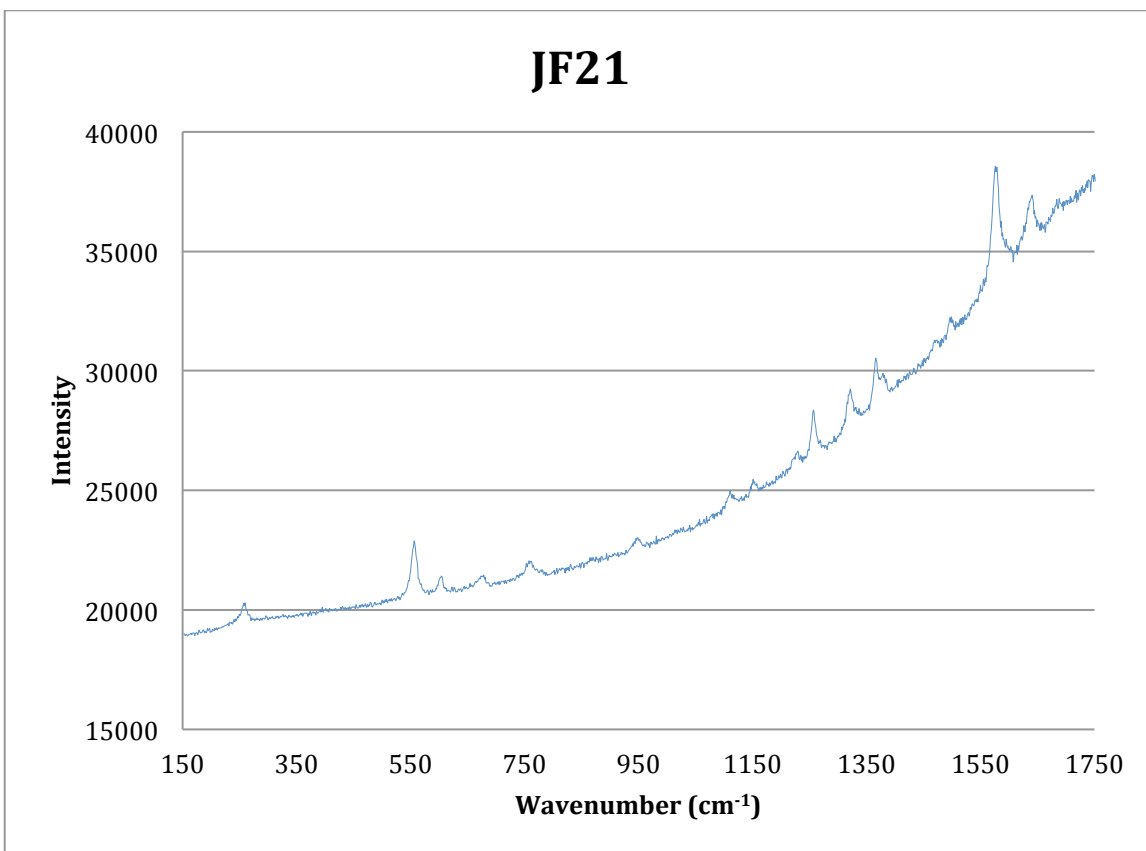
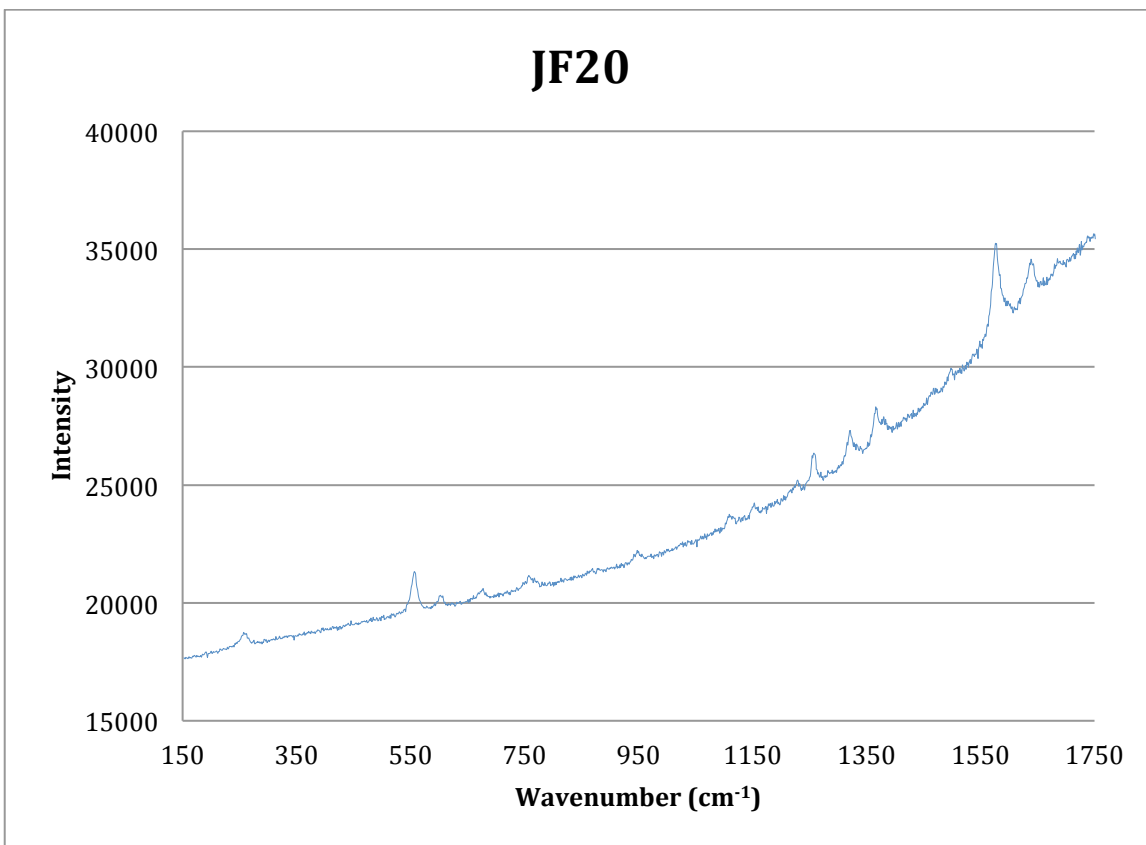
## JF17



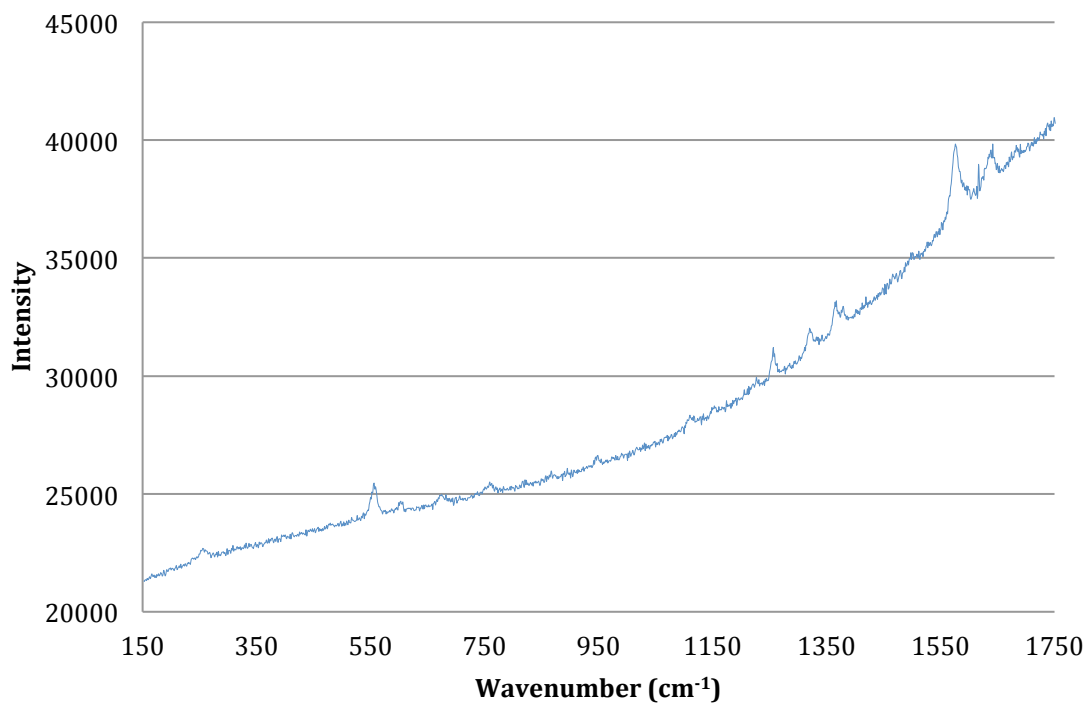
## JF18



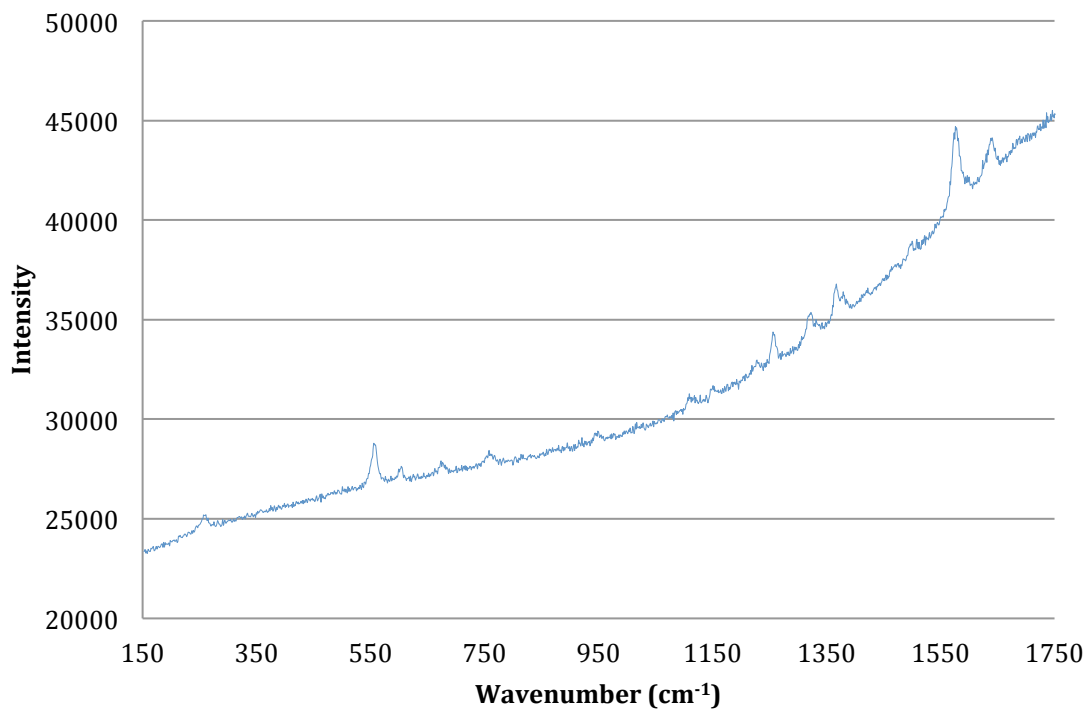


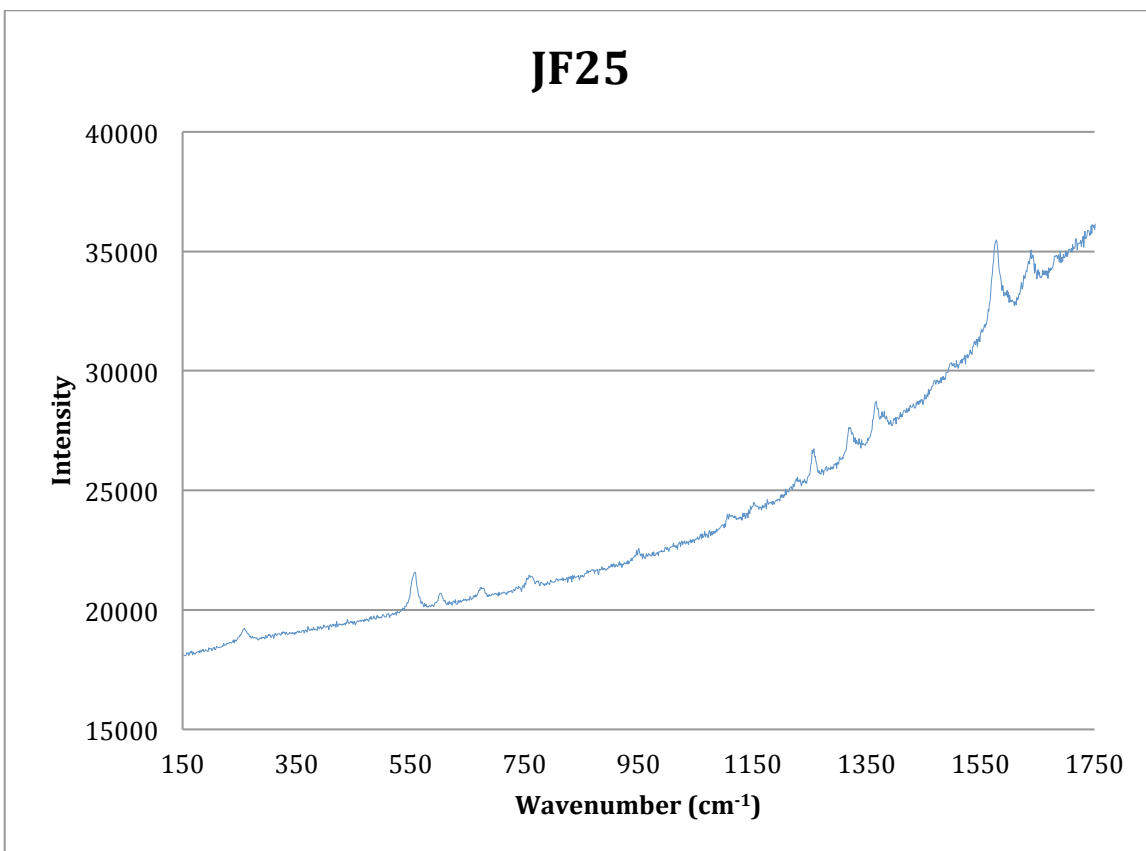
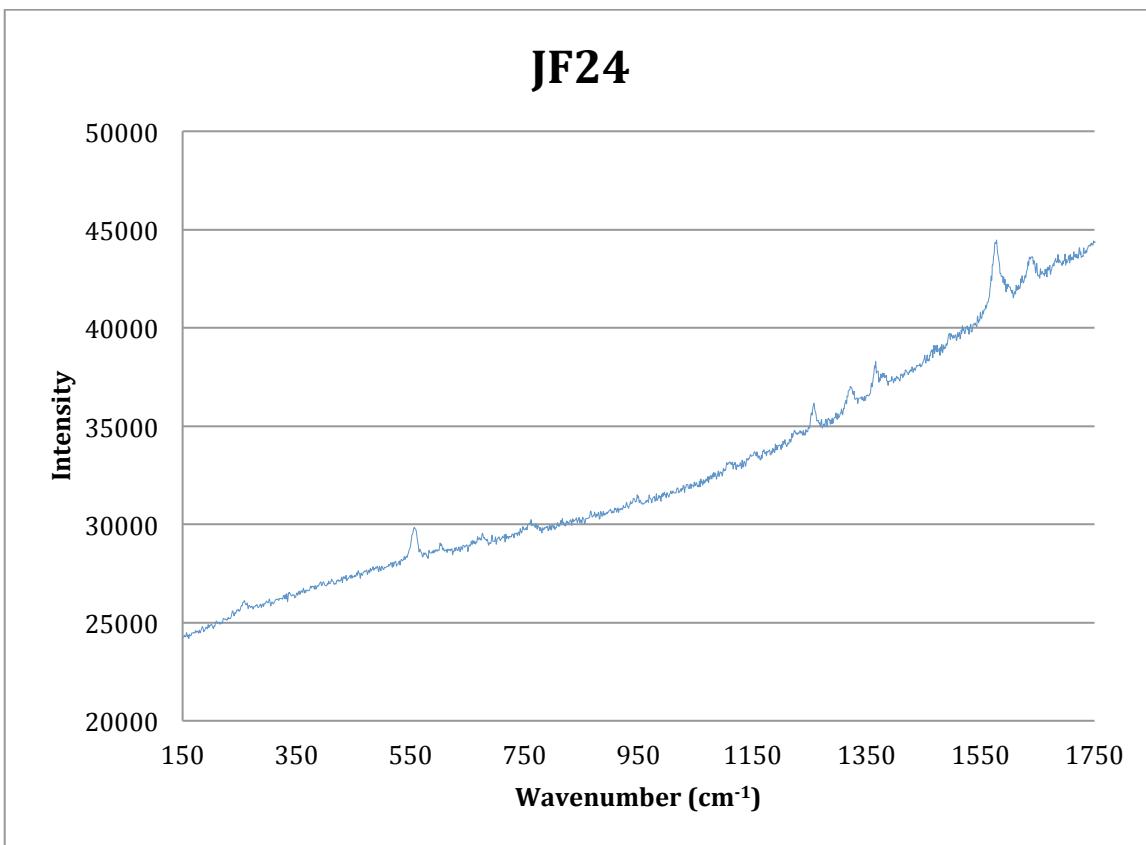


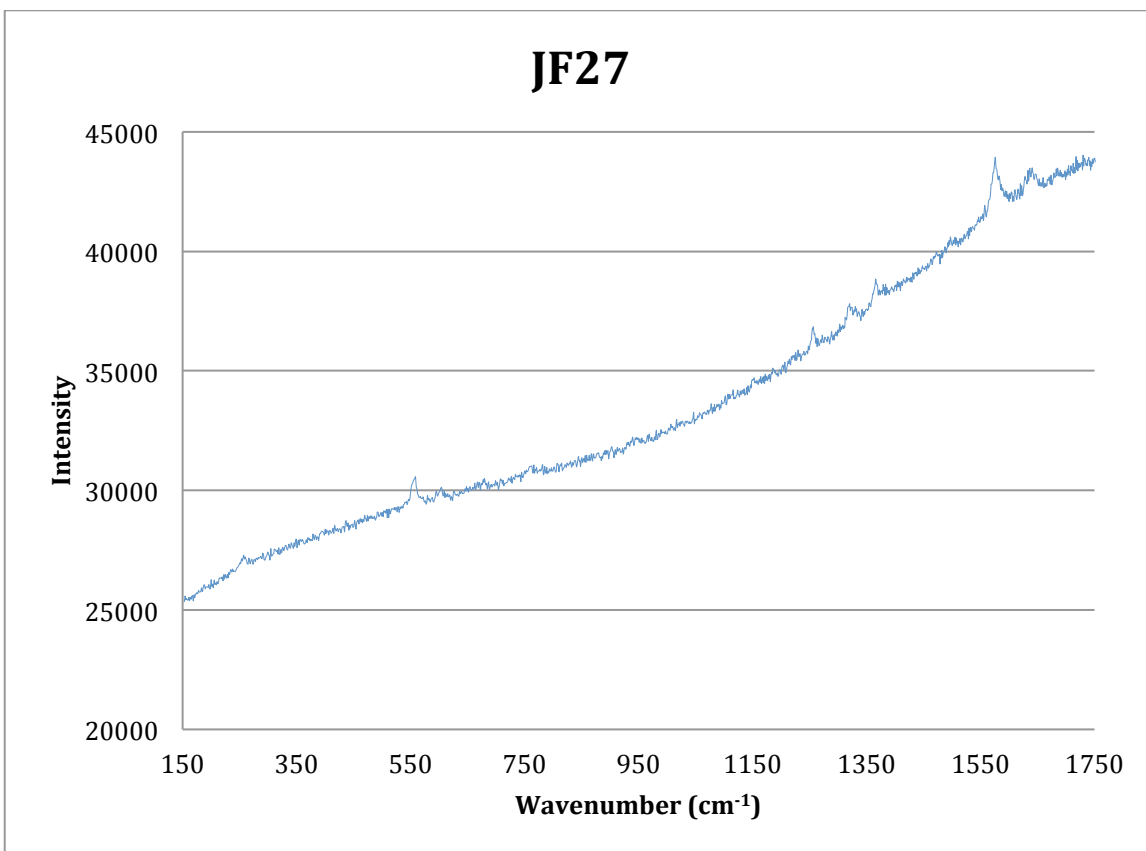
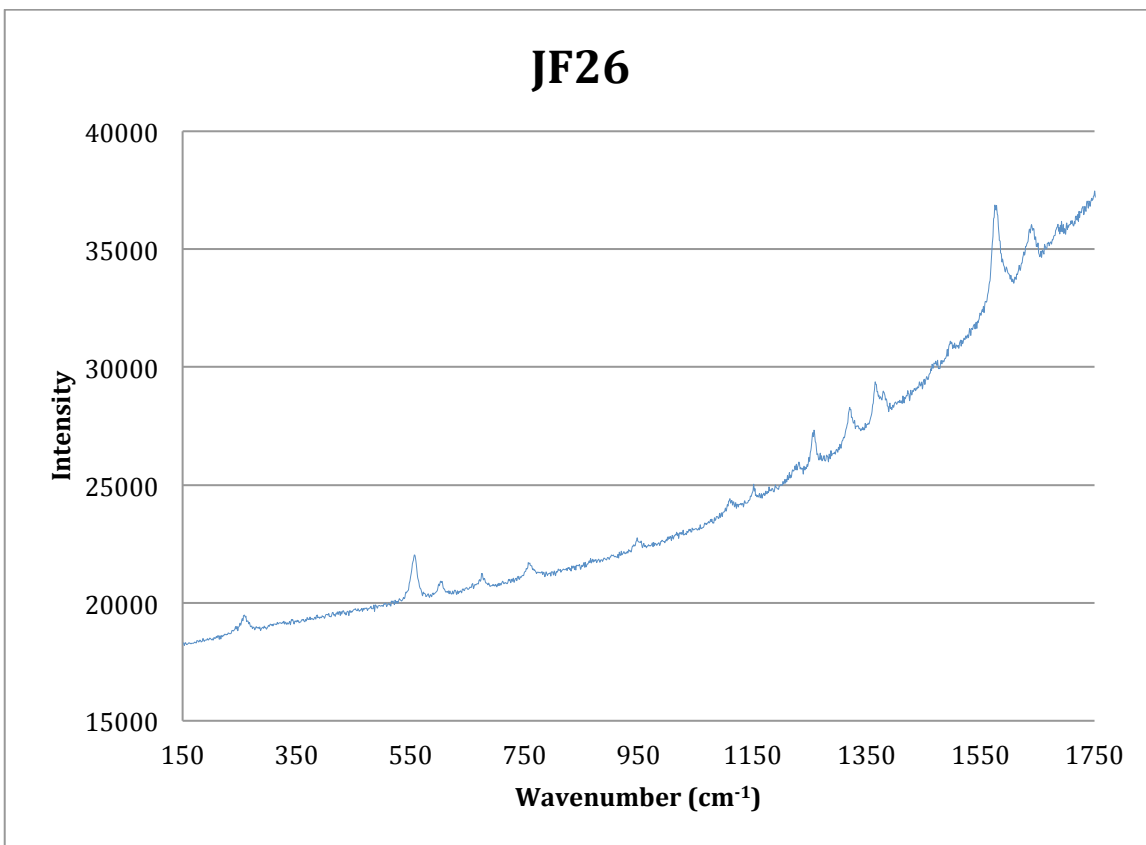
## JF22



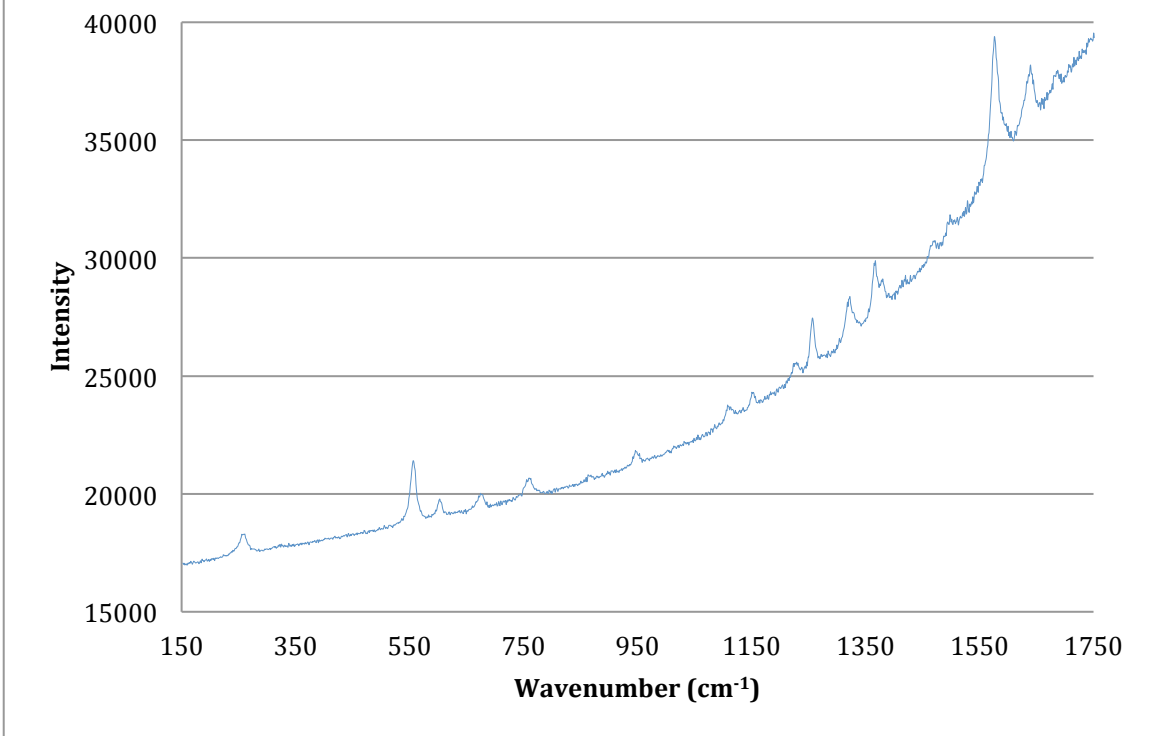
## JF23







# JF28



### 6.3 Appendix C – Raman shifts (wavenumbers - $\text{cm}^{-1}$ )

Indigo Standard (Aldrich)	Indigo Standard (Kremer)	MB Standard (Kremer)	JF 01	JF 02	JF 03	JF 04
-	-	-	-	-	-	-
252	-	254	-	258	-	258
266	261	-	-	-	-	-
275	-	-	-	-	-	-
-	-	-	-	-	-	-
-	-	-	-	-	-	-
-	-	-	-	-	-	-
546	548	554	554	554	555	557
600	-	599	603	601	-	604
-	-	634	-	-	-	-
-	675	672	677	675	-	673
-	773	758	760	756	763	760
-	-	-	-	-	-	-
-	-	864	-	-	-	-
-	-	950	-	-	-	944
-	-	-	-	-	-	-
-	-	-	-	-	-	-
-	-	1018	-	-	-	-
-	-	-	-	-	-	-
-	-	1111	-	1105	-	1110
-	-	-	-	-	-	-
-	-	1151	-	1152	-	1154
-	-	-	-	-	-	-
-	-	1226	-	-	-	-
1249	-	1257	1254	1256	1255	1257
-	1298	-	-	-	-	-
-	-	1317	1318	1318	1316	1322
-	-	1367	1365	1365	1366	1366
-	-	-	-	1382	-	1382
-	-	1464	1471	1468	-	1469
-	-	-	1502	-	-	1497
-	-	-	-	-	-	-
-	-	-	-	-	-	-
1573	1581	1573	1576	1576	1576	1577
-	-	-	-	-	-	-
-	1634	1631	1640	1637	1640	1640
-	1703	-	-	1688	-	1682

JF 05	JF 06	JF 07	JF 08	JF 09	JF 10	JF 11
-	-	-	-	-	-	-
257	-	259	260	259	258	257
-	-	-	-	-	-	-
-	-	-	-	-	-	-
-	-	-	-	-	-	-
-	-	-	-	-	-	-
558	556	556	557	557	556	556
603	-	601	604	603	604	601
-	-	-	-	-	-	-
676	-	675	675	672	679	674
757	755	762	760	760	757	756
-	-	-	-	-	-	-
-	-	-	-	-	-	-
949	-	-	-	948	949	946
-	-	-	-	-	-	-
-	-	-	-	-	-	-
-	-	-	-	-	-	-
1109	-	1111	1109	1111	1114	1109
-	-	-	-	-	-	-
1154	-	-	1150	1152	1152	-
-	-	-	-	-	-	-
1225	-	-	1228	1226	1228	1230
1257	1256	1256	1258	1255	1256	1257
-	-	-	-	-	-	-
1322	-	1318	1322	1321	1320	1321
1366	1365	1363	1367	1365	1366	1366
-	1378	-	1381	1379	1381	-
1472	1471	1465	1466	1474	-	1464
1495	-	1495	1497	1496	-	1496
-	-	-	1511	-	-	-
-	-	-	-	-	-	-
1577	1575	1577	1576	1577	1577	1576
-	-	-	-	-	-	-
1636	1637	1639	1641	1642	1640	1638
1685	-	1686	1684	-	1684	1685

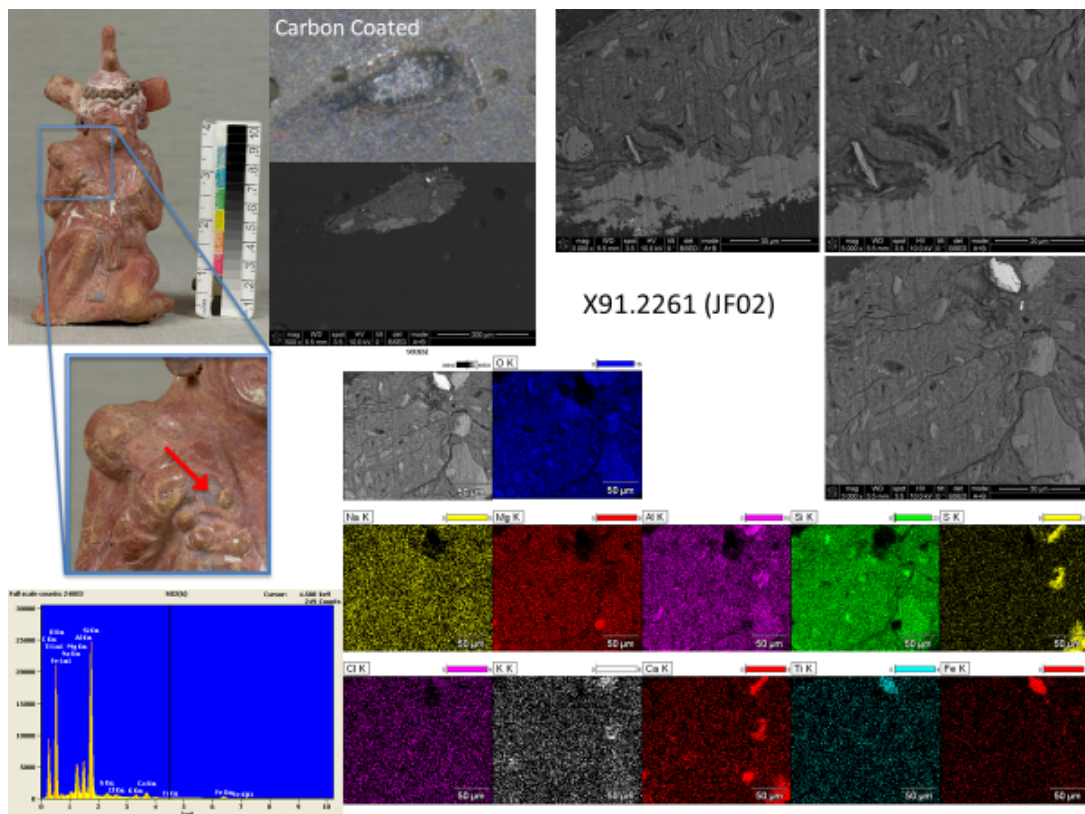
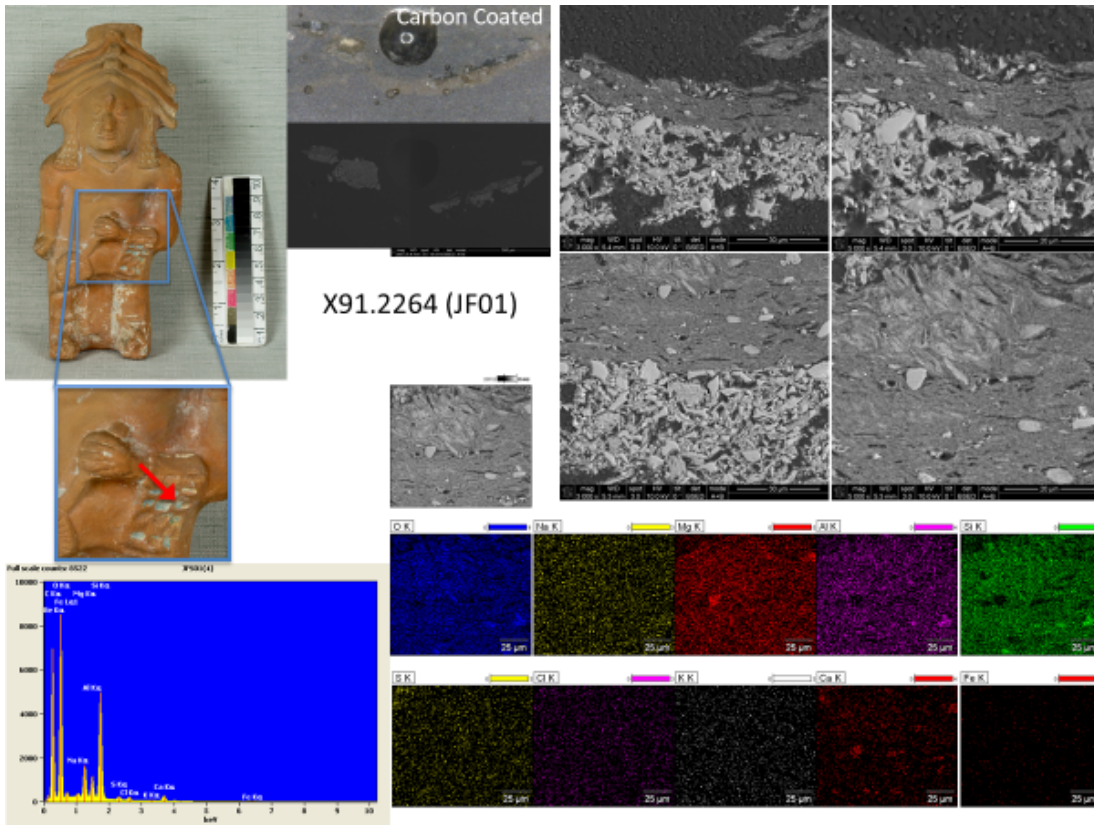
JF 12	JF 13	JF 14	JF 15	JF 16	JF 17	JF 18
-	-	-	-	-	-	-
-	256	260	257	258	262	257
-	-	-	-	-	-	-
-	-	-	-	-	-	-
-	-	-	-	-	-	-
-	-	-	-	-	-	-
555	556	557	555	557	557	556
-	602	602	602	604	602	602
-	-	-	-	-	-	-
675	671	677	676	675	676	673
-	757	762	760	769	759	758
-	-	-	-	-	-	-
-	-	-	-	-	-	865
950	947	949	948	948	948	946
-	-	-	-	-	-	-
-	-	-	-	-	-	-
-	-	-	-	-	-	-
-	-	1111	1112	1107	1108	1109
-	-	-	-	-	-	-
-	-	1153	-	1151	1153	1152
-	-	-	-	-	-	-
-	1225	1228	1230	1225	-	1226
1253	1257	1257	1256	1257	1257	1257
-	-	-	-	-	-	-
1324	1322	1322	1319	1320	1321	1320
-	1366	1365	1364	1366	1368	1365
1384	-	-	1380	-	1382	-
-	-	1471	-	1471	-	1471
-	1497	1496	1498	1495	1497	1499
-	-	-	-	1509	-	-
-	-	-	-	-	-	-
1576	1576	1577	1577	1577	1576	1576
-	-	-	-	-	-	-
1638	1638	1635	1640	1640	1640	1638
1683	1686	1689	1686	1687	1683	1682

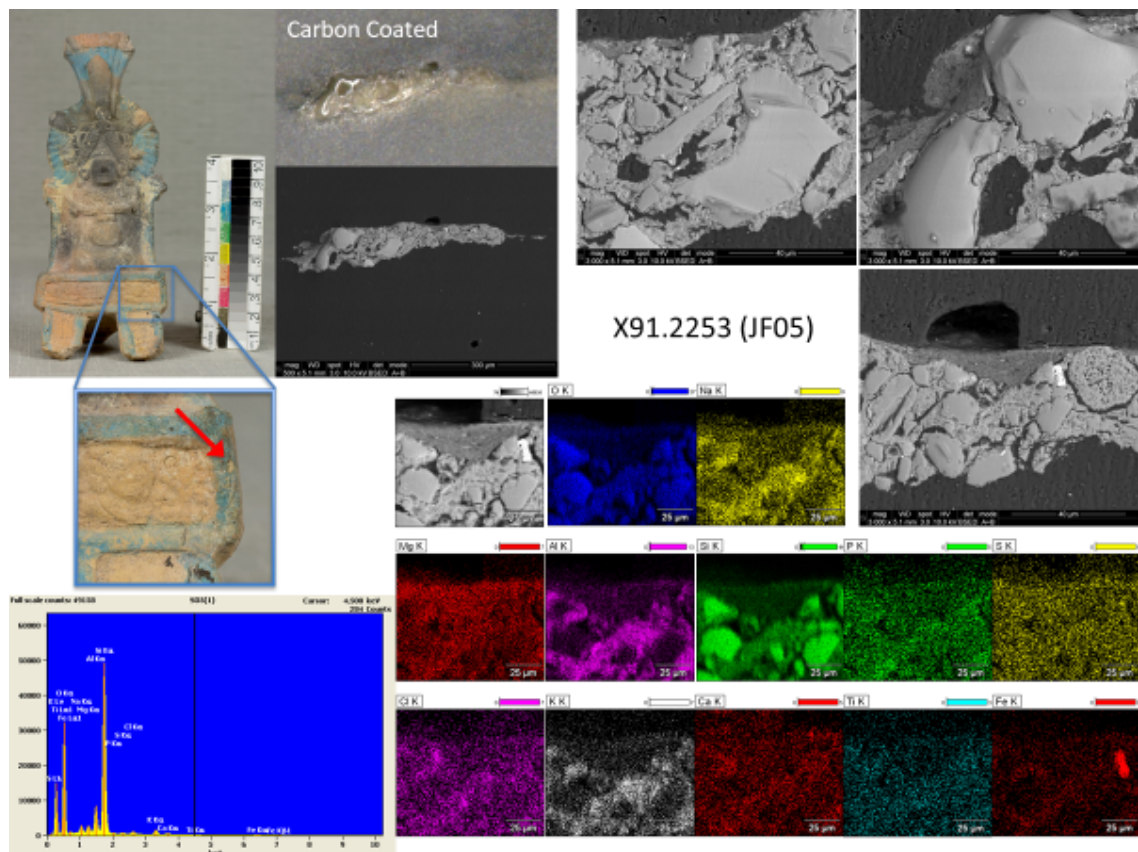
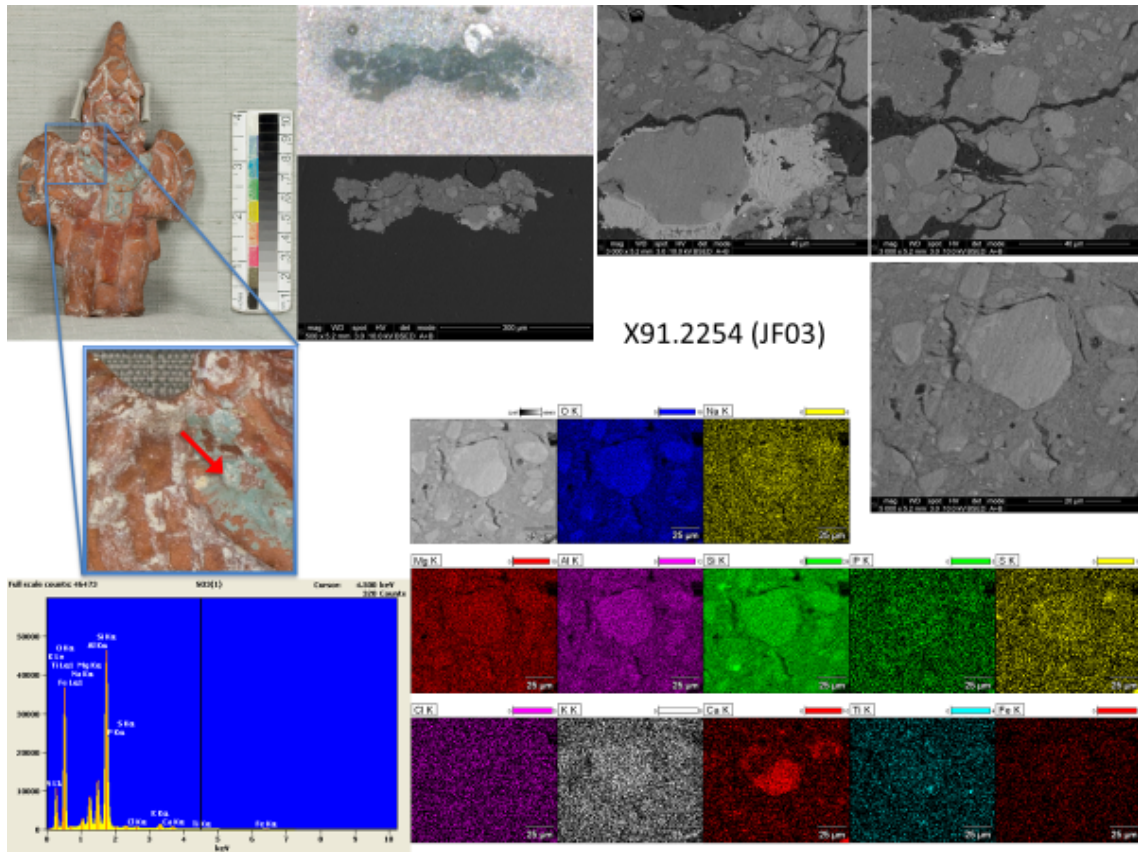


JF 19	JF 20	JF 21	JF 22	JF 23	JF 24	JF 25
-	-	-	-	-	-	-
-	258	257	256	258	257	258
-	-	-	-	-	-	-
-	-	-	-	-	-	-
-	-	-	-	-	-	-
-	-	-	-	-	-	-
-	556	556	556	557	556	556
-	603	602	599	604	602	602
-	-	-	-	-	-	-
-	676	675	676	673	676	675
-	758	759	759	758	761	760
-	-	-	-	-	-	-
-	-	865	-	-	-	-
-	948	945	945	949	948	950
-	-	-	-	-	-	-
-	-	-	-	-	-	-
-	1027	-	-	-	-	-
-	-	-	-	-	-	-
-	1109	1109	1106	1109	1110	1109
-	-	-	-	-	-	-
-	1153	1151	1148	1151	1154	1152
-	-	-	-	-	-	-
-	1229	1224	1228	1228	1224	1229
-	1257	1257	1256	1257	1257	1256
-	-	-	-	-	-	-
-	1320	1320	1319	1321	1322	1320
-	1367	1366	1366	1366	1366	1366
-	1380	1381	1379	1379	1380	1381
-	1468	1471	1467	1464	1468	1470
-	1498	1498	1499	1498	1495	1497
-	-	-	-	-	-	-
-	-	-	-	-	-	-
-	1576	1577	1576	1576	1576	1577
-	-	-	-	-	-	-
-	1639	1639	1637	1639	1638	1638
-	1685	1684	1692	1689	1686	1682

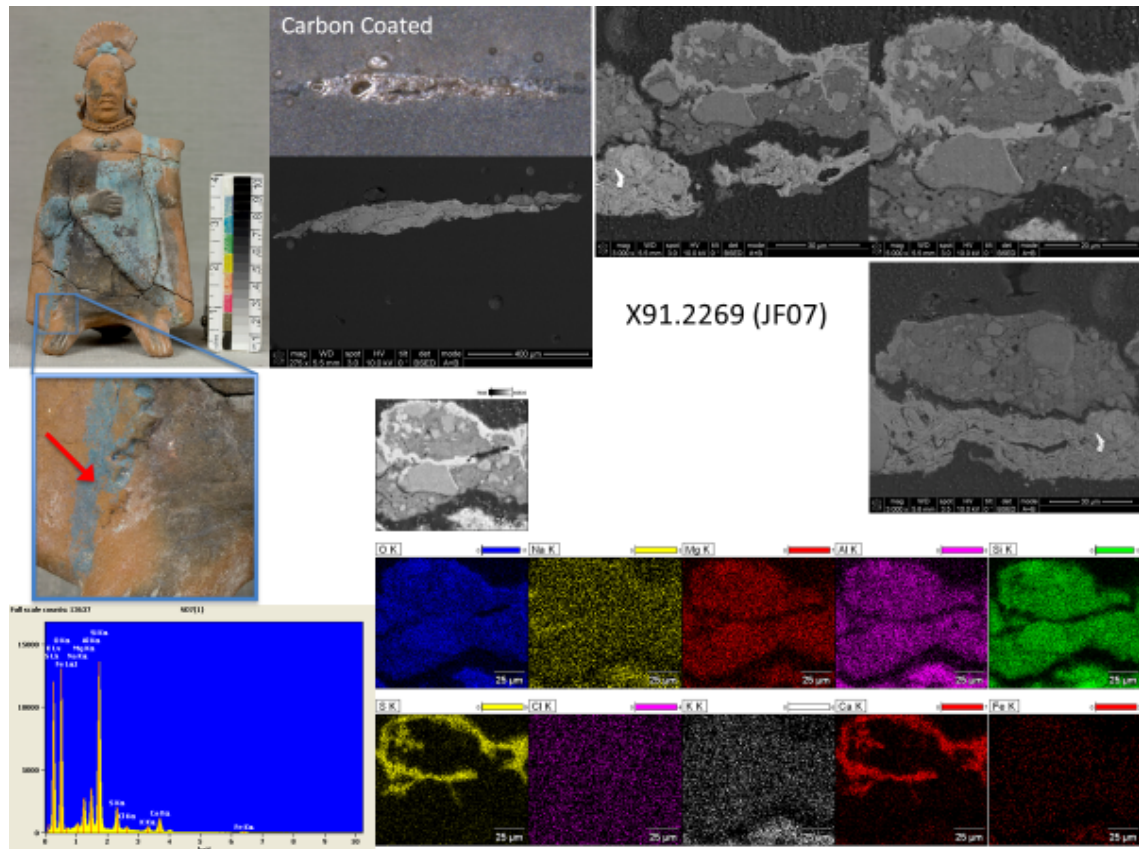
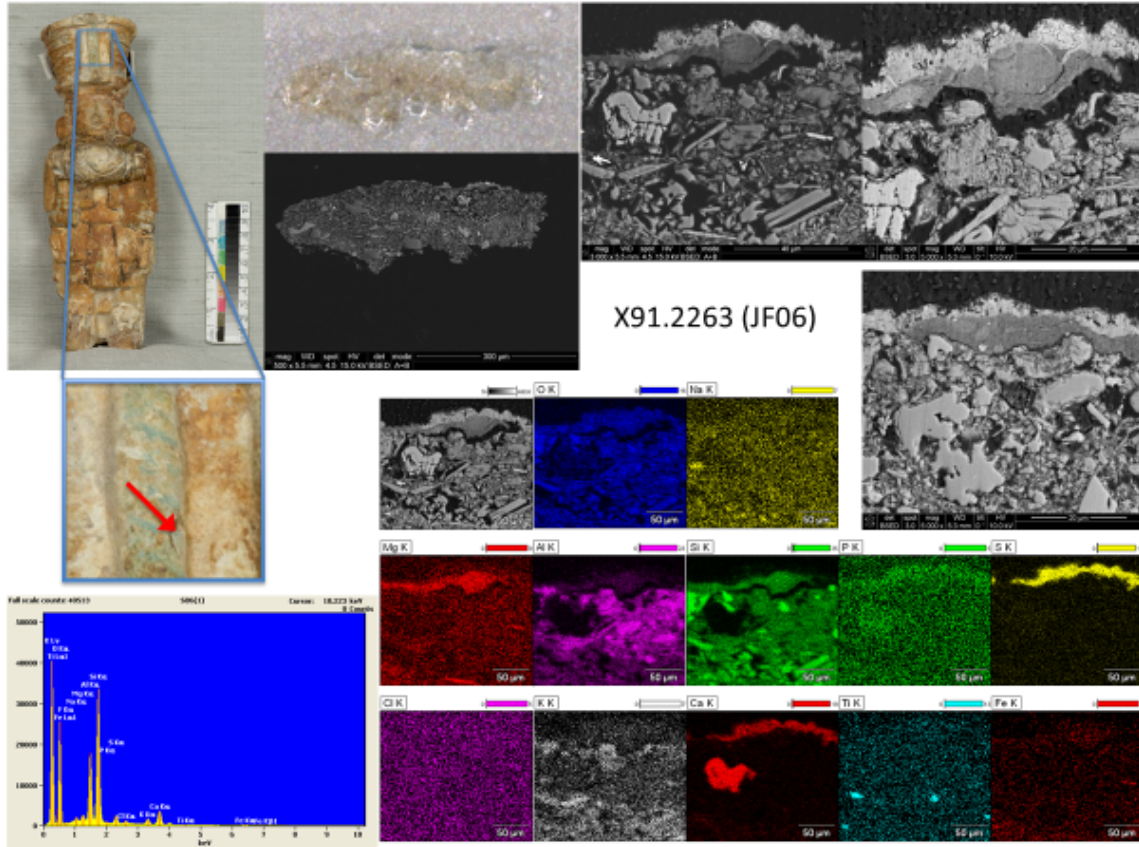
JF 26	JF 27	JF 28	JF 29	JF 30
-	-	-	-	-
258	257	258	-	-
-	-	-	-	-
-	-	-	-	-
-	-	-	-	-
-	-	-	-	-
557	555	557	-	-
603	604	603	-	-
-	-	-	-	-
677	680	675	-	-
759	761	759	-	-
-	-	-	-	-
-	-	864	-	-
946	-	947	-	-
-	-	-	-	-
-	-	-	-	-
-	-	-	-	-
1110	-	1109	-	-
-	-	-	-	-
1153	1151	1152	-	-
-	-	-	-	-
1227	-	1226	-	-
1257	1255	1257	-	-
-	-	-	-	-
1321	1319	1321	-	-
1365	1366	1366	-	-
1380	1379	1380	-	-
1469	1472	1468	-	-
1499	1497	1498	-	-
-	-	-	-	-
-	-	-	-	-
1577	1576	1577	-	-
-	-	-	-	-
1639	1641	1639	-	-
1687	1683	1686	-	-

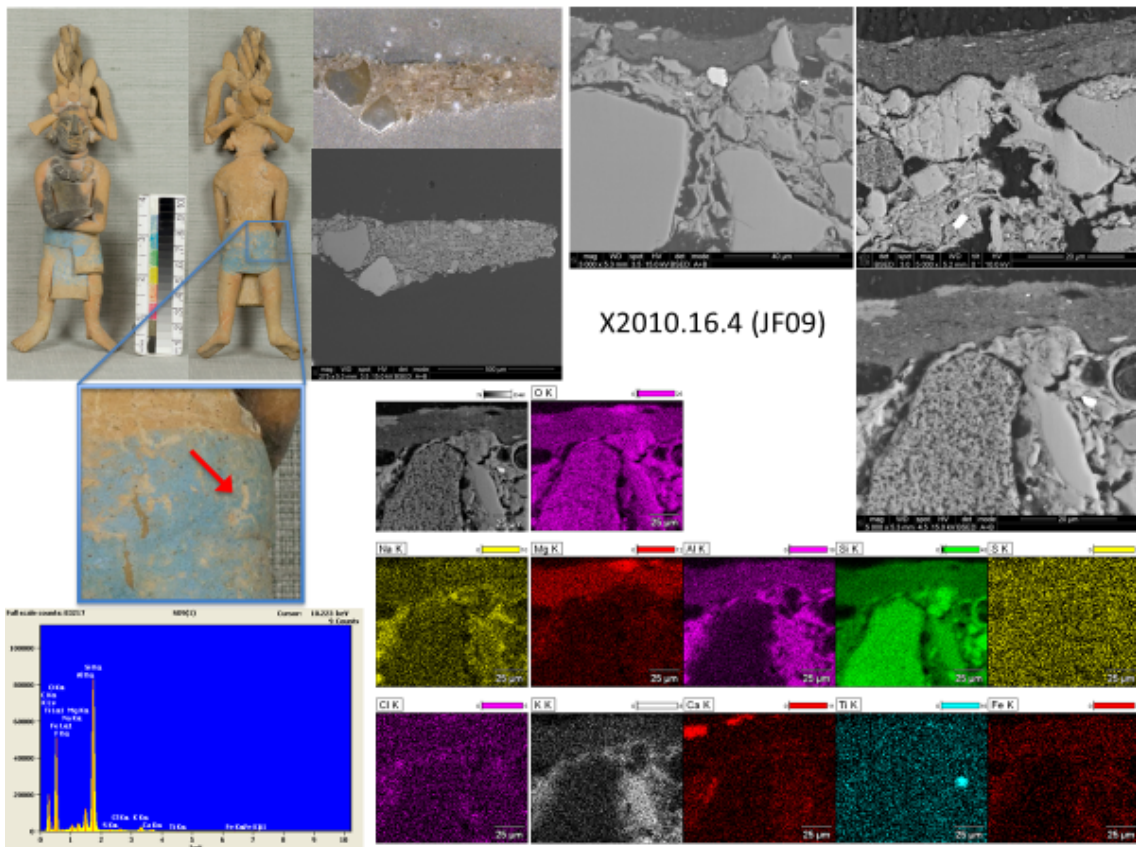
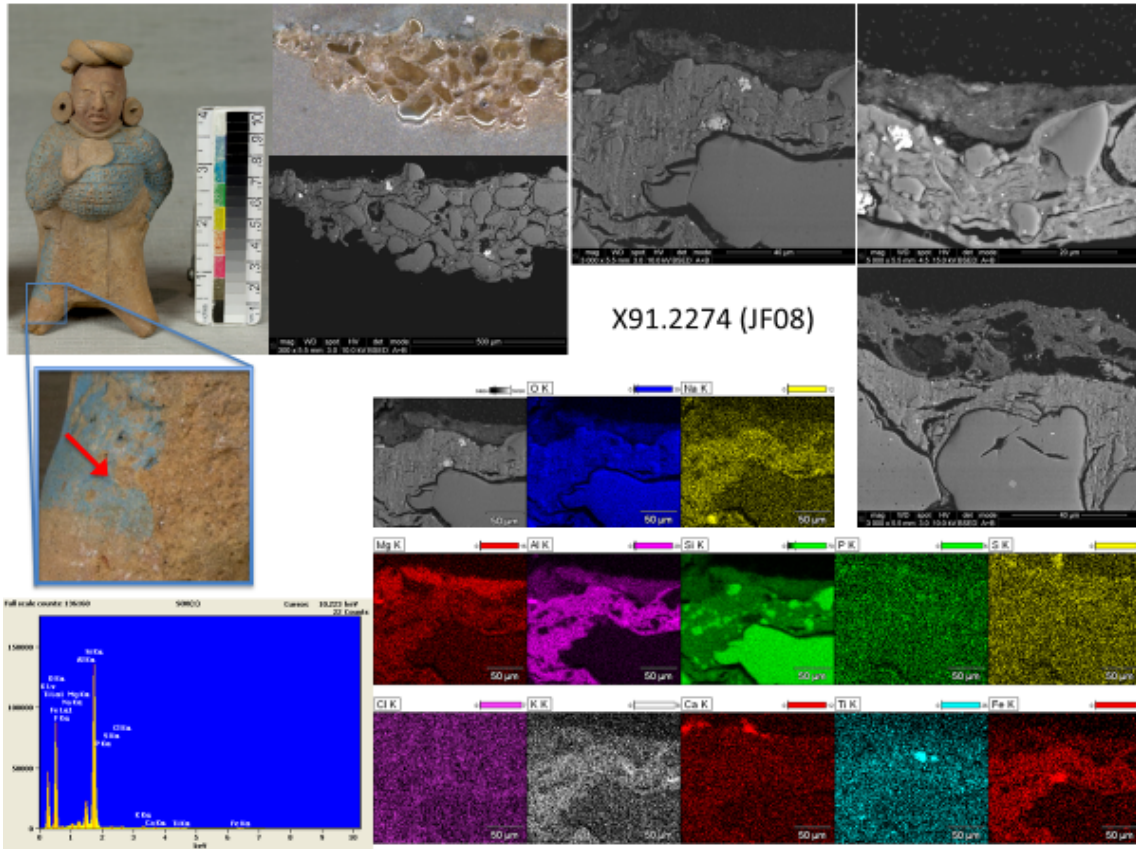
## 6.4 Appendix D – SEM-EDS micrographs and elemental mapping



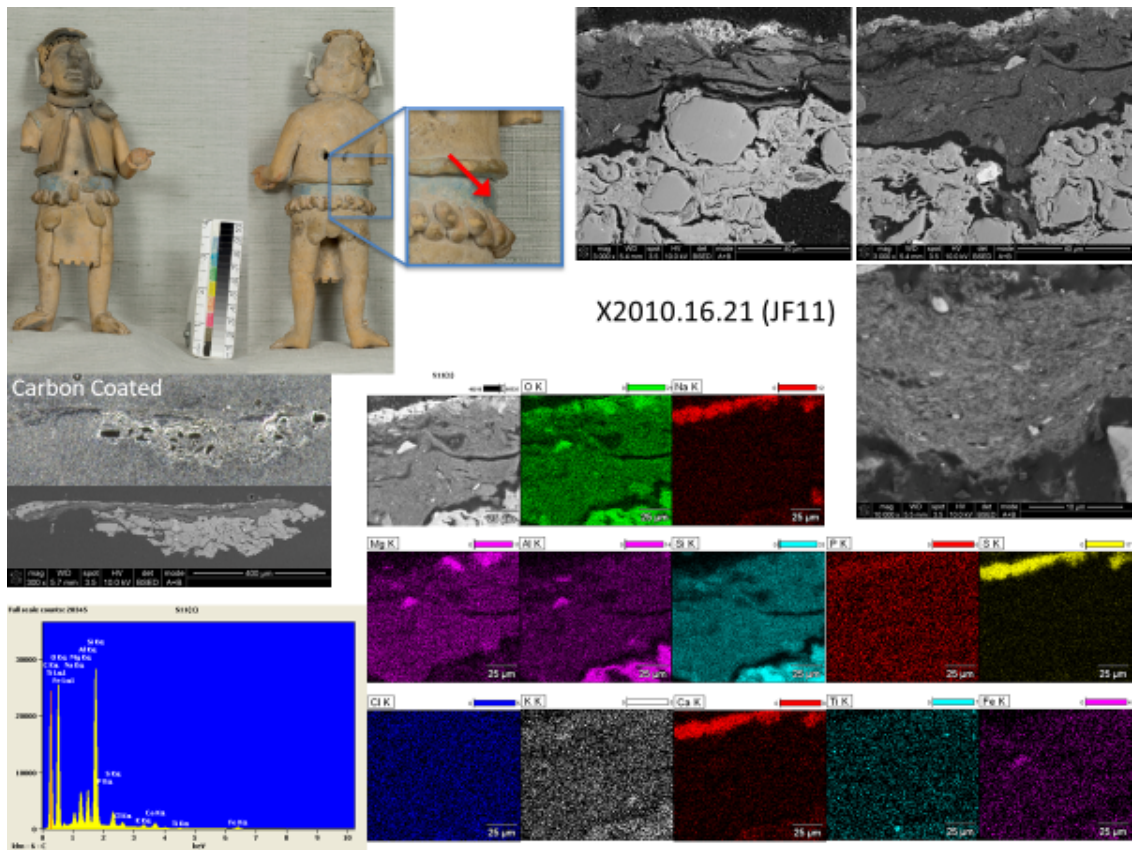
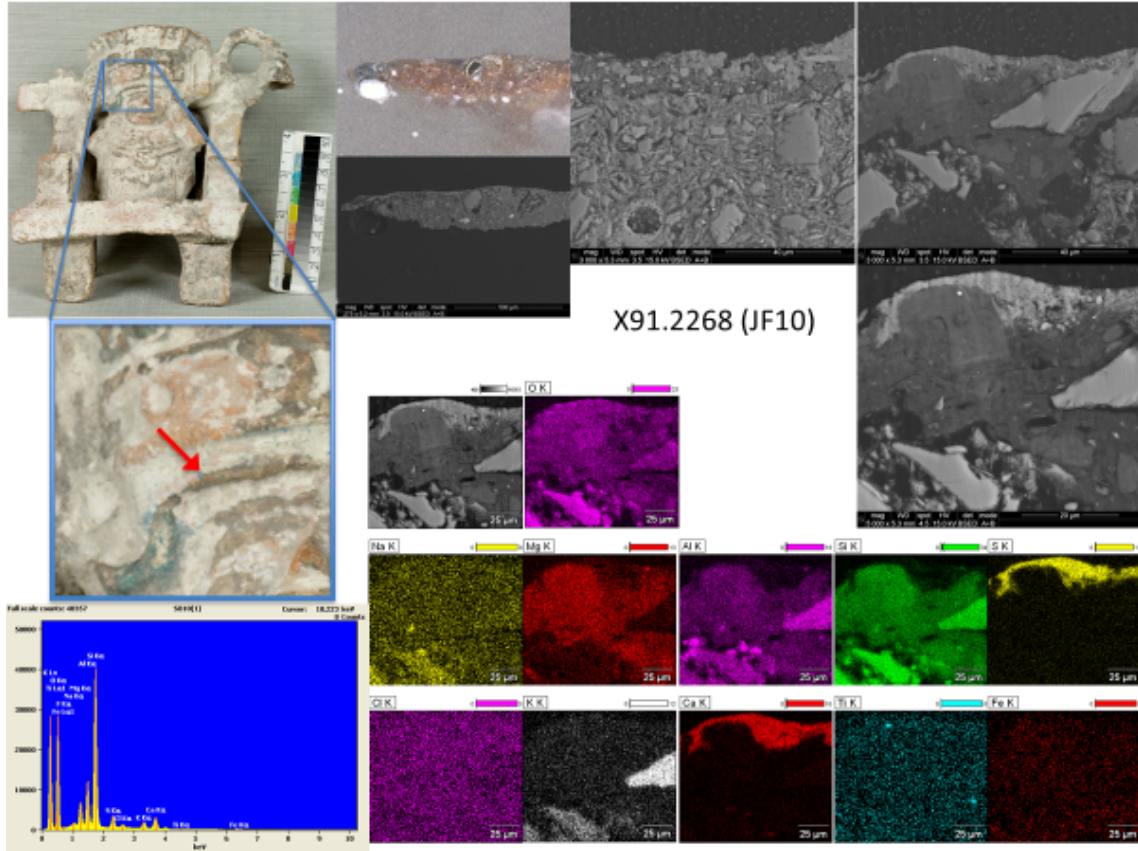


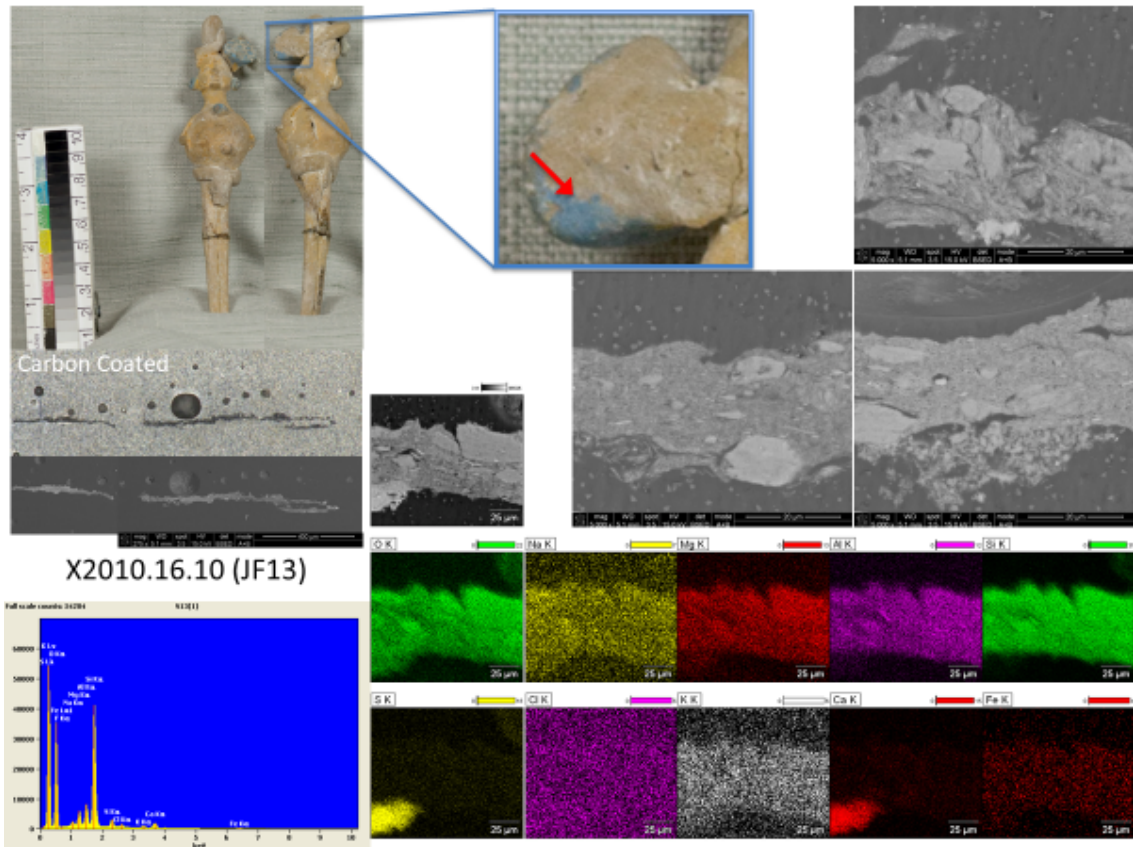
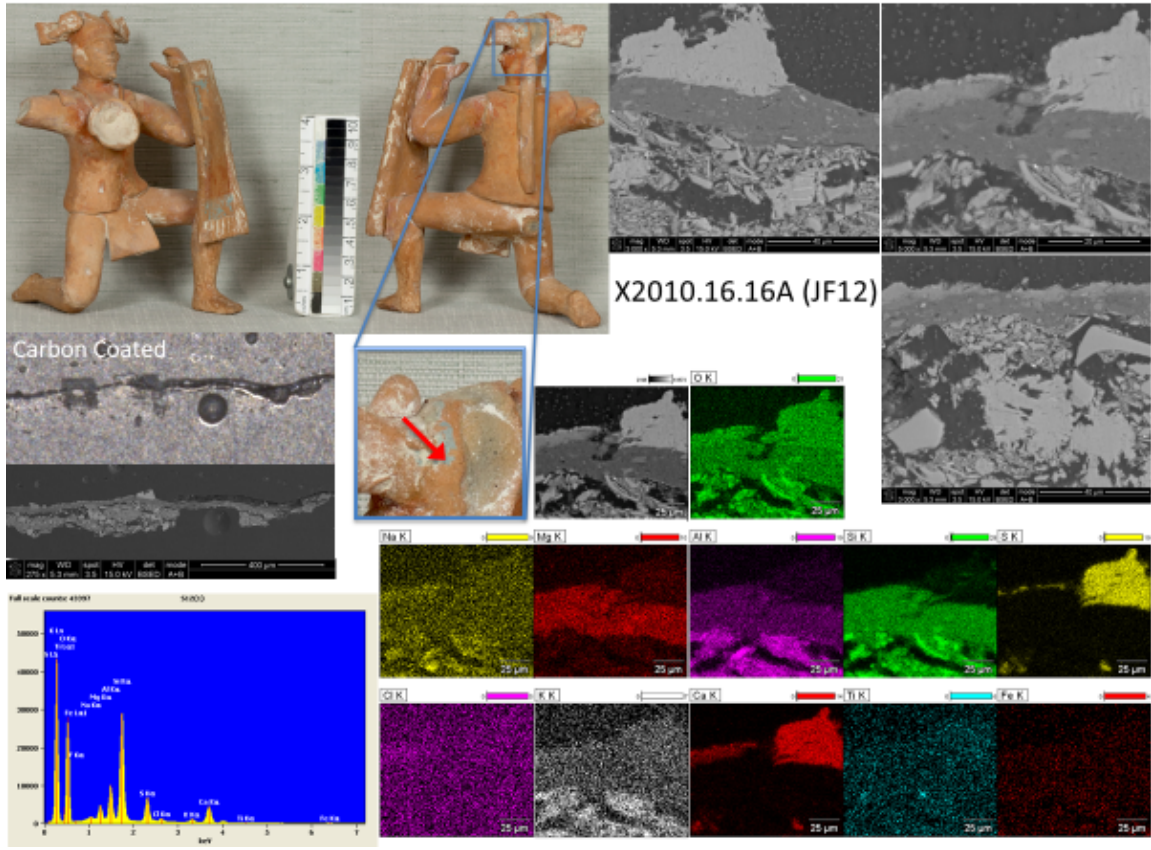




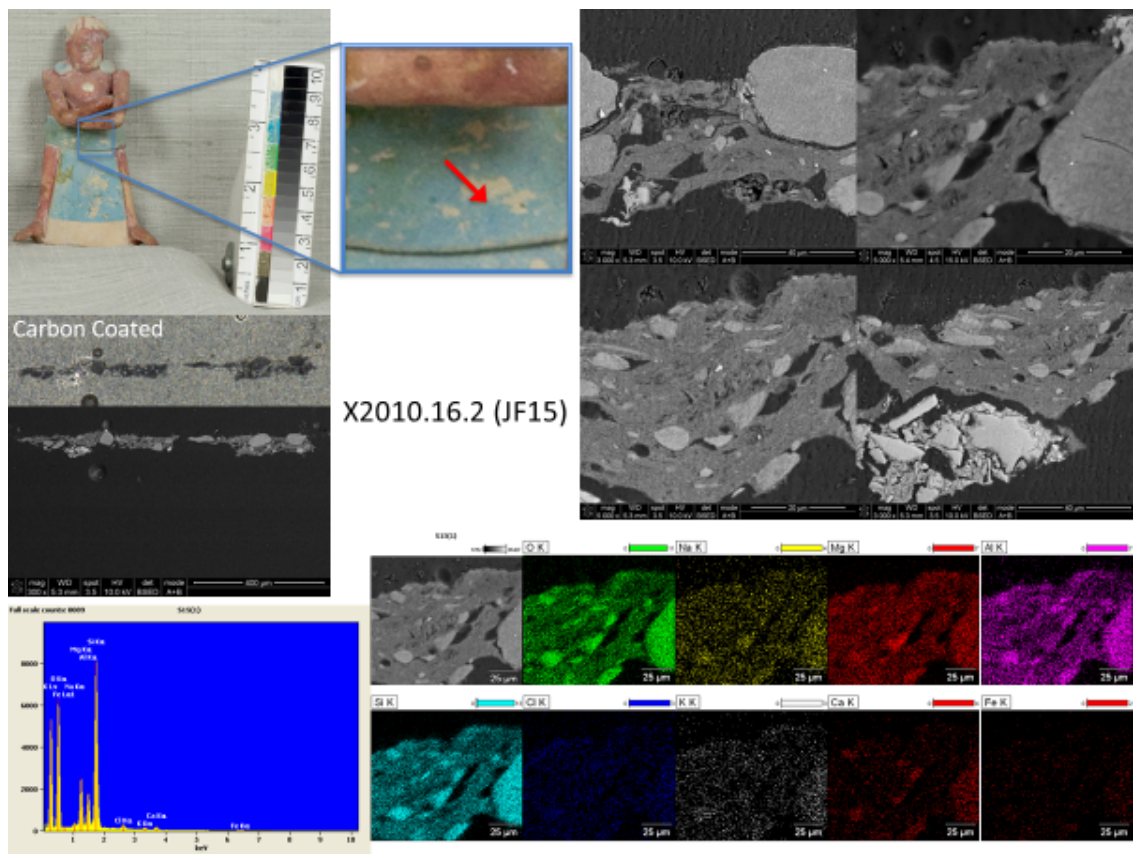
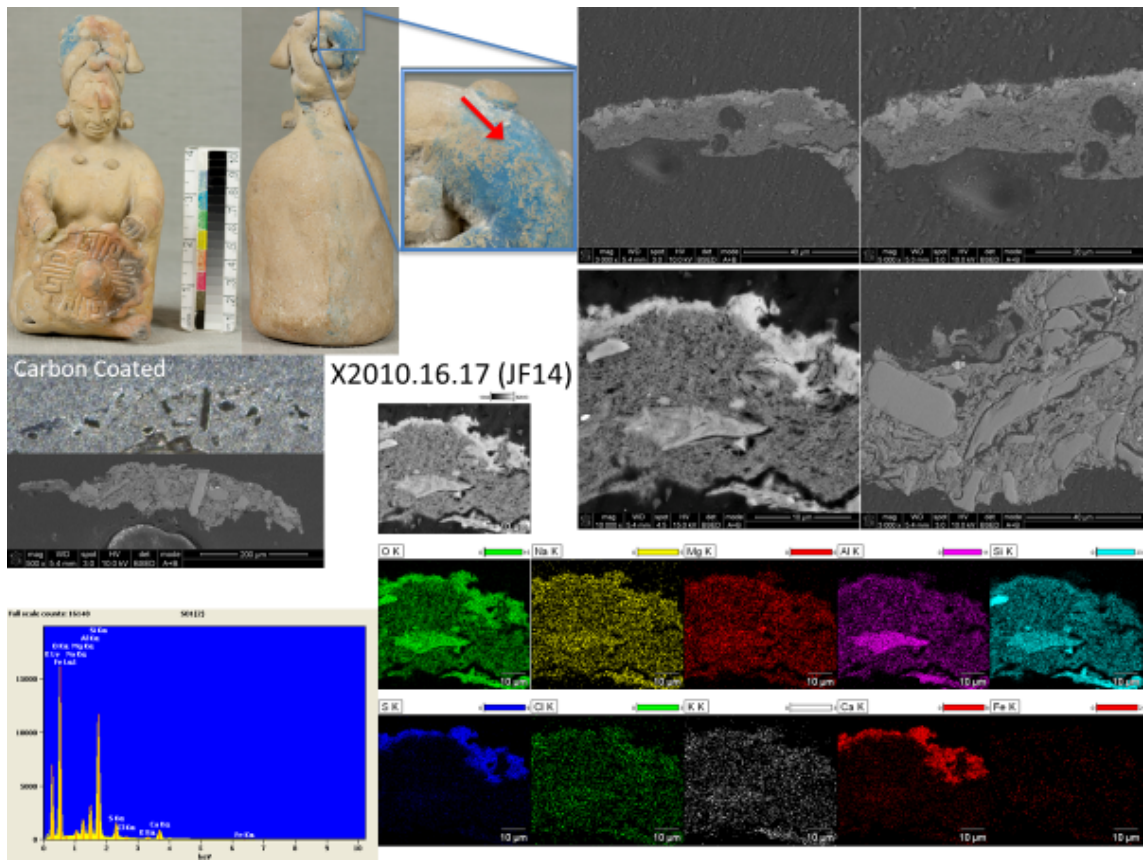


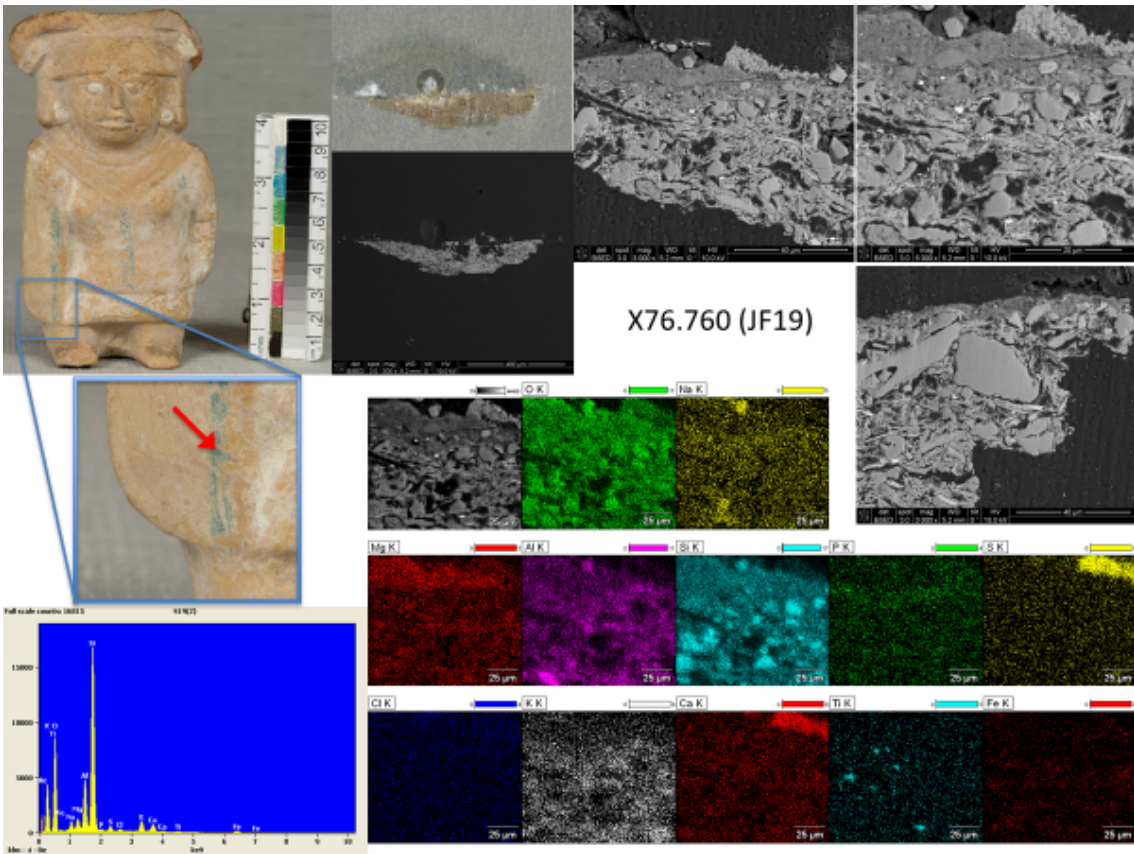
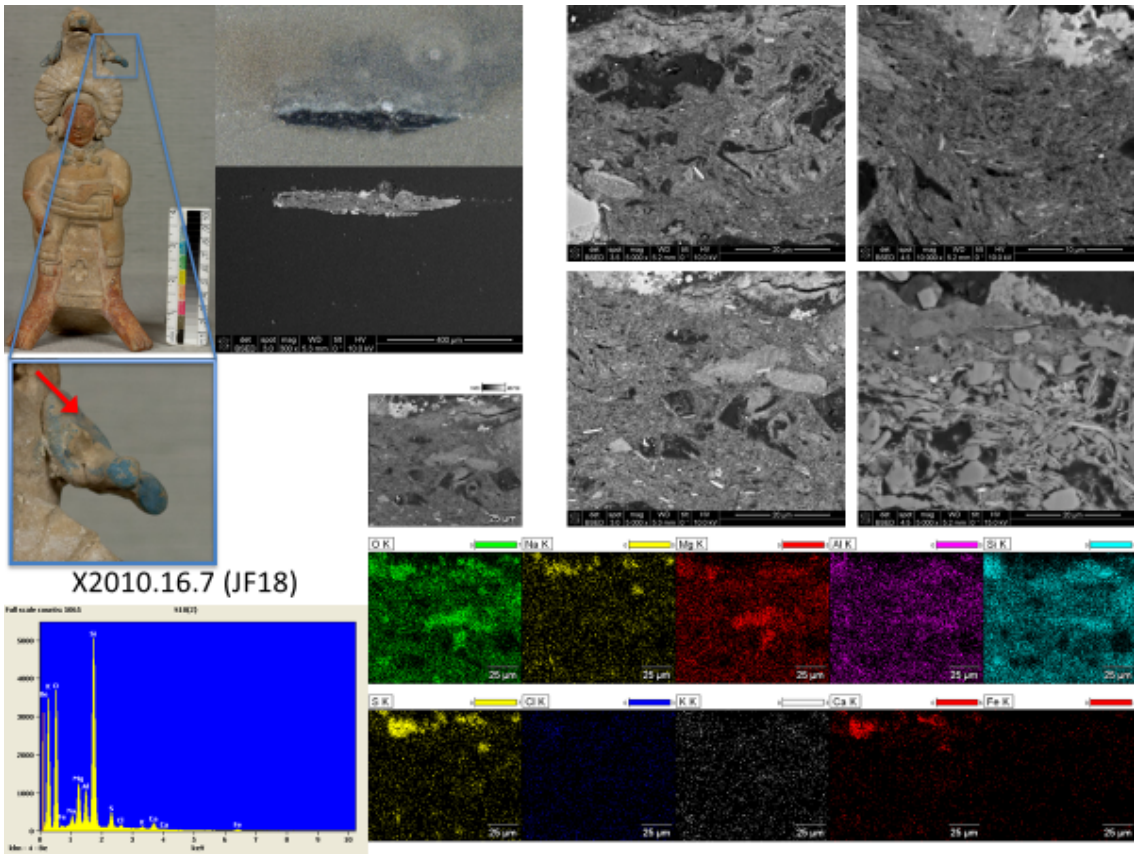




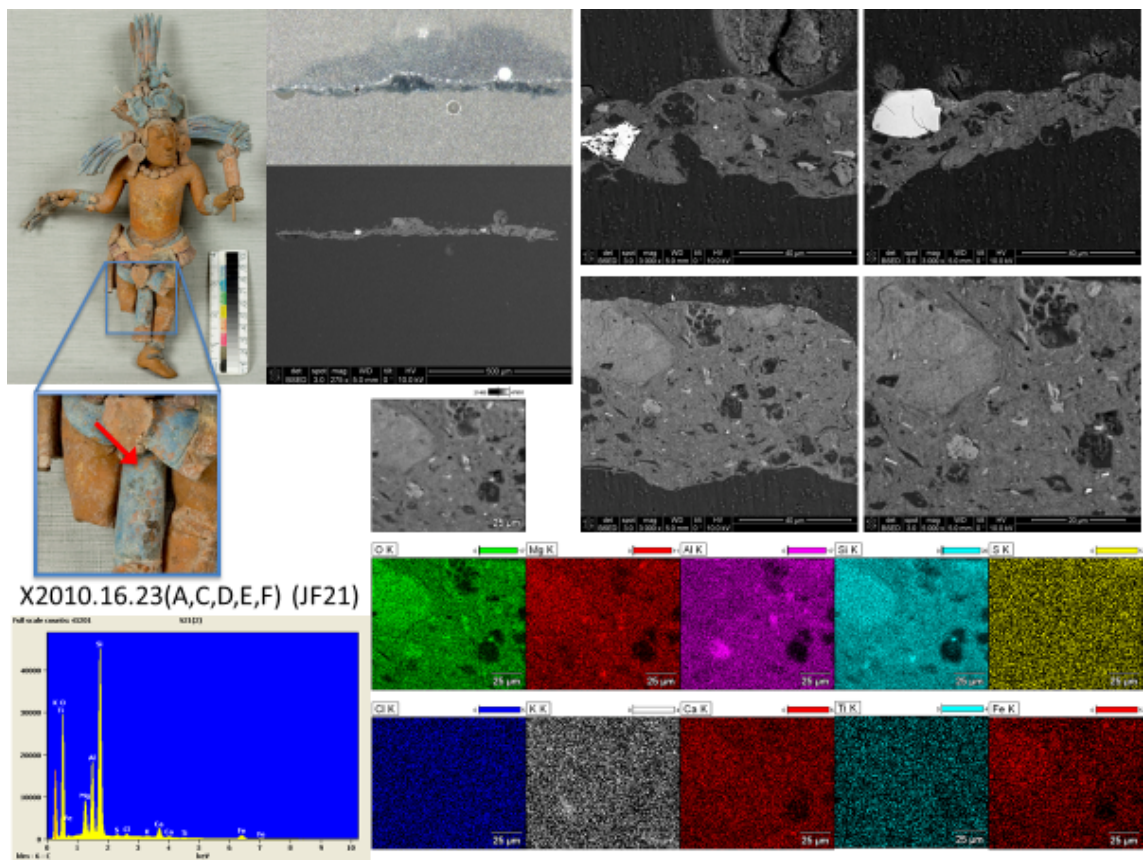
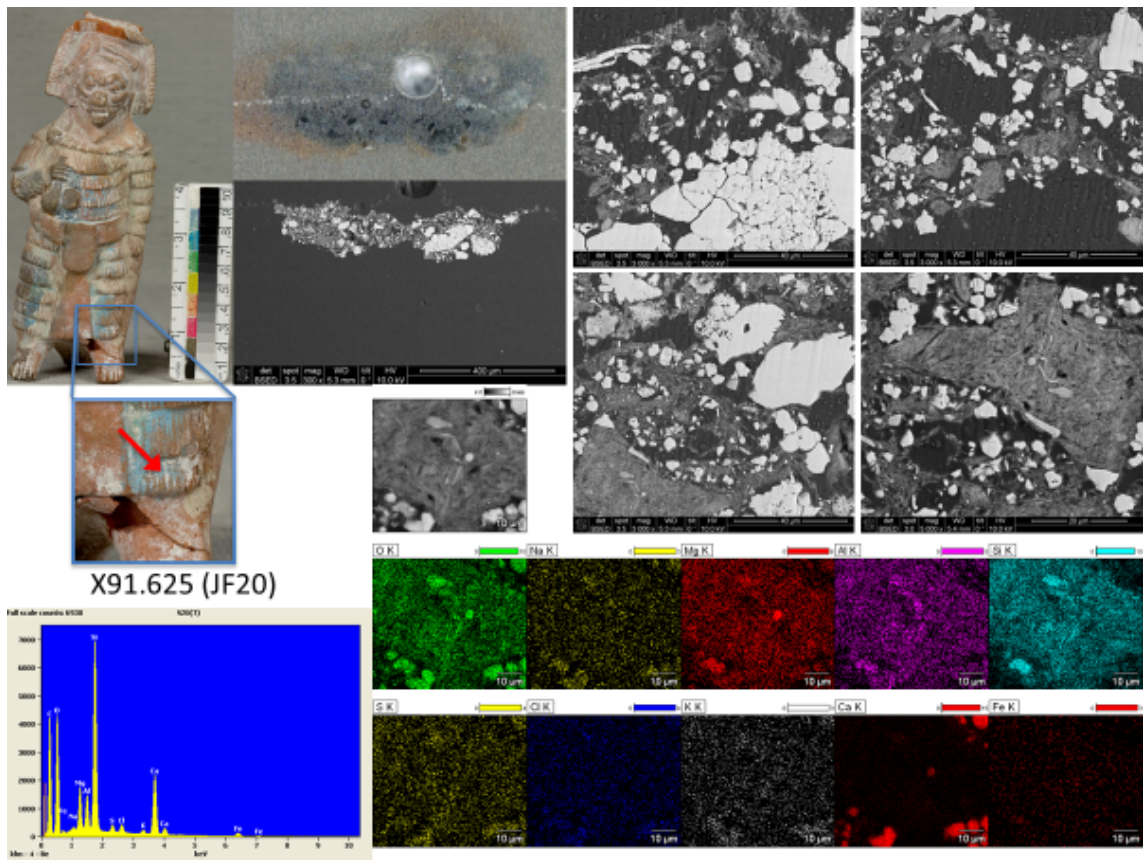


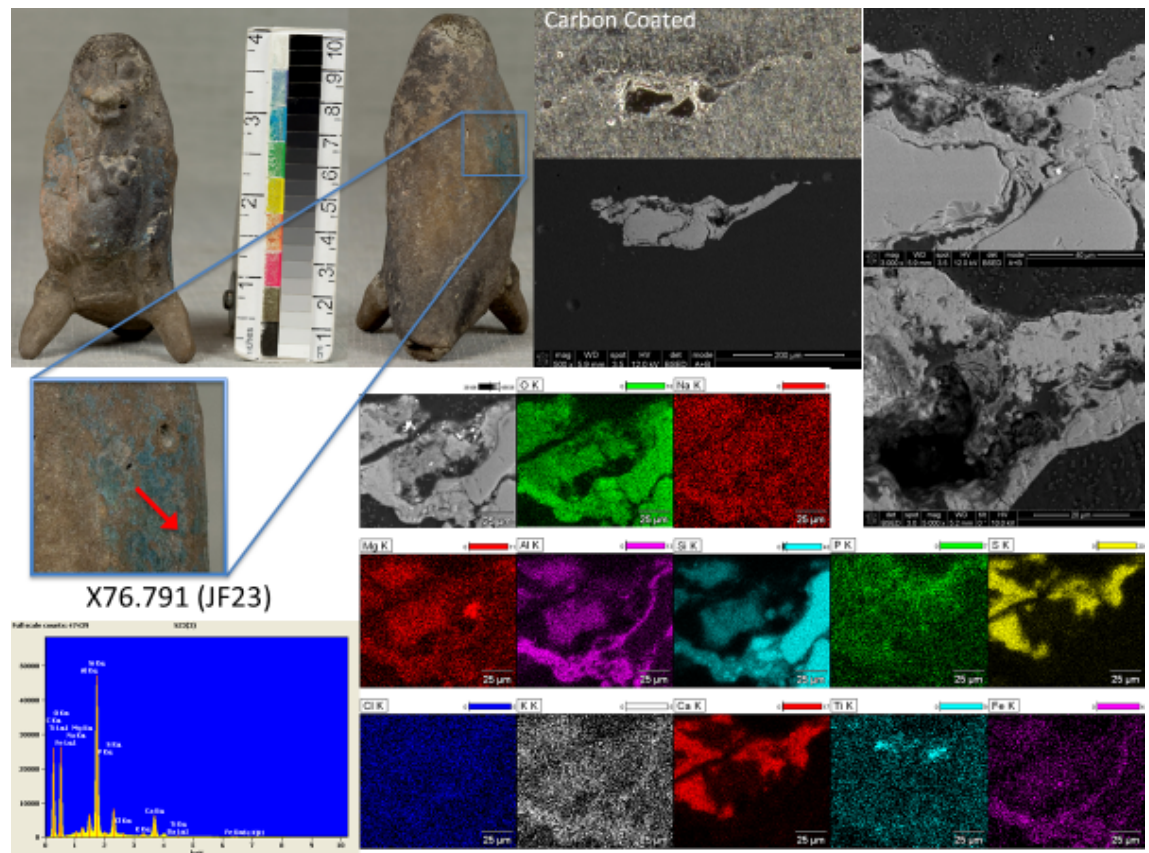
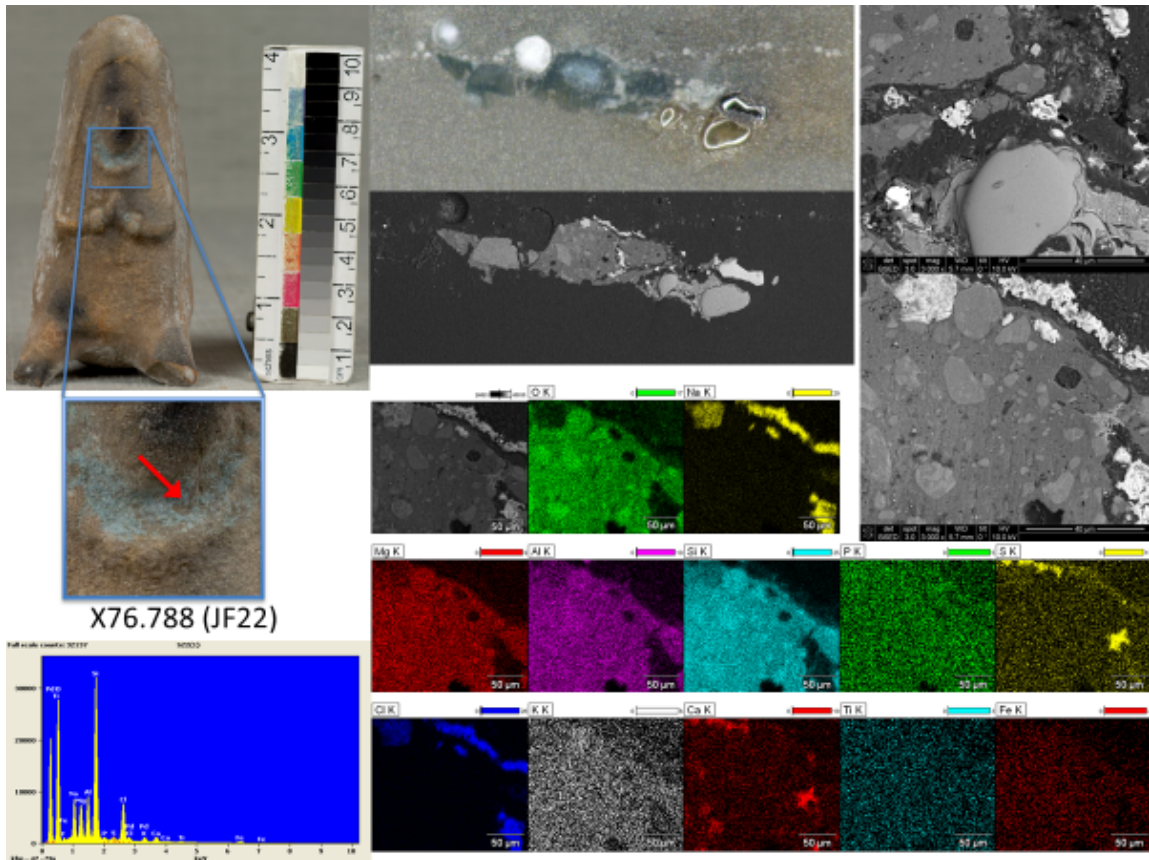




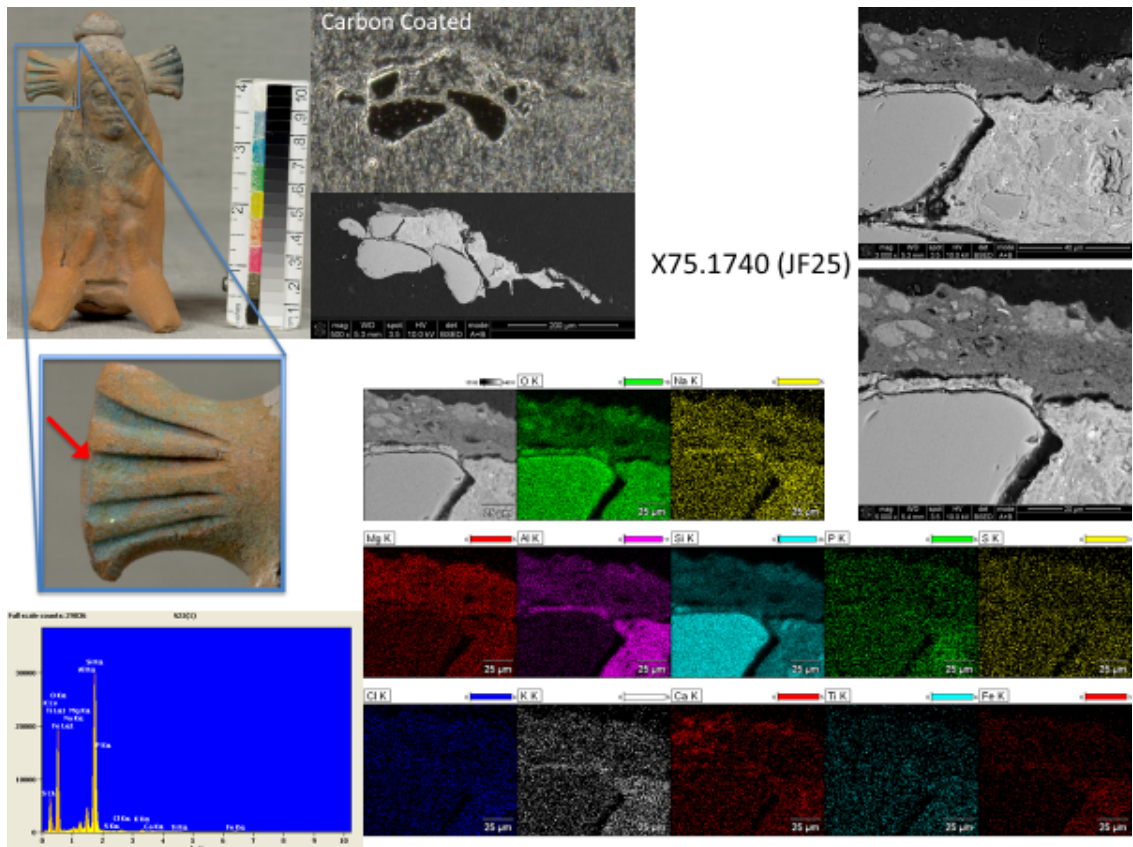
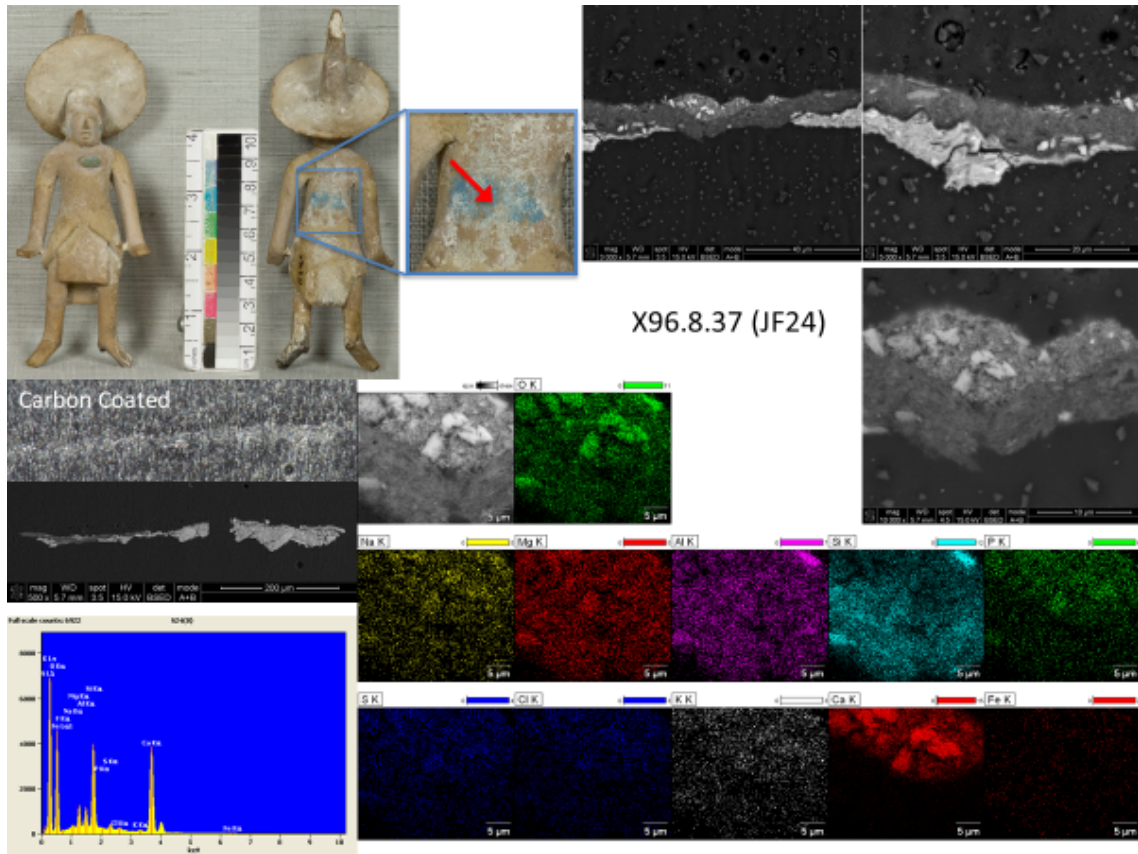


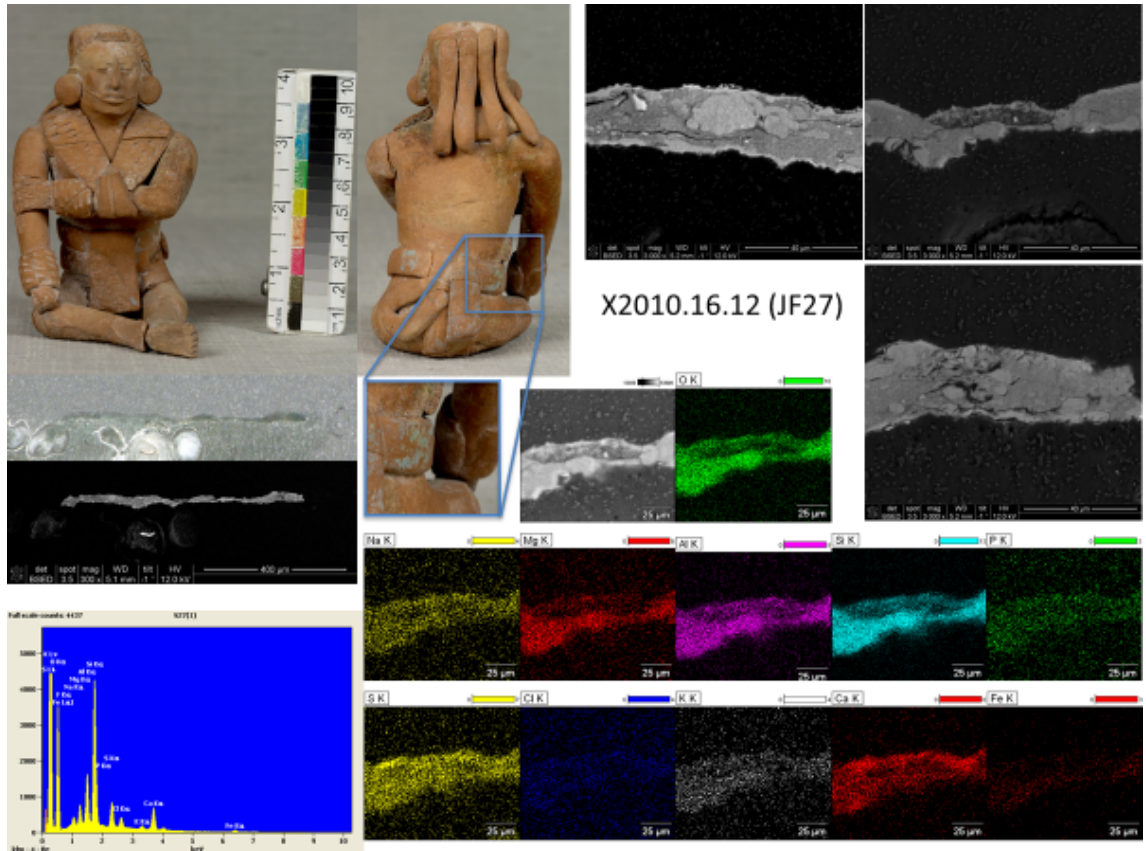
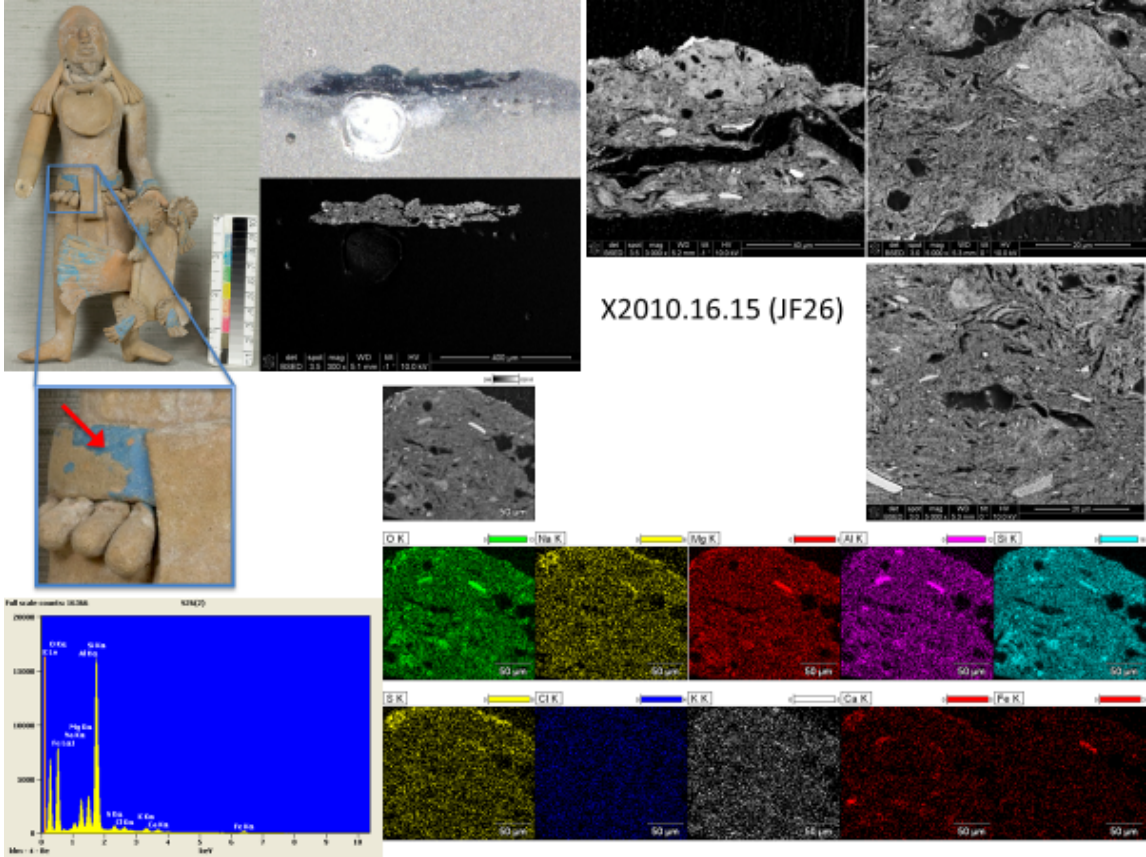




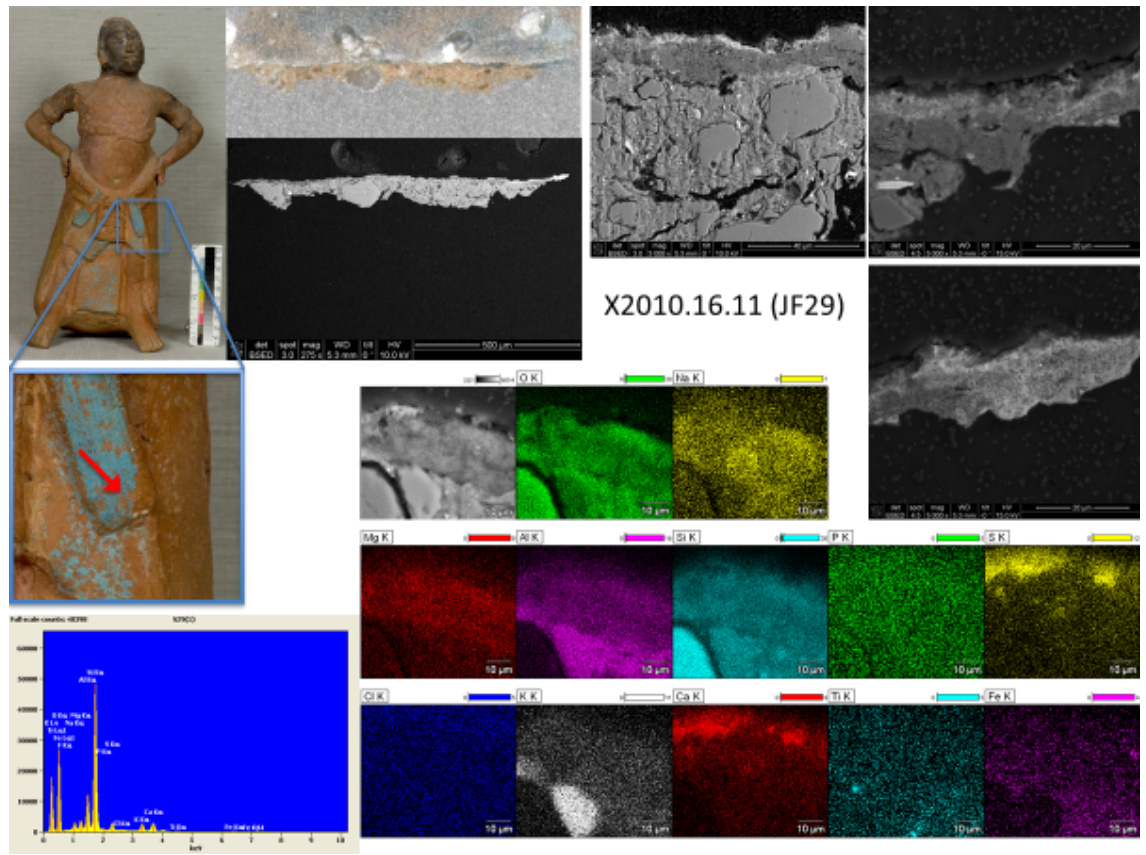
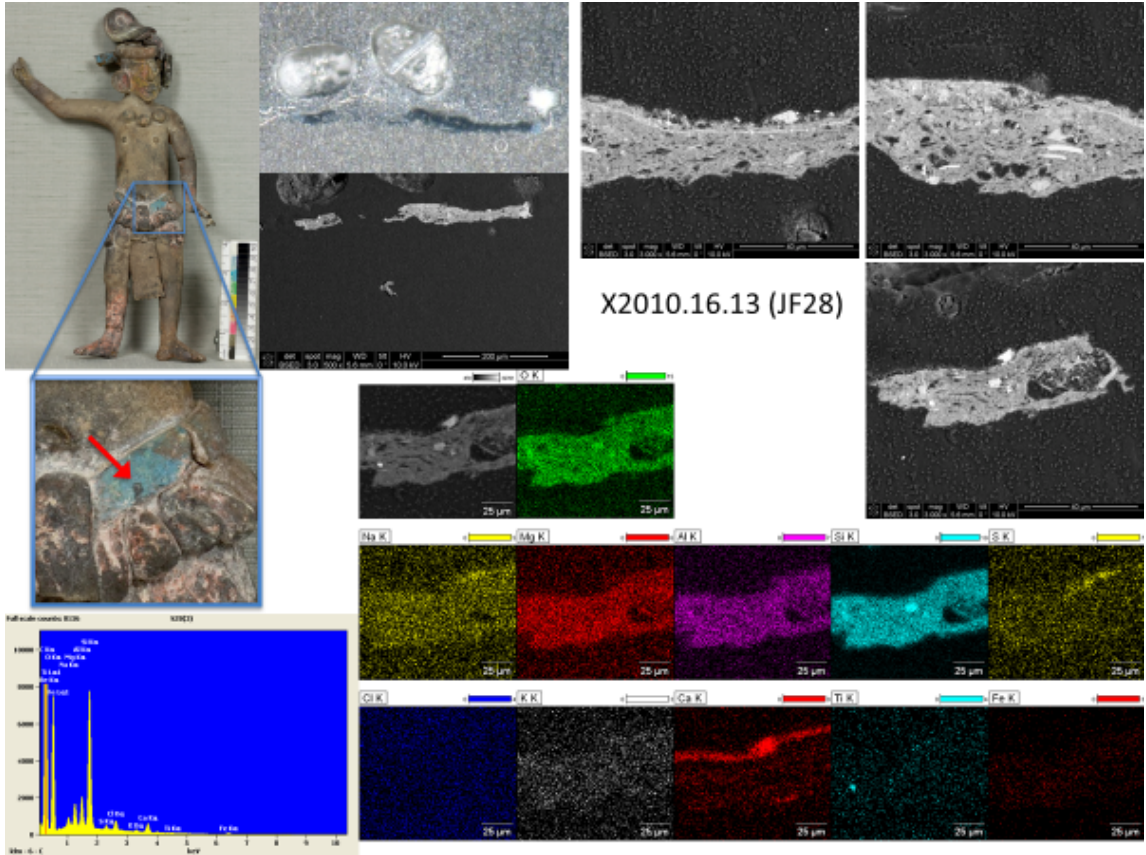












## 7 References

- BRAINARD, D. H. 2003. Color appearance and color difference specification. *The science of color*, 2, 191-216.
- BRODA, J. 2000. Mesoamerican astronomy and the ritual calendar. *Astronomy Across Cultures*. Springer.
- CHIARI, G., GIUSTETTO, R., DRUZIK, J., DOEHNE, E. & RICCHIARDI, G. 2008. Pre-columbian nanotechnology: reconciling the mysteries of the maya blue pigment. *Applied Physics A*, 90, 3-7.
- COE, M. D. & HOUSTON, S. D. 2015. *The Maya*. Ninth ed.: Thames & Hudson.
- COOK DE LEONARD, C. 1964. Extraneous influences in Jaina figurines. *Actas y memorias*, 1, 361.
- CORSON, C. 1976. *Maya Anthropomorphic Figurines from Jaina Island, Campeche*, Ballena Press.
- CREAMER, W. 1987. Mesoamerica as a concept: An archaeological view from Central America. *Latin American Research Review*, 22, 35-62.
- DE PABLO GALÁN, L. 1996. Palygorskite in Eocene-Oligocene lagoonal environment, Yucatan, Mexico. *Revista Mexicana de Ciencias Geológicas*, 13, 6.
- DEJOIE, C., MARTINETTO, P., DOORYHEE, E., BROWN, R., BLANC, S., BORDAT, P., STROBEL, P., ODIER, P., PORCHER, F. & DEL RIO, M. S. Diffusion of indigo molecules inside the palygorskite clay channels. MRS Proceedings, 2011. Cambridge Univ Press, mrsf10-1319-ww06-01.
- DEMAREST, A. 2004. *Ancient Maya: the rise and fall of a rainforest civilization*, Cambridge University Press.
- DOMÉNECH, A., DOMÉNECH-CARBÓ, M. T., DEL RÍO, M. S., DE AGREDOS PASCUAL, M. L. V. & LIMA, E. 2009. Maya Blue as a nanostructured polyfunctional hybrid organic-inorganic material: the need to change paradigms. *New Journal of Chemistry*, 33, 2371-2379.
- DOMÉNECH, A., DOMÉNECH-CARBÓ, M. T. & VÁZQUEZ DE AGREDOS PASCUAL, M. L. 2006. Dehydroindigo: a new piece into the Maya Blue puzzle from the voltammetry of microparticles approach. *The Journal of Physical Chemistry B*, 110, 6027-6039.
- FERNÁNDEZ, M. A. 1946. Los adoratorios de la Isla de Jaina. *Revista mexicana de estudios antropológicos*, 8, 243-260.
- GETTENS, R. J. 1962. Maya Blue: an unsolved problem in ancient pigments. *American Antiquity*, 557-564.



- GIUSTETTO, R., LEVY, D., WAHYUDI, O., RICCHIARDI, G. & VITILLO, J. G. 2003. Crystal structure refinement of a sepiolite/indigo Maya Blue pigment using molecular modelling and synchrotron diffraction. *European Journal of Mineralogy*, 23, 449-466.
- GIUSTETTO, R., LLABRÉS I XAMENA, F. X., RICCHIARDI, G., BORDIGA, S., DAMIN, A., GOBETTO, R. & CHIEROTTI, M. R. 2005. Maya Blue: a computational and spectroscopic study. *The Journal of Physical Chemistry B*, 109, 19360-19368.
- GOLDSTEIN, M. M. 1980. MAYA FIGURINES FROM CAMPECHE, MEXICO: CLASSIFICATION ON THE BASIS OF CLAY CHEMISTRY, STYLE AND ICONOGRAPHY.
- HALPERIN, C. T. 2014. *Maya figurines: Intersections between state and household*, University of Texas Press.
- HENDERSON, J. S. 1997. *The world of the ancient Maya*, Cornell University Press.
- HODELL, D. A., CURTIS, J. H. & BRENNER, M. 1995. Possible role of climate in the collapse of Classic Maya civilization.
- HUBBARD, B., KUANG, W., MOSER, A., FACEY, G. A. & DETELLIER, C. 2003. Structural study of Maya Blue: textural, thermal and solidstate multinuclear magnetic resonance characterization of the palygorskite-indigo and sepiolite-indigo adducts. *Clays and clay minerals*, 51, 318-326.
- HUNTER, R. S. & HAROLD, R. W. 1987. *The measurement of appearance*, John Wiley & Sons.
- JOSÉ-YACAMÁN, M., RENDÓN, L., ARENAS, J. & PUCHE, M. C. S. 1996. Maya blue paint: an ancient nanostructured material. *Science*, 273, 223.
- KARAPANAYIOTIS, T., VILLAR, S. E. J., BOWEN, R. D. & EDWARDS, H. G. 2004. Raman spectroscopic and structural studies of indigo and its four 6, 6' -dihalogeno analogues. *Analyst*, 129, 613-618.
- LEONA, M., CASADIO, F., BACCI, M. & PICOLLO, M. 2004. Identification of the Pre-Columbian Pigment Mayablue on Works of Art by Noninvasive UV-Vis and Raman Spectroscopic Techniques. *Journal of the American Institute for Conservation*, 43, 39-54.
- LUCERO, L., AOYAMA, K., CYPHERS, A., DEMAREST, A., INOMATA, T., LECOUNT, L., PUGH, T., RICE, P., SCARBOROUGH, V. & LUCERO, L. 2003. The politics of ritual: The emergence of Classic Maya rulers. *Current Anthropology*, 44, 523-558.
- MCVICKER, D. 2012. Figurines are us? The social organization of Jaina Island, Campeche, Mexico. *Ancient Mesoamerica*, 23, 211-234.
- MILLER, M. E. 1975. *Jaina Figurines: A Study of Maya Iconography*, Art Museum, Princeton University.

- PIÑA CHÁN, R. 1996. Las figurillas de Jaina. *Arqueología mexicana*, 3, 52-59.
- REINEN, D., KÖHL, P. & MÜLLER, C. 2004. The nature of the colour centres in 'Maya blue'— the incorporation of organic pigment molecules into the palygorskite lattice. *Zeitschrift für anorganische und allgemeine Chemie*, 630, 97-103.
- RICHARDSON, D. & RICHARDSON, S. 2016. *Indigo* [Online]. Asian Textile Studies. [Accessed].
- SÁNCHEZ DEL RÍO, M., DOMÈNECH, A., DOMÈNECH-CARBÓ, M., VÁZQUEZ DE AGREDOS PASCUAL, M., SUÁREZ, M. & GARCÍA-ROMERO, E. 2011. The Maya blue pigment. *Developments in Palygorskite-Sepiolite Research. Developments in Clay Science*, 3, 293-452.
- SÁNCHEZ DEL RÍO, M., PICQUART, M., HARO - PONIATOWSKI, E., VAN ELSLANDE, E. & HUGO UC, V. 2006. On the Raman spectrum of Maya blue. *Journal of Raman Spectroscopy*, 37, 1046-1053.
- SANZ, E., ARTEAGA, A., GARCÍA, M., CÁMARA, C. & DIETZ, C. 2012. Chromatographic analysis of indigo from Maya Blue by LC-DAD-QTOF. *Journal of Archaeological Science*, 39, 3516-3523.
- SHARER, R. J. & TRAXLER, L. P. 2006. *The ancient maya*, Stanford University Press.
- SHEPARD, A. & GOTTLIEB, H. B. 1962. Maya blue: alternative hypotheses. *Notes from a ceramic laboratory*, 43-64.
- SMITH, M. E. & BERDAN, F. F. 2003. Spatial structure of the Mesoamerican world system. *The Postclassic Mesoamerican World, University of Utah Press, Salt Lake City*, 21-31.
- SPLITSTOSER, J. C., DILLEHAY, T. D., WOUTERS, J. & CLARO, A. 2016. Early pre-Hispanic use of indigo blue in Peru. *Science Advances*, 2, e1501623.
- ŠPRAJC, I. 2009. Astronomy and its role in ancient Mesoamerica. *Proceedings of the International Astronomical Union*, 5, 87-95.
- TATSCH, E. & SCHRADER, B. 1995. Near - infrared fourier transform Raman spectroscopy of indigoids. *Journal of Raman Spectroscopy*, 26, 467-473.
- TZADIK, C. 2014. *Jaina Figurines: The Survey, Characterization of Materials, and Treatment of Figures from the Fowler Museum Collection*. Master of Arts, University of California, Los Angeles.
- VAN OLPHEN, H. 1966. Maya Blue: A Clay-Organic Pigment? *Science*, 154, 645-646.
- VANDENABEELE, P., BODÉ, S., ALONSO, A. & MOENS, L. 2005. Raman spectroscopic analysis of the Maya wall paintings in Ek'Balam, Mexico. *Spectrochimica Acta Part A: Molecular and Biomolecular Spectroscopy*, 61, 2349-2356.

WHETZEL, N. 2016. Measuring color using Hunter L, a, b versus CIE 1976 L\*a\*b\*.

WITKE, K., BRZEZINKA, K.-W. & LAMPRECHT, I. 2003. Is the indigo molecule perturbed in planarity by matrices? *Journal of molecular structure*, 661, 235-238.